Response to Referee Henk Eskes

We thank the reviewer Henk Eskes for the careful reading and the usefulmments. Below we give the reviewer's comment, our response, and the changed text in the manuscript. The page and line numbers refer to the mark-up version of the manuscript.

General remarks:

1.The reader may find the title and abstract confusing. It suggests that the authors are improving the operational TROPOMI retrieval product, while actually the paper discusses and upgrade of the retrieval product implemented at DLR. This should be made more clear at the top of the abstract and in the title. I suggest the authors make clear which retrieval product they refer to, for instance by calling it the DLR TROPOMI NO₂ European product. Maybe good to add the word "scientific" as opposed to the "operational" retrieval.

We have updated the title to "*An improved TROPOMI tropospheric NO₂ research product over Europe*" and referred the data to "*the DLR TROPOMI NO₂ European product*" throughout the paper.

2.The preformance of the POLYPHEMUS model is not easy to judge. The resolution of this model is not very high, 0.2x0.3 degree, while TROPOMI has a resolution of 0.05 degree. The CAMS models for instance run at 0.1x0.1 degree. This resolution is in between the TM5-MP and TROPOMI. Would higher resolution produce a major further improvement? I would like to see a comparison between POLYPHEMUS and TROPOMI as extra figure. The POLYPHEMUS model seems to produce very low free tropospheric NO₂ concentrations. Is this expected to impact the retrieval?

The 0.2x0.3 degree is selected for POLYPHEMUS/DLR due to the feasibility in terms of runtime and affordability in terms of computing resources. We have analysed the effect of model resolution using a priori NO₂ profiles from LOTOS-EUROS, which constitutes one of the state-of-the-art atmospheric chemistry models used by the regional Copernicus Atmosphere Monitoring Service (CAMS, http://www.copernicus-atmosphere.eu). Figure R1 shows the differences in the tropospheric NO₂ columns retrieved by altering the model resolution for LOTOS-EUROS (0.1x0.1 degree - 0.2x0.3 degree) in February 2019. The increase of the spatial resolution from 0.2x0.3 to 0.1x0.1 degree improves the tropospheric NO₂ columns moderately by up to 5×10^{14} molec/cm² or 11% for polluted regions.
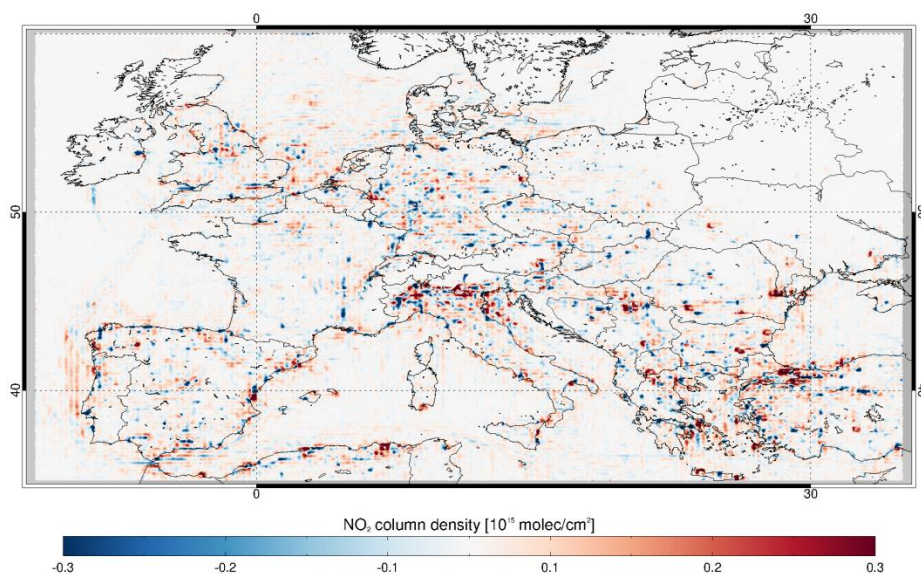
Figure R1. Differences in the tropospheric NO$_2$ columns retrieved by altering the model resolutions (0.1x0.1 degree - 0.2x0.3 degree) for LOTOS-EUROS a priori NO$_2$ profiles in February 2019.

We have included a new Fig. 11 in page 20 comparing the tropospheric NO$_2$ columns from TROPOMI measurements and POLYPHEMUS/DLR simulations (using the satellite averaging kernel) and included the description in pages 19 as "*Figure 11 compares the tropospheric NO$_2$ columns from TROPOMI measurements and POLYPHEMUS/DLR simulations. The satellite averaging kernel, which describes the vertical sensitivity of measurements of NO$_2$ concentrations, is applied to reduce the systematic biases caused by unrealistic a priori profile information. From Fig. 11, POLYPHEMUS/DLR NO$_2$ columns are generally higher than satellite measurements, which can be partly related to the use of the TNO-MACC emission dataset (Denier van der Gon et al., 2010). An update of the POLYPHEMUS/DLR model using the more recent TNO-MACC_II emission (Kuenen et al., 2014) is planned for the near future. We note here that the profile shape is of far more importance than the column bias for the interpretation of satellite retrievals.*"
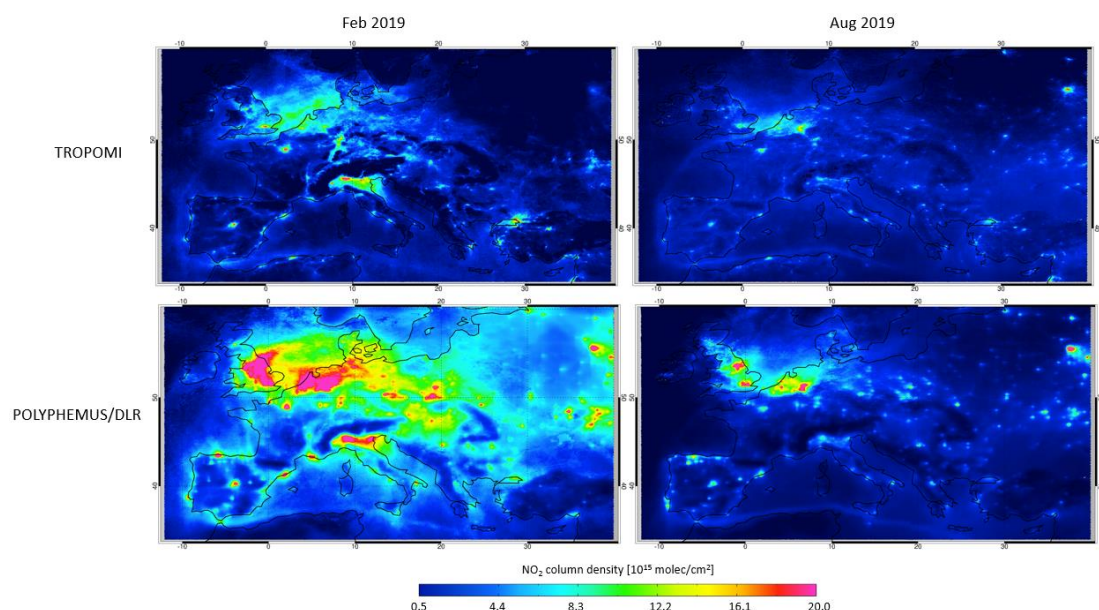
Figure 11. Tropospheric NO$_2$ columns from TROPOMI measurements (retrieved with the POLYPHEMUS/DLR a priori NO$_2$ profiles) and POLYPHEMUS/DLR simulations (using the satellite averaging kernel) over Europe in February and August 2019. Only TROPOMI measurements with cloud radiance fraction less than 0.5 are included.

Despite the use of outdated emissions, the POLYPHEMUS/DLR is in general reliable, as indicated in a validation exercise in Fig. R2 comparing the near-surface NO$_2$ concentrations from POLYPHEMUS/DLR and ground-based EEA air quality monitoring stations (https://discomap.eea.europa.eu/map/fme/AirQualityExport.htm). The correlation coefficients are generally higher than 0.6 for polluted hot spots, and the biases are generally lower than 20 uq/m^3 or 38%.
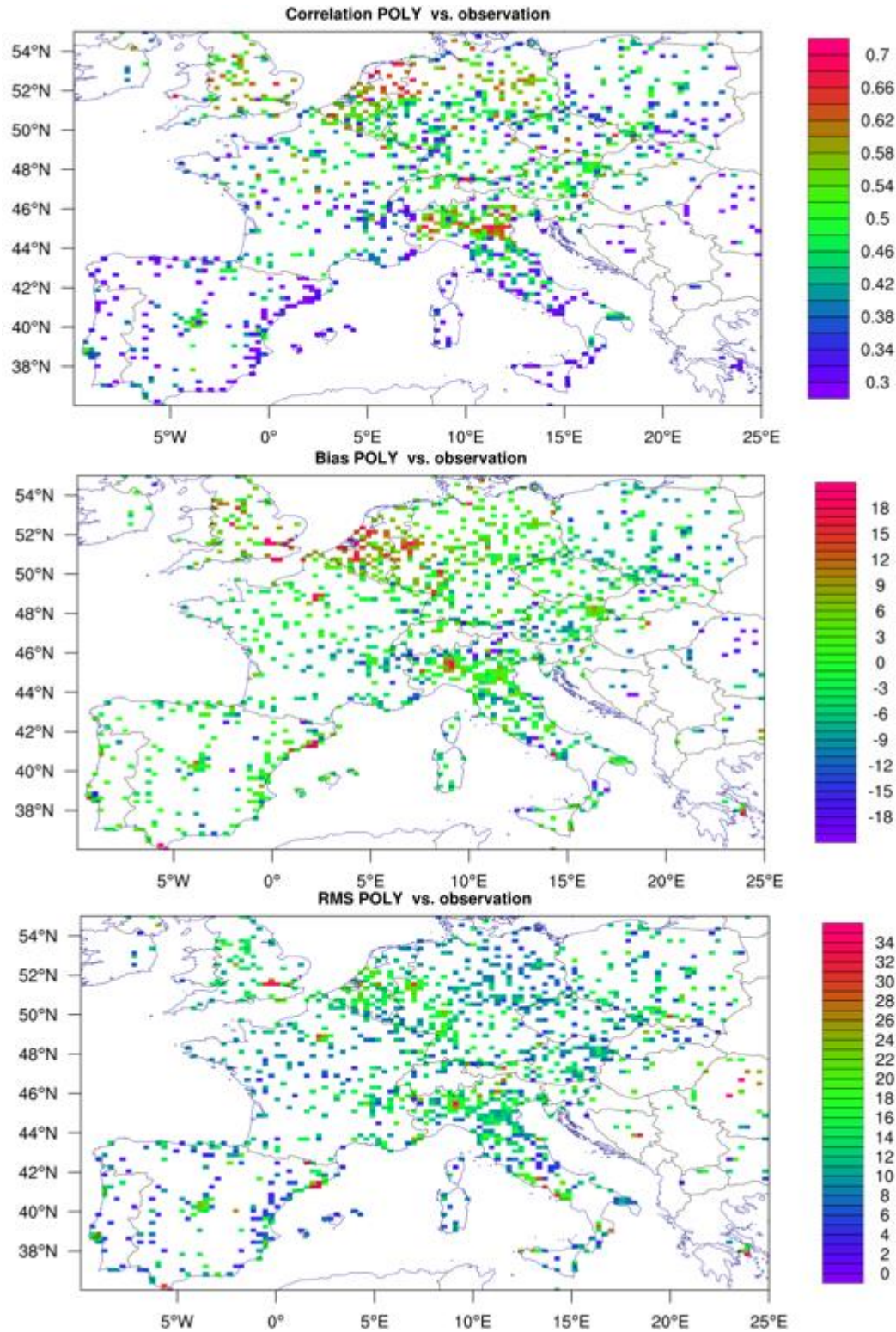
Figure R2. Comparisons of near-surface NO$_2$ concentrations [uq/m^3] from POLYPHEMUS/DLR simulations and ground-based air quality monitoring stations (POLYPHEMUS/DLR results – ground-based observations) for Europe in 2018.
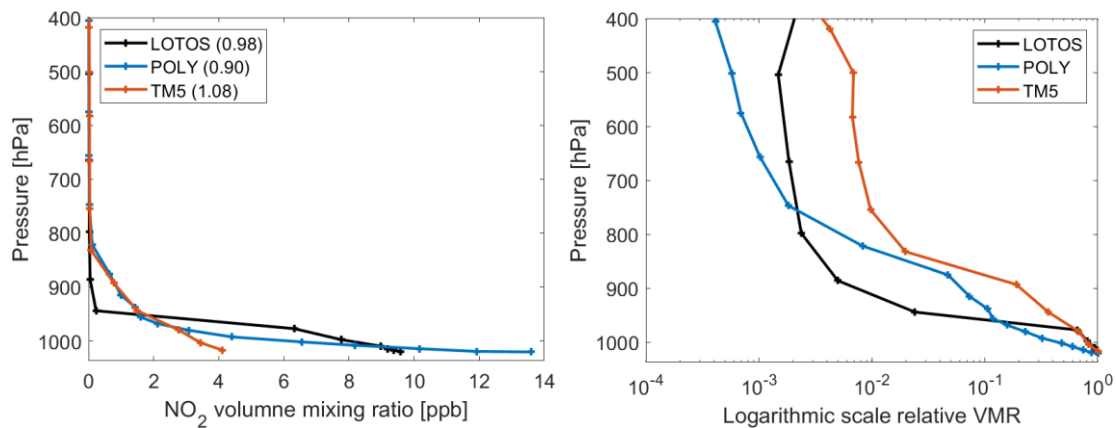
Figure R3. A priori NO$_2$ profiles from the chemistry transport models LOTOS-EUROS, POLYPHEMUS/DLR, and TM5-MP over Hamburg in Germany (53.55°N, 9.99°E) on 1 February 2019. The calculated clear-sky tropospheric AMF is given in the bracket next to each label in the legend. Normalized profiles (to the lowest values) are also shown on a logarithm scale.

We have compared a priori NO$_2$ profiles from LOTOS-EUROS, POLYPHEMUS/DLR, and TM5-MP over Hamburg in Fig. R3. POLYPHEMUS/DLR shows the largest surface layer NO$_2$ concentration (Fig. R3 left panel) and the steepest profile shape (Fig. R3 right panel), which yields the smallest tropospheric AMF. LOTOS-EUROS shows lower free tropospheric concentration and larger surface concentration than TM5-MP, and thus the tropospheric AMF is lower by 9%.
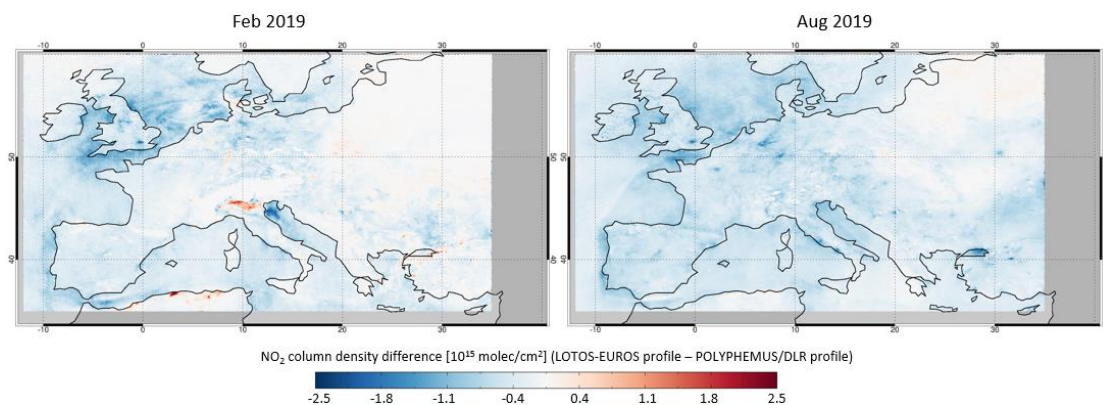
Figure R4. Differences in the tropospheric NO$_2$ columns retrieved using the POLYPHEMUS/DLR and LOTOS-EUROS a priori NO$_2$ profiles over Europe in February and August 2019.

Figure R4 compares the tropospheric NO$_2$ columns retrieved using POLYPHEMUS/DLR and LOTOS-EUROS a priori NO$_2$ profiles, where the use of LOTOS-EUROS reduces the tropospheric NO$_2$ columns by up to ~1×10^{15} molec/cm^2, e.g. over the ocean partly due to difference in the shipping emissions.

3.It would be of interest to extend the comparisons with the operational TROPOMI product and also list differences with other (regional) retrievals like the TROPOMI-POMINO approach for Asia. Maybe in the form of a table listing the choices for albedo, cloud, stratosphere, a-priori for several retrievals. For the validation, Table 4, it would be nice if also the operational retrieval could be added (now there is only the comparison with the old DLR retrieval in brackets).

We have extended the comparison with different retrievals in Table 1 in page 9.

Table 1. Overview of tropospheric NO$_2$ column retrievals. See Table 2 for details of the chemistry transport models used to obtain the a priori NO$_2$ profiles for the DLR improved retrieval in this work.

	DLR reference retrieval	DLR improved algorithm	KNMI operational product	POMINO-TROPOMI product	ECCC product
reference	This work	This work	(van Geffen et al., 2020a, b)	(Lin et al., 2014; Liu et al., 2019a)	(Griffin et al., 2019)
Region	Global	Europe	Global	China	Canada
Stratospheric correction	STREAM	DSTREAM	Data assimilation	Same as KNMI	Same as KNMI
Surface albedo	OMI LER climatology	TROPOMI GE_LER data	OMI LER climatology	MODIS BRDF	MODIS albedo climatology
A priori NO$_2$ profile	TM5-MP	POLYPHEMUS/DLR	TM5-MP	GEOS-Chem	GEM-MACH
Cloud parameter	OCRA/ROCINN_CRB version 1.x	OCRA/ROCINN_CAL version 2.1	FESCO-S	Recalculated cloud fraction with aerosol correction	Same as KNMI
Aerosol treatment	Implicit correction	Implicit correction	Implicit correction	Explicit correction	Explicit correction

We have included the validation results for the operational product in Tables 5 and 6 in pages 31-32.

Table 5. The Pearson correlation coefficient R, as well as the slope S and intercept I (in 1×10^{15} molec/cm^2) obtained with the robust Theil–Sen estimator for the monthly TROPOMI tropospheric NO$_2$ product compared to MAX-DOAS data. Stations are ordered by increasing mean difference. Values for the DLR improved algorithm (DLRimp) are given, and the values for the DLR reference algorithm (DLRref) and the KNMI operational product (KNMIop) are reported for comparison.

Station	R			S			I		
	DLRimp	DLRref	KNMIop	DLRimp	DLRref	KNMIop	DLRimp	DLRref	KNMIop
Athens	0.85	0.87	0.81	0.65	0.42	0.45	0.33	0.25	0.33
De Bilt	0.63	0.72	0.80	0.42	0.25	0.77	1.69	1.31	-0.57
Thessaloniki_ciri	0.91	0.95	0.91	0.51	0.45	0.26	-0.80	0.14	1.23
Thessaloniki_lap	0.79	0.86	0.90	0.35	0.30	0.37	1.97	1.09	0.93
Bremen	0.85	0.71	0.70	0.58	0.44	0.40	-0.24	-0.20	0.79
Uccle	0.85	0.81	0.44	0.70	0.42	0.27	-0.52	-0.24	2.26
Cabauw	0.75	0.67	0.43	0.41	0.21	0.33	1.08	1.24	1.98
Munich	0.57	0.72	0.63	0.35	0.39	0.42	1.44	0.29	1.35
Mainz	0.85	0.87	0.81	0.39	0.28	0.50	1.65	0.82	0.02

Table 6. Similar as Table 5 but for the mean difference (MD, SAT-GB in 1×10^{15} molec/cm^2), standard deviation (STD, in 1×10^{15} molec/cm^2), and relative difference (RD, in %) for the monthly TROPOMI tropospheric NO$_2$ product compared to MAX-DOAS data.

Station	MD			STD			RD		
	DLRimp	DLRref	KNMIop	DLRimp	DLRref	KNMIop	DLRimp	DLRref	KNMIop
Athens	-1.6	-3.5	-3.1	1.2	1.4	1.3	-26	-53	-48
De Bilt	-2.0	-3.5	-2.1	1.8	1.6	1.3	-27	-51	-30
Thessaloniki_ciri	-2.2	-3.4	-3.8	1.5	2.0	4.0	-34	-54	-51
Thessaloniki_lap	-2.4	-3.7	-3.5	2.6	2.6	2.3	-27	-49	-46
Bremen	-2.6	-3.7	-3.1	1.0	1.2	1.4	-45	-61	-46
Uccle	-2.6	-4.5	-4.3	1.3	1.5	2.9	-34	-55	-45
Cabauw	-3.2	-4.7	-2.9	1.8	2.0	2.1	-40	-59	-36
Munich	-3.4	-4.6	-3.3	2.5	2.3	2.8	-39	-56	-38
Mainz	-4.4	-5.6	-5.1	3.0	2.8	2.5	-40	-60	-49

4.The word "improved" is used many times in the paper, not only for the final NO$_2$ result, but also for the retrieval aspects like cloud parameters, albedo, a-priori. To my opinion one should be a bit careful with this term. One can claim something is improved if there is a better match with independent observations, or if obvious biases are removed. This is not always clear. The main conclusion of the paper is an increase of the NO$_2$ columns which better agrees with MAXDOAS (smaller bias).

We have rephrased the word "improved" e.g. to "*new*" in line 24 and 500, "*updated*" in line 405, and "*corrected*" in line 299, "*higher*" in line 327.

5.The uncertainty estimates for the individual aspects of the retrieval: cloud fraction/pressure, albedo, profiles could be discussed in more detail. It seems the authors make use of numbers from De Smedt et al, instead of deriving typical uncertainties for GE-LER, ROCINN, POLYPHEMUS. It would be good to have some rough estimates of uncertainty reductions for the individual terms in the new versus old retrieval.

We have updated the uncertainty estimates in pages 26-27 as *"The estimated parameter uncertainties considered in the AMF uncertainty budget include 0.0016 for GE_LER albedo (Loyola et al., 2020b), 75 hPa for POLYPHEMUS/DLR profile height (estimated from the profile height standard deviation), 0.05 for the OCRA cloud fraction, and 50 hPa ROCINN_CAL cloud pressure (Loyola et al., 2020a). "*

We have included a Table 3 in page 25 showing the individual changes of each step (as suggested by the other reviewer) and the uncertainty reduction.

Table 3. Main settings for the step-by-step improvements and results of the tropospheric NO_2 retrievals for the different steps of the updates for Munich (48.15N, 11.57E). The tropospheric NO_2 columns (VCDtrop) are given in absolute values (molec/cm^2), and the percentage numbers in the brackets are changes relative to the reference case. The uncertainties in the tropospheric NO_2 columns (VCDtropErr) are given in relative values.

	Sect. 2.3 (Reference)	Sect. 4.1	Sect. 4.2	Sect. 4.3.1	Sect. 4.3.2 (Improved)
Surface albedo	OMI LER climatology	TROPOMI GE_LER data	TROPOMI GE_LER data	TROPOMI GE_LER data	TROPOMI GE_LER data
A priori NO_2 profile	TM5-MP	TM5-MP	POLYPHEMUS/DLR	POLYPHEMUS/DLR	POLYPHEMUS/DLR
Cloud parameter	OCRA/ROCINN_CRB version 1.x	OCRA/ROCINN_CRB version 1.x	OCRA/ROCINN_CRB version 1.x	OCRA/ROCINN_CRB version 2.1	OCRA/ROCINN_CAL version 2.1
VCDtrop (Feb. 2019)	1.02×10^{16}	1.07×10^{16} (+4.9%)	1.51×10^{16} (+48.0%)	1.57×10^{16} (+53.9%)	1.43×10^{16} (+40.2%)
VCDtropErr (Feb. 2019)	65%	62%	57%	56%	53%
VCDtrop (Aug. 2019)	3.86×10^{15}	4.03×10^{15} (+4.4%)	5.02×10^{16} (+30.1%)	5.13×10^{16} (+32.9%)	4.59×10^{16} (+18.9%)
VCDtropErr (Aug. 2019)	41%	41%	37%	36%	35%

6.In our experience with the operational product the impact of the free troposphere is not negligible. This may be discussed in more detail.

Comparing to the operational data assimilation technique that applies actual meteorological fields, one general limitation of modified reference sector methods is the possible misinterpretation of tropospheric background column over clean regions as stratospheric column. To overcome this issue, (D)STREAM makes use of cloudy pixels with medium altitudes, which directly reflect the actual stratospheric column as the tropospheric column is mostly shielded. However, the broad-scale free tropospheric diffuse NO_2 cannot be fully distinguished from stratospheric NO_2 by (D)STREAM. We have included more discussions in page 7 regarding the tropospheric background as *"Due to the use of cloudy pixels, which directly reflect the actual stratospheric column as the tropospheric column is mostly shielded,*

STREAM reduces the bias caused by the free-tropospheric contamination or tropospheric background in the reference region, in comparison with other modified reference sector methods (Beirle et al., 2016). However, the broad-scale free tropospheric diffuse NO₂ might not be fully separated from the stratospheric NO₂, which is a general limitation of the modified reference sector methods."

7.The paper mentions that the datasets are available upon request. A brief description of the product would be useful, e.g. are the input fields like GE-LER and OCRA/ROCINN cloud parameters included? Are averaging kernels included?

We have included an introduction of the product file in Data Availability as "*The DLR TROPOMI NO₂ product are published as HDF version 5 files. For each ground pixel, the TROPOMI data product provides the retrieval results (e.g., the slant column, stratospheric column, and tropospheric column of NO₂), input information (such as the GE_LER surface albedo, POLYPHEMUS/DLR a priori NO₂ profiles, and OCRA/ROCINN cloud parameters), uncertainty estimate, processing quality flag, and averaging kernel.* "

8.And finally, it would be nice if the authors can provide some recommendations for the future development of the (operational and scientific) TROPOMI NO₂ retrievals in the conclusions section!

We have extended the future works in page 35 regarding the POLYPHEMUS/DLR a priori profile, GE_LER surface albedo, and MA-DOAS validation.

Detailed remarks:

Title: Improved compared to what? The retrieval and reference should be clearly defined.

We have updated the title and texts accordingly. Please refer to major comment 1.

l12: Uncertainty strat column = 3.5 10^14 "for polluted conditions". This is a bit strange: the stratosphere does not have polluted conditions.

We have updated the expression in line 12 as "3.5×10^{14} molec/cm² *in case of significant tropospheric sources*".

l25: Decrease from 55 to 34 %: what is the 55% reference?

We have clarified the reference in line 26 as "The implementation of the algorithm improvements leads to a decrease of the relative difference from -55.3% to -34.7% on average *in comparison with the DLR reference retrieval*."

l25: At the end of section 6 it is shown that the comparison with MAXDOAS is affected significantly by the differences in the sensitivity profiles for MAXDOAS compared to TROPOMI. With kernel smoothing the remaining difference is about -20%. It would be interesting to mention this.

We have included the texts in line 26 as "*When the satellite averaging kernels are used to remove the contribution of a priori profile shape, the relative difference decrease further to ~-20%.*"

l65: There is no reference to the data assimilation approach. It would be useful to explain a bit more this alternative approach.

We have included references in line 67 as "*(Eskes et al., 2003; Dirksen et al., 2011)*" and extended the description in line 69 as "*Advantages of the data assimilation approach include a realistic error estimation and the capture of small-scale dynamical and chemical variability of stratospheric NO_2.*"

l120: Improvements compared to what? To the previous DLR algorithm or compared to the operational algorithm, or both? Even at the end of the introduction it is still somewhat unclear which two retrievals are compared.

We have updated the sentence in 125 as "a number of improvements to the tropospheric NO_2 retrieval over Europe are introduced *for the DLR product*."

l151: An intensity offset correction is used, while this is not done in the operational retrieval. Would be good to have a brief discussion of the impact of this intensity offset term. How do the slant columns compare with the operational algorithm?

Though the precise physical origin of such an intensity offset has not been fully discussed, the intensity offset correction is included in the DLR product to reduce the fitting residues. Figure R5. illustrates the effect of applying a linear intensity offset correction, which decreases the NO_2 columns by up to 11% and the fitting residues by up to 23% mainly over the cloud-free ocean, likely due to the compensation of inelastic vibrational Raman scattering in water bodies (Vountas et al., 2003).
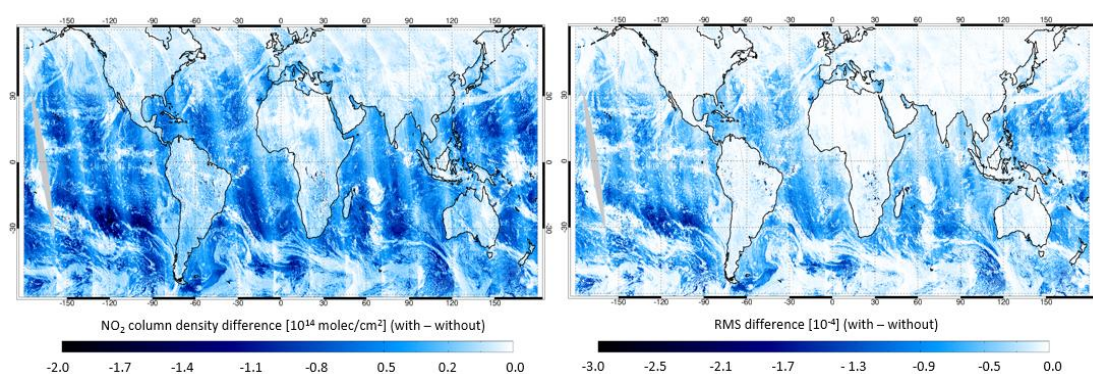

NO₂ column density difference [10¹⁴ molec/cm²] (with – without)   RMS difference [10⁻⁴] (with – without)

-2.0   -1.7   -1.4   -1.1   -0.8   0.5   0.2   0.0   -3.0   -2.5   -2.1   -1.7   - 1.3   -0.9   -0.5   0.0

Figure R5. Difference in NO$_2$ columns (slant columns scaled by geometric AMFs) and fitting residues (retrieval root mean square, RMS) estimated with and without a linear intensity offset correction (with-without) on 5 February 2019.

Figure R6 compares the DLR and KNMI NO$_2$ slant columns, with similar spatial distribution to Fig. R5 mainly reflecting the differences of the intensity offset correction. The results are in agreement with van Geffen et al., 2020. We have referred to *van Geffen et al., 2020* for further discussion in line 158.

NO$_2$ column density difference [10^{14} molec/cm^2] (DLR improved – KNMI operational)
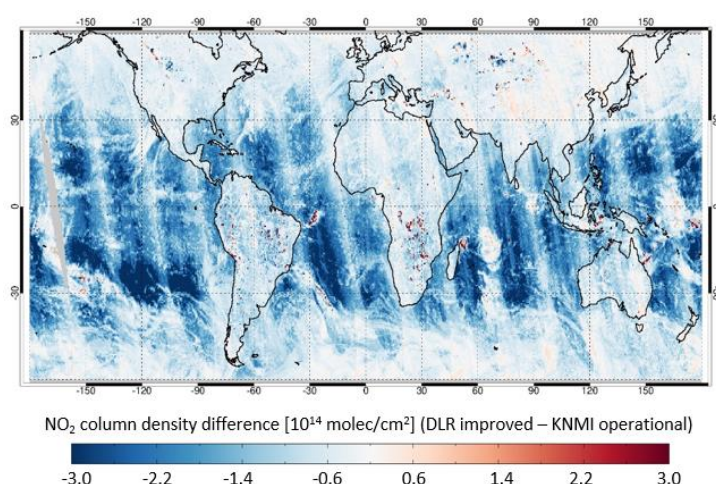
Figure R6. Difference in NO$_2$ columns (slant columns scaled by geometric AMFs) from the DLR improved algorithm and KNMI operational product (DLR-KNMI) on 5 February 2019.

Sec 2.2 STREAM: How does STREAM distinguish the stratospheric background from a free tropospheric background? Please add some discussion on the free troposphere, which is supposed to be included in the tropospheric NO$_2$ column.

Please refer to major comment 6.

l182: "average bias of 1e13 molec/cm2 with respect to the ground-based zenith-scattered light differential optical absorption spectroscopy (ZSL-DOAS) measurements" This is a very small number. Please provide the uncertainty range on this comparison. STREAM produces a somewhat larger column than the assimilation approach because it does not distinguish stratosphere from free troposphere.

We have included the uncertainty in line 193 as "an average bias of 1$\pm$8$\times$10^{13} molec/cm^2".

Sec 3.1, description of DSTREAM: I am wondering if there is any interference between DSTREAM and the destriping? The directional part removes east-west

biases. Does the destriping do something similar? Is destriping done before STREAM is calculated, or after?

The interference between DSTREAM and the de-striping is expected to be small.

We first have corrected the mistake in the label of Fig. 3 in page 11 as "The de-striping is ~~not~~ implemented here." The correct figure without de-striping is shown in Fig. R7, which shows similar impact of local time changes across the orbit as the results with de-striping.
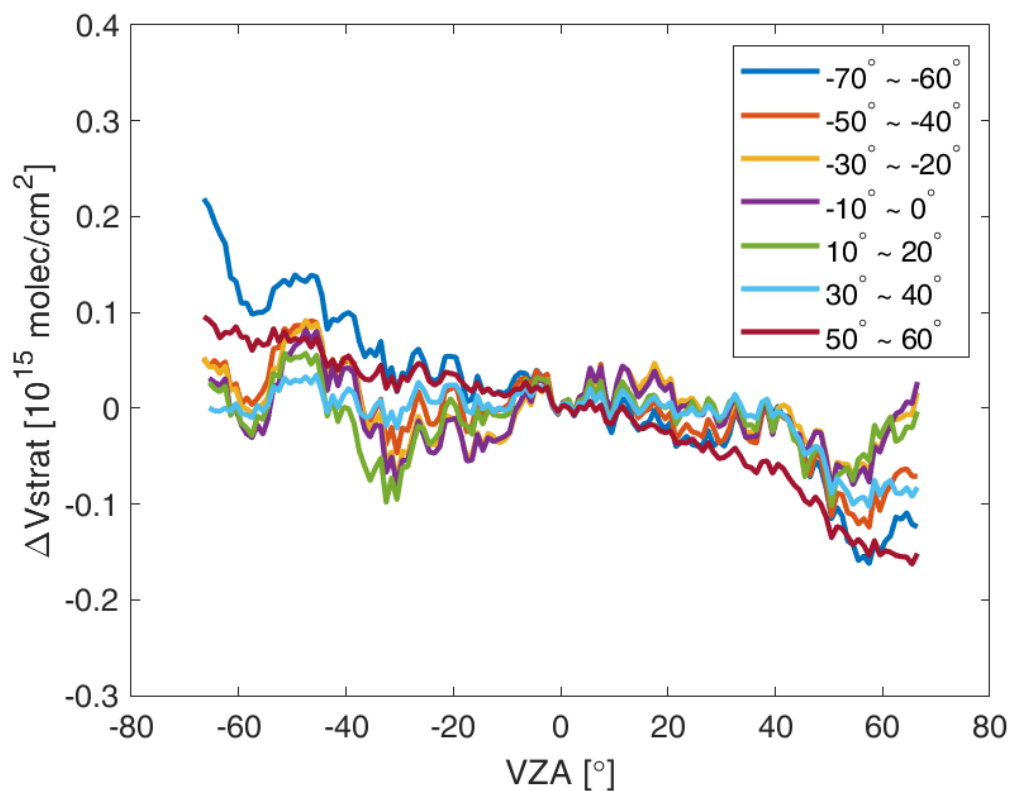

Figure R7. Similar as Fig. 3 in the manuscript but for measurements without de-striping correction.
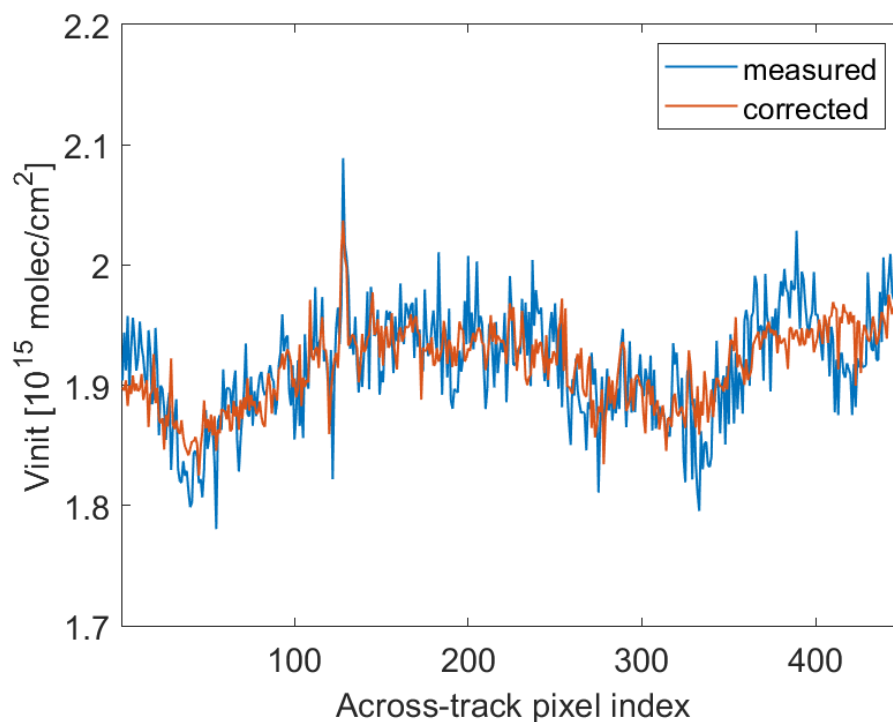
Figure R8. NO$_2$ slant columns (scaled by geometric AMFs) averaged for clean regions between 20°S and 20°N with and without de-striping correction for orbit 6748 on 1 February 2019.

The de-striping correction is implemented before the (D)STREAM. Figure R8 shows the effect of applying the empirical de-striping correction. According to the box-car averaging method (Boersma et al., 2011), the total NO$_2$ columns from 60 adjacent viewing angles are averaged for every TROPOMI along-track array. In comparison to the operational de-striping relying on CTM, only relatively small-scale variation is removed, and the larger-scale directional part may not be captured.

l 257: Why is this latitude weighting introduced? Even though the diurnal cycle effect is smaller at the equator, I would assume it could still be modelled with STREAM? For instance, average slopes with viewing angle could be accomodated as a function of latitude also near the equator.
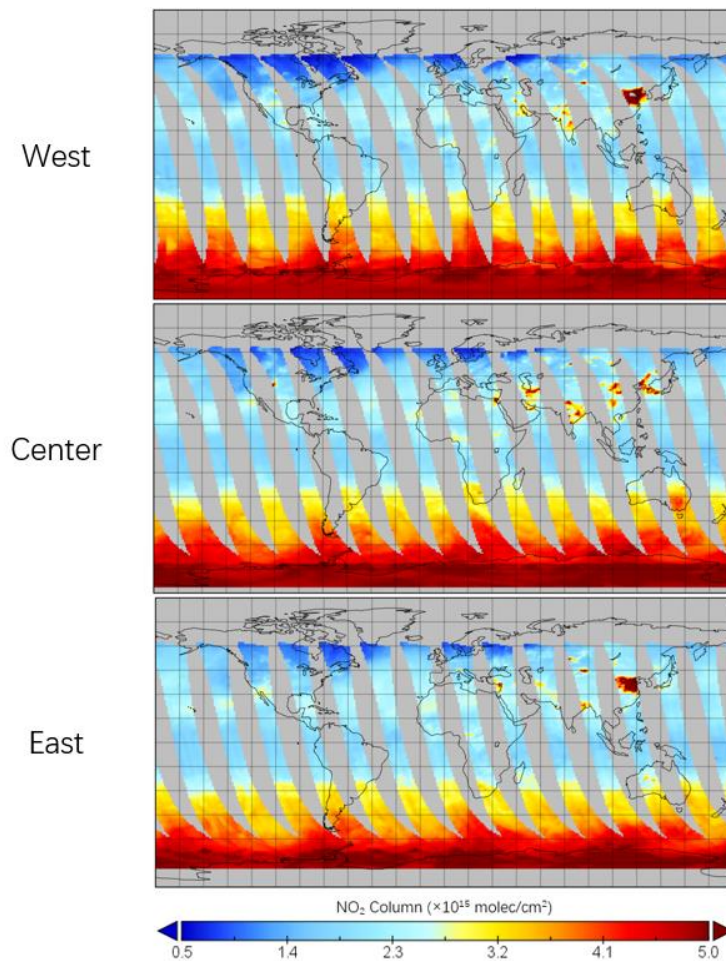
Figure R9. NO$_2$ columns (slant columns scaled by geometric AMFs) for the eastern, central, and western segments of the orbit swath.

The main consideration of the latitude weighting is to reduce interpolation errors for low latitudes with less orbital overlap, as shown in Fig. R9 and explained in line 267.

l273: Can the difference with the model (3.5e14) be considered a true uncertainty estimate? Or is it a lower limit, e.g. because of the finite model resolution?

3.5e14 can be regarded as a lower limit due to the use of 0.75 degree resolution for the synthetic data.

l 290: Does the GE-LER approach also provide an uncertainty estimate?

In the near future an independent Neural Network will be trained and implemented for error estimation. We have updated the conclusion accordingly.

l290: How sensitive is the GE-LER to L1B calibration errors? How has the GE-LER been validated, e.g has it been compared with MODIS-based BRDF results? Please

add some more info for the reader to judge the performance of the GE-LER approach.

Large L1B calibration errors will significantly affect the GE_LER retrieval. For UV fitting window, like O_3, SO_2, and HCHO, the GE_LER data has been validated with representative products, such as OMI and GOME-2 LER climatologies. A first comparison of NO_2 GE_LER data has shown a general good agreement with S5P/KNMI and GOME-2 LER climatology, particularly for oceans and the polluted continents, as shown in Fig. R10 for example. We are currently composing a paper about an extensive validation of the GE_LER products.
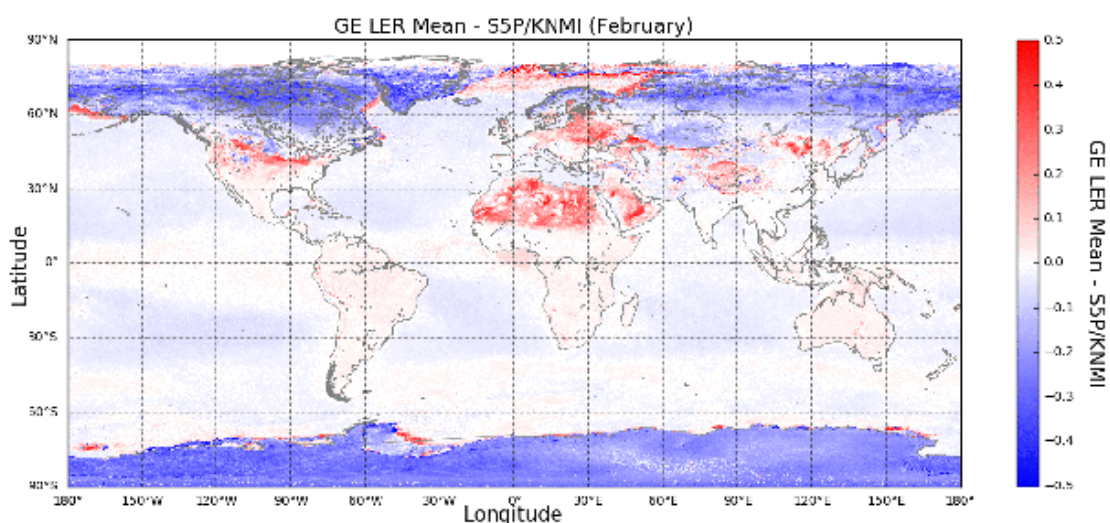

Figure R10. S5P/KNMI LER climatology at 460 nm and GE_LER retrieved from TROPOMI data (February 2018-2020) in the NO_2 window.

l315: "The surface LER values from GE_LER are lower than the climatological OMI values by 0.03 on average" Is this a statement for February or August? It seems that the average differences in August are smaller than in February (by looking at the figures).

We have corrected the statement in line 331 as "*The mean differences between the surface LER values from GE_LER and OMI climatological values are lower than 0.03.*"

Fig. 7: Please comment on the very low albedo values over the Mediterranean compared to the OMI LER.

The very low albedo values could be due to errors in the input parameters, such as SCD or the constant term of DOAS polynomial. As compared to the OMI LER based on years of data, the GE_LER used in this study considered a short time period of data, as explained in line 334. We have included the expression in line 335 as "which makes GE_LER more likely affected by aerosol contamination *or outliers in the input data*". Further analyses are required to explain the low values.

Sec 4.2: Please provide the definition of the POLYPHEMUS European domain (lat-lon domain boundaries).

We have included the domain in line 346 as "for Europe *(34.0N-60.4N, 12.0W-40.2E)* in this study".

l339: "European TNO-MACC". Please specify the version and reference year.

We have included the version and reference year in line 356 as "European TNO-MACC *(from 2011 with base year 2005)*".

l349: "The profile shape from POLYPHEMUS/DLR agree better with the MAX-DOAS measurements". The profiling capabilities of the MAXDOAS instruments are limited and often also quite uncertain. Part of this profile shape is a-priori defined. So, does it make sense to compare these profiles?

We have removed the comparison of profiles and updated the expression in line 367 as "*In comparison with the tropospheric AMF calculated using the MAX-DOAS NO_2 profile, the bias reduces from 0.32 (48.5%) for TM5-MP to -0.04 (-6.0%) for POLYPHEMUS/DLR.*"

Fig.10: It would be nice to also show a direct comparison of POLYPHEMUS tropospheric NO_2 column against TROPOMI (using the averaging kernels), e.g. also for February and August. Would it be possible to add these plots?

We have included the plot in pages 19-20. Please refer to major comment 2.

Sec. 4.2: Has POLYPHEMUS been compared to the CAMS regional modelling results? If so, please provide a brief summary of these comparisons. Please provide more detail on how the model has been validated in general, e.g. against observations of NO_2.

Please refer to the major comment 2 for the comparison between POLYPHEMUS/DLR and EUROS-LOTOS as well as the validation of POLYPHEMUS/DLR.

Sec. 4.2: Fig.9 indicates that POLYPHEMUS has basically very low concentrations of NO_2 in the free troposphere. Even though the free tropospheric column is small, this may have quite a significant impact on the AMF, and may in part be a reason why we see only red colors in Fig. 10. With larger free tropospheric NOx concentrations I would expect more blue colors especially in the more remote areas away from the main pollution hotspots. Please comment on this.

From Fig 9 left panel, POLYPHEMUS/DLR shows larger free tropospheric NO_2 concentration. Please refer to major comment 2 for further discussions.

Fig.11: "comparisons with version 1.x " Please be more explicit. Do you show cf(2.1)-cf(1.x) or cf(1.x)-cf(2.1)? What is x in "1.x" in this case?

We have updated the plot in page 21 with text *"(version 2.1 – version 1.x)"*. We have added the description *"(1.0 and 1.1)"* in line 402.

Fig.12: Why do you show a normalised CF instead of a mean CF?

We have changed the Fig. 13 in page 22 to show the mean CF instead of a normalized one.

Is Fig.12 consistent with Figs. 11 and 13 and the text? Fig.12 indicates smaller CF at the right side of the orbit in v2.1, while e.g. line 389 mentions an increase of the cloud fraction?

We have updated the plot. Please refer to the previous reply.

Fig.13: Again: do you show cf(2.1)-cf(1.x) or cf(1.x)-cf(2.1)?

We have updated the Fig.14 in page 22 with *"(version 2.1 – version 1.x)"*.

Fig.13: Is there any evidence that the new v2.1 cloud pressures are better than the old ones? Please discuss this in more detail.

The biggest change for ROCINN between v1.x and version 2.1 is the replacement of the coarse MERIS surface albedo climatology used in v1.x with an actual surface albedo retrieval with the matching TROPOMI scene information in real time (GE_LER retrieval). Hence, shortcomings of a climatology (e.g. spatial resolution, short term temporal variations like snow/ice coverage, cloud contamination) are largely reduced by the GE_LER retrieval which is based on TROPOMI data themselves and performed at the same time with the TROPOMI measurements, hence it is more representative of the actual scene conditions than a climatology can be. Although the ROCINN retrieval scheme for cloud height and optical thickness / cloud albedo itself did not change, an improvement for those parameters is achieved indirectly through the improved surface albedo, particularly over scenes with rapidly varying surface conditions like snow/ice.

Fig.14: How can I understand the reduction in NO_2 over the Po Valley? The cloud pressure does not seem to change much here.

The reduction in NO₂ over the Po Valley is mainly due to a new check in the version 2.1 processor: if the cloud fraction is smaller than 0.1 and the height difference between the retrieved cloud height and the surface height is lower than 100 m, the scene is assumed to be cloud-free. We have included the explanation in page 23 as "*The NO₂ reductions over the Po Valley are related to an additional check implemented in the version 2.1 processor: the pixel is assumed to be cloud-free for the almost clear-sky condition (cloud fraction < 0.1) with the retrieved cloud height very close to the surface height (difference < 100 m). This correction improves the data yield of the TROPOMI cloud products compared with other satellite cloud products; the performance of this correction under different surface conditions (dark, bright, snow, ice) or under presence of different types of low-level aerosols (fog, smoke, dust, ash) is under investigation.*"

l407: Could you also provide the average % difference in the AMF in winter and summer for CAL vs CBR?

We have included the relative difference as "by more than 1×10^{15} molec/cm^2 *(18%)* for polluted regions in winter" in line 441 and "less than 5×10^{14} molec/cm^2 *(10%)* for summer" in line 443.

Fig. 16: Please be explicit what is shown: CRB-CAL or CAL-CRB

We have included the information (CAL cloud -CRB cloud) in the figure in page 25.

l419: Please also provide the % increase in winter and summer.

We have included the relative difference in line 454 as "enhanced by 2×10^{15} molec/cm^2 *(37%)* in winter and 8×10^{14} molec/cm^2 *(15%)* in summer".

Figures 8, 10, 16 provide the contributions to Fig. 18. However, it would be good to also have the numbers for the contributions of the various terms (new STREAM, new profiles, GE-LER, CAL) to the increase. Could such numbers be provided for February and August?

We have included the individual changes of each step in Table 3. Please refer to major comment 5.

l427: I think it is good to refer to van Geffen 2020 here, who discuss this in detail. The 4.5e14 is similar/close to the 5.2e15 estimated for the operational retrieval.

Done.

l433: The table in the paper of De Smedt is mentioned. Are these numbers used without any modification? Are these consistent with estimates for e.g. the GE-LER

and OCRA/ROCINN CAL uncertainties? I suggest to include the relevant numbers in the text! Some more discussion on the uncertainties related to GE-LER, OCRA and ROCINN would be very relevant. For clear sky the AMF uncertainty is estimated as 20%.

we have updated the uncertainty estimation. Please refer to major comment 5.

l469: "which is mostly explained by the relatively low sensitivity of spaceborne measurements near the surface, the aerosol shielding effect, and the gradient smoothing effect." This is not so clear. The retrieval accounts for the lower sensitivity at the surface, and with the new GE-LER these uncertainties are hopefully reduced. The aerosol shielding effect was discussed as implicitly accounted for via the cloud retrieval. So it is not clear if a bias should remain due to these effects.

We have reformulated the expression in page 30 as "The NO_2 levels are underestimated by 34% by TROPOMI with a standard deviation of 16%, *which is likely explained by comparison errors (such as the gradient smoothing effect, the comparison choices, and the inherent difference in sensitivity), partly by* the remaining impact of structural uncertainties in the satellite data (Boersma et al., 2016, such as the impact of the choice of the a priori NO_2 profiles and/or the albedo database assumed for the satellite AMF calculations), and by the different measurement types or the specific conditions of the validation sites." Please see also the discussion to the last comment for the conclusion section.

Table 4: It would be great if also numbers for the operational product could be included.

We have included the operational validation. Please refer to major comment 3.

Figure 23: Nice to see that also the operational product is included!

Fig. 24: Nice to see this plot! The sensitivity profiles of MAXDOAS and satellite are very different, so it is good to demonstrate the impact on the comparison.

l500: "see Sec 5.2" ? Section 5.2 discusses the uncertainties and does not discuss the kernels.

We have removed the expression in line 542.

Conclusions section: It would be relevant to comment on the differences between the new DLR retrieval (and inputs) and other NO_2 retrieval approaches (operational, NASA, POMINO, ECCC, BEHR, Bremen) and discuss possible recommendations following from this comparison of retrieval methods.

We have included the comparison in page 35 as "*The TROPOMI NO$_2$ research product from DLR is a complement to the operational product due to the use of independent approaches for stratosphere-troposphere separation and AMF calculation. Comparing to the other regional TROPOMI NO$_2$ product, the DLR European retrieval reduces the potential biases introduced by using inputs from different instruments or climatologies and confirms the importance of applying more realistic input parameters with better resolution for AMF calculation.*"

Conclusions section: The bias in the updated retrieval against MAXDOAS is reduced from 55 to 34%, but is still substantial. Do the authors have an opinion what are the main retrieval aspects causing this difference? How can this gap between surface and satellite observations be closed? Something is said about this in section 6, but it would be interesting to discuss it again in the conclusions, and perhaps including recommendations for a way foreward.

Part of the remaining biases are likely related to the spatial heterogeneity effect (e.g. Pinardi 2020; Goldberg 2019), limiting the comparison of a satellite pixel (even if smaller for TROPOMI than what we were used to before) to ground-based data having a few-to-some Km length line-of-sight sensibility. Tang et al., 2021 calculated the sub-grid variability from airborne campaign measurements over Korea and Los Angeles basin, finding between 15 and 20% impact for TROPOMI pixel size. Illustration of this effect around Uccle site, based on TROPOMI data itself, is discussed in Sect. 6, Fig 22, with impact up to 19% in summer.

We have included more recommendations in page 36 as "*Further improvements in the ground-based validation include using the full MAXDOAS line-of-sight sensitivity and the intersect with the TROPOMI pixel(s) or having more ground-based instruments located within a TROPOMI pixel. More frequent ground-based measurements and measurements in more than one direction might better sample the temporal and spatial variability around the measurement sites (Richter and Lange, 2021; Dimitropopulou et al., 2020).*"

References

Boersma, K. F., Eskes, H. J., Dirksen, R. J., van der A, R. J., Veefkind, J. P., Stammes, P., Huijnen, V., Kleipool, Q. L., Sneep, M., Claas, J., Leitão, J., Richter, A., Zhou, Y., and Brunner, D.: An improved tropospheric NO$_2$ column retrieval algorithm for the Ozone Monitoring Instrument, Atmos. Meas. Tech., 4, 1905–1928, 2011.

Tang, W., Edwards, D. P., Emmons, L. K., Worden, H. M., Judd, L. M., Lamsal, L. N., Al-Saadi, J. A., Janz, S. J., Crawford, J. H., Deeter, M. N., Pfister, G., Buchholz, R. R., Gaubert, B., and Nowlan, C. R.: Assessing sub-grid variability within satellite pixels

over urban regions using airborne mapping spectrometer measurements, Atmos. Meas. Tech., 14, 4639–4655, 2021.

van Geffen, J., Boersma, K. F., Eskes, H., Sneep, M., Ter Linden, M., Zara, M., and Veefkind, J. P.: S5P TROPOMI NO_2 slant column retrieval: method, stability, uncertainties and comparisons with OMI, Atmos. Meas. Tech., 13, 1315–1335, 2020.

Vountas, M., Richter, A., Wittrock, F., and Burrows, J.: Inelastic scattering in ocean water and its impact on trace gas retrievals from satellite data, Atmos. Chem. Phys., 3, 1365–1375, 2003.

~~An improved tropospheric NO$_2$ column retrieval algorithm for TROPOMI over Europe~~An improved TROPOMI tropospheric NO$_2$ research product over Europe

Song Liu[1,*], Pieter Valks[1], Gaia Pinardi[2], Jian Xu[1,3], Ka Lok Chan[1], Athina Argyrouli[1,4], Ronny Lutz[1], Steffen Beirle[5], Ehsan Khorsandi[6], Frank Baier[6], Vincent Huijnen[7], Alkiviadis Bais[8], Sebastian Donner[5], Steffen Dörner[5], Myrto Gratsea[9], François Hendrick[2], Dimitris Karagkiozidis[8], Kezia Lange[10], Ankie J.M. Piters[7], Julia Remmers[5], Andreas Richter[10], Michel Van Roozendael[2], Thomas Wagner[5], Mark Wenig[11], and Diego G. Loyola[1]

[1]Deutsches Zentrum für Luft- und Raumfahrt (DLR), Institut für Methodik der Fernerkundung (IMF), Oberpfaffenhofen, Germany
[2]Royal Belgian Institute for Space Aeronomy (BIRA-IASB), Brussels, Belgium
[3]National Space Science Center, Chinese Academy of Sciences, Beijing, China
[4]Technical University of Munich (TUM), Department of Civil, Geo and Environmental Engineering, Chair of Remote Sensing Technology, Munich, Germany
[5]Max Planck Institute for Chemistry (MPI-C), Mainz, Germany
[6]Deutsches Zentrum für Luft- und Raumfahrt (DLR), German Remote Sensing Data Center (DFD), Oberpfaffenhofen, Germany
[7]Royal Netherlands Meteorological Institute (KNMI), De Bilt, the Netherlands
[8]Laboratory of Atmospheric Physics, Aristotle University of Thessaloniki (AUTH), Thessaloniki, Greece
[9]Institute for Environmental Research and Sustainable Development, National Observatory of Athens, Greece
[10]Institute of Environmental Physics (IUP-UB), University of Bremen, Bremen, Germany
[11]Meteorological Institute (MIM), Ludwig-Maximilians-Universität München (LMU), Munich, Germany
[*]now at: School of Environmental Science and Engineering, Southern University of Science and Technology, Shenzhen, China

Correspondence: Song Liu ~~(Song.Liu@dlr.de)~~(lius7@sustech.edu.cn)

Abstract.

Launched in October 2017, the TROPOspheric Monitoring Instrument (TROPOMI) aboard Sentinel-5 Precursor provides the potential to monitor air quality over point sources across the globe with a spatial resolution as high as 5.5 km×3.5 km (7 km×3.5 km before 6 August 2019). The DLR nitrogen dioxide (NO$_2$) retrieval algorithm for the TROPOMI instrument

5   consists of three steps: the spectral fitting of the slant column, the separation of stratospheric and tropospheric contributions, and the conversion of the slant column to a vertical column using an air mass factor (AMF) calculation. In this work, an improved DLR tropospheric NO$_2$ retrieval algorithm from TROPOMI measurements over Europe is presented.

The stratospheric estimation is implemented using the STRatospheric Estimation Algorithm from Mainz (STREAM), which was developed as a verification algorithm for TROPOMI and does not require chemistry transport model data as input. A direc-

10 tionally dependent STREAM (DSTREAM) is developed to correct for the dependency of the stratospheric NO$_2$ on the viewing geometry by up to 2×10^{14} molec/cm^2. Applied to synthetic TROPOMI data, the uncertainty in the stratospheric column is 3.5×10^{14} molec/cm^2 for ~~polluted conditions~~in case of significant tropospheric sources. Applied to actual measurements, the

smooth variation of stratospheric NO$_2$ at low latitudes is conserved, and stronger stratospheric variation at higher latitudes are captured.

15   For AMF calculation, the climatological surface albedo data is replaced by geometry-dependent effective Lambertian equivalent reflectivity (GE_LER) obtained directly from TROPOMI measurements with a high spatial resolution. Mesoscale-resolution a priori NO$_2$ profiles are obtained from the regional POLYPHEMUS/DLR chemistry transport model with the TNO-MACC emission inventory. Based on the latest TROPOMI operational cloud parameters, a more realistic cloud treatment is provided by a clouds-as-layers (CAL) model, which treats the clouds as uniform layers of water droplets, instead of

20   the clouds-as-reflecting-boundaries (CRB) model, in which clouds are simplified as Lambertian reflectors.

For the error analysis, the tropospheric AMF uncertainty, which is the largest source of NO$_2$ uncertainty for polluted scenarios, ranges between 20% and 50%, leading to a total uncertainty in the tropospheric NO$_2$ column in the 30-60% range. From a validation performed with ground-based multi-axis differential optical absorption spectroscopy (MAX-DOAS) measurements, the ~~improved~~new DLR tropospheric NO$_2$ data shows good correlations for nine European urban/suburban stations with an

25   average correlation coefficient of 0.78. The implementation of the algorithm improvements leads to a decrease of the relative difference from -55.3% to -34.7% on average in comparison with the DLR reference retrieval. When the satellite averaging kernels are used to remove the contribution of a priori profile shape, the relative difference decrease further to $\sim$-20%.

1   Introduction

Tropospheric nitrogen dioxide (NO$_2$) is an important atmospheric trace gas because of its contribution to the formation of

30   tropospheric ozone, urban haze, and acid deposition (Charlson and Ahlquist, 1969; Crutzen, 1970; McCormick, 2013). NO$_2$ is a prominent air pollutant affecting the human respiratory system (World Health Organization, 2006). Substantial amounts of NO$_2$ are produced in the boundary layer from combustion processes. In Europe, cities regularly exceed the air quality standards for NO$_2$ (European Commission, 2017), with road transport as the largest contributor, ahead of the energy and the industry sectors (Crippa et al., 2018).

35   To monitor and quantify the NO$_2$ column, NO$_2$ measurements have been provided for more than a decade on a global scale and daily basis by European satellite instruments, such as Global Ozone Monitoring Experiment (GOME) (Burrows et al., 1999), SCanning Imaging Absorption SpectroMeter for Atmospheric CHartographY (SCIAMACHY) (Bovensmann et al., 1999), Ozone Monitoring Instrument (OMI) (Levelt et al., 2006, 2018), and Global Ozone Monitoring Experiment-2 (GOME-2) (Callies et al., 2000; Munro et al., 2006, 2016), complementary to sparse measurements by ground-based instruments.

40   The satellite-based NO$_2$ dataset has been extended by the new generation TROPOspheric Monitoring Instrument (TROPOMI) (Veefkind et al., 2012) with an unprecedented spatial resolution of 5.5 km in the along-track direction (7 km before 6 August 2019) and 3.5 km in the across-track direction.

TROPOMI is a nadir-viewing push-broom imaging spectrometer aboard the European Space Agency (ESA) Sentinel-5 Precursor satellite, launched on 13 October 2017. The TROPOMI instrument measures the Earth's backscattered radiance

45   and extraterrestrial solar irradiance in the spectral range between the ultraviolet and the shortwave infrared. The spectral

resolution and sampling are 0.54 and 0.20 nm in the visible channel (400 - 496 nm) used for the detection of NO_2. From a sun-synchronous polar orbit, TROPOMI provides trace gas measurements as well as cloud and aerosol properties with an ascending node equatorial crossing at ~13:30 local time. The swath width is ~2600 km in the direction across the track of the satellite, allowing daily global coverage.

50   NO_2 measurements from TROPOMI have been widely used for ground level concentration estimates (e.g. Cooper et al., 2020; Li et al., 2020) and emission estimates (e.g. Lorente et al., 2019; Beirle et al., 2019; van der A et al., 2020; Huber et al., 2020). The high spatial resolution and good data quality allow a detailed analysis of local distribution and evolution of NO_2 (e.g. Stavrakou et al., 2020; Goldberg et al., 2021; Georgoulias et al., 2020), which are particularly important and helpful during the COVID-19 pandemic (e.g. Bauwens et al., 2020; Liu et al., 2020a; Goldberg et al., 2020; Huang and Sun, 2020;
55   Ding et al., 2020; Biswal et al., 2020; Koukouli et al., 2021).

Independent from the operational processing, the NO_2 retrieval algorithm for the TROPOMI instrument developed at DLR starts with the calculation of the slant column (the concentration integrated along the total light path through the atmosphere along the way from the sun to the satellite) from the TROPOMI reflectance spectra using the differential optical absorption spectroscopy (DOAS) method (Platt and Stutz, 2008). To determine the tropospheric NO_2 slant column, the stratospheric
60   contribution is estimated and removed from the total slant column, after which both total and tropospheric slant columns are converted to vertical columns by the application of air mass factors (AMF).

The retrieval of tropospheric NO_2 columns from total column data requires an accurate stratospheric estimation, a procedure referred to as stratosphere-troposphere separation (e.g. Leue et al., 2001; Bucsela et al., 2006). One typical stratosphere-troposphere-separation algorithm is the modified reference sector method, which uses measurements over regions with negli-
65   gible tropospheric NO_2 abundance to estimate the stratospheric NO_2 columns based on the assumption of longitudinally homogeneous stratospheric NO_2 fields. A more sophisticated approach used by the operational TROPOMI NO_2 retrieval relying on a chemistry transport model is data assimilation (Eskes et al., 2003; Dirksen et al., 2011), in which the three-dimensional distributions of NO_2 are regularly updated such that the modelled stratospheric NO_2 concentrations are in close agreement with satellite measurements for low-tropospheric contributions. Advantages of the data assimilation approach include a real-
70   istic error estimation and the capture of small-scale dynamical and chemical variability of stratospheric NO_2. Compared to data assimilation, the modified reference sector method is in general simple and requires no additional model input. Therefore, the STRatospheric Estimation Algorithm from Mainz (STREAM) method (Beirle et al., 2016), which belongs to the modified reference sector methods, has been developed as a verification algorithm for TROPOMI, as a complement to the operational stratospheric correction based on data assimilation.

75   The quality of satellite tropospheric NO_2 measurements is strongly related to the tropospheric AMFs, which are determined with a radiative transfer model and depend on ancillary information such as surface albedo, vertical shape of the a priori NO_2 profile, cloud, and aerosol. The importance of these parameters in NO_2 retrievals has been recognized for OMI (e.g. Heckel et al., 2011; Lin et al., 2014; Laughner et al., 2018; Qin et al., 2019), GOME-2 (e.g. Valks et al., 2011; Lorente et al., 2018; Liu et al., 2019b, 2020c), and TROPOMI (e.g. Griffin et al., 2019; Liu et al., 2020b; Zhao et al., 2020; Ialongo et al., 2020; Tack
80   et al., 2021).

The surface albedo has implications for satellite retrievals of aerosols, clouds, and trace gases including NO_2. Most of current satellite NO_2 retrievals (Boersma et al., 2011; Liu et al., 2019b, 2020c; van Geffen et al., 2020b) rely on monthly Lambertian-equivalent reflectivity (LER) climatologies derived from satellite measurements such as OMI (Kleipool et al., 2008) and GOME-2 (Tilstra et al., 2017, 2019). However, this simple assumption of isotropic surface reflection can introduce a bias by up to 35% in the NO_2 AMF calculation (Lorente et al., 2018). To account for the geometry-dependent surface scattering characteristics, previous works have applied measurements from the MODerate resolution Imaging Spectroradiometer (MODIS) dataset (e.g. Vasilkov et al., 2017; Qin et al., 2019). In this study we use a new algorithm developed at DLR to retrieve geometry-dependent effective LER (GE_LER) in the VIS based on the full-physics inverse learning machine (FP_ILM) technique (Loyola et al., 2020b). Compared to the typical climatological LER or the directionally dependent (DLER) data (Tilstra et al., 2021), the GE_LER data represents better the actual surface conditions such as snow/ice scenarios based on each single TROPOMI measurements with a high spatial resolution. GE_LER has been successfully applied in the retrievals of TROPOMI total ozone columns in the UV (Loyola et al., 2020b) and cloud parameters in the NIR (Loyola et al., 2020a) and is being used in the corresponding operational version 2.1 cloud products (see introduction below).

The varying sensitivity of the satellite to NO_2 at different altitudes is considered in the tropospheric AMF calculation using vertically resolved box-AMFs and a priori NO_2 profiles. Typically prescribed by a chemistry transport model, the importance of applying a priori NO_2 profiles with sufficiently detailed resolution has been addressed (e.g. Russell et al., 2011; McLinden et al., 2014; Kuhlmann et al., 2015; Boersma et al., 2016; Laughner et al., 2016), particularly for TROPOMI with a small pixel size (Griffin et al., 2019; Liu et al., 2020b; Ialongo et al., 2020; Tack et al., 2021). Routine simulations of tropospheric trace gases and aerosols have been provided by POLYPHEMUS/DLR since 2014 with a spatial resolution of $0.2° \times 0.3°$ (latitude, longitude) covering Europe and parts of North Africa. POLYPHEMUS/DLR is an air quality modelling platform operated at DLR based on the POLYPHEMUS chemistry transport model (Mallet et al., 2007) coupled to the Weather Research and Forecasting (WRF) model (Skamarock et al., 2008) with the TNO-MACC emission inventory (Denier van der Gon et al., 2010). It has been further developed within the PASODOBLE project for sensitivity studies of the mountainous Black Forest region (Bergemann et al., 2012) and to cover urban areas in southern Bavaria (Khorsandi et al., 2018). It uses the TNO-MACC emission inventory (Kuenen et al., 2014). Daily model forecasts are freely available via DLR Geospatial Web Services (http://wdc.dlr.de/cgi-bin/produkt_4d_w?).

The NO_2 retrieval is affected by the presence of clouds, because high clouds shield underlying parts of the atmosphere, and low clouds can enhance the NO_2 absorption due to cloud albedo and multiple scattering if they are below or at the same height as the NO_2 layer (Martin et al., 2002; Kokhanovsky and Rozanov, 2008). The operational cloud retrieval for TROPOMI is implemented using Optical Cloud Recognition Algorithm (OCRA) and Retrieval Of Cloud Information using Neural Networks (ROCINN). In addition to the retrieval product based on the assumption that clouds are simple Lambertian reflecting surfaces, referred to as Clouds-as-Reflecting-Boundaries (CRB) model, a more sophisticated set of cloud products is provided by OCRA/ROCINN, which considers clouds as optically uniform layers of scattering liquid water spherical particles, referred to as Clouds-as-Layers (CAL) model. The more realistic CAL model is regarded as the preferred method, particularly for small TROPOMI ground pixels and for low clouds (Compernolle et al., 2021). With an updated OCRA/ROCINN processor

~~version 2.1~~ version 2.1 processor for OCRA/ROCINN in operation since August 2020, new features such as the application of GE_LER to describe the surface albedo have been added in OCRA/ROCINN (Loyola et al., 2020a).

The satellite NO_2 data has been widely validated by comparison with correlative ground-based multi-axis differential optical absorption spectroscopy (MAX-DOAS) measurements (e.g. Celarier et al., 2008; Irie et al., 2008; Ma et al., 2013; Pinardi et al., 2014, 2015; Drosoglou et al., 2017, 2018; Chan et al., 2020; Pinardi et al., 2020). MAX-DOAS measures the vertically resolved abundances of atmospheric trace species in the lowermost troposphere (Hönninger et al., 2004; Wagner et al., 2004; Wittrock et al., 2004; Heckel et al., 2005). Based on the scattered sky light under different viewing directions, high NO_2 sensitivity close to the surface is obtained for the smallest elevation angles, whereas measurements at higher elevations provide information on the rest of the column.

In this paper, a number of improvements to the tropospheric NO_2 retrieval over Europe are introduced for the DLR product. To estimate and remove the stratospheric contribution, an improved STREAM algorithm is developed and evaluated by applying it to synthetic TROPOMI data and actual satellite observations. To calculate the tropospheric AMFs, the surface albedo is described by the GE_LER data consistently in both NO_2 and cloud retrievals; a priori NO_2 profiles are obtained from the regional POLYPHEMUS/DLR chemistry transport model; the OCRA/ROCINN_CAL cloud model from the new version 2.1 ~~OCRA/ROCINN~~ processor is used for cloud correction.

In Sect. 2, we introduce the reference algorithm at DLR for the TROPOMI NO_2 retrieval, which is based on an improved algorithm originally designed for GOME-2 (Liu et al., 2019b) and adapted for TROPOMI measurements with optimization related to the specific instrumental aspects. In Sects. 3 and 4, we improve the stratosphere-troposphere separation and the tropospheric AMF calculation, respectively. In Sect. 5, examples of applying the retrieval algorithm to TROPOMI measurements are shown, and the error estimate is discussed. In Sect. 6, we show a comprehensive validation of the TROPOMI NO_2 data using ground-based MAX-DOAS observations in Europe.

2 DLR reference retrieval for TROPOMI NO_2 measurement

2.1 DOAS slant column retrieval

Applied to the backscattered spectra measured by TROPOMI, the DOAS fit (Platt and Stutz, 2008) is a least-squares inversion to isolate the trace gas absorption from the background processes, which are approximated by a fifth-order polynomial $P(\lambda)$ at wavelength λ:

$$\ln\left[\frac{I(\lambda)+offset(\lambda)}{I^0(\lambda)}\right] = -\sum_g S_g \sigma_g(\lambda) - \alpha_R R(\lambda) - P(\lambda). \tag{1}$$

The measurement-based term is defined as the natural logarithm of the measured earthshine radiance spectrum $I(\lambda)$ divided by the daily solar irradiance spectrum $I^0(\lambda)$. The DOAS fit is performed in the 405-465 nm wavelength range for consistency with other NO_2 retrievals from TROPOMI (van Geffen et al., 2020a) and the heritage instrument OMI (van Geffen et al., 2015; Zara et al., 2018).
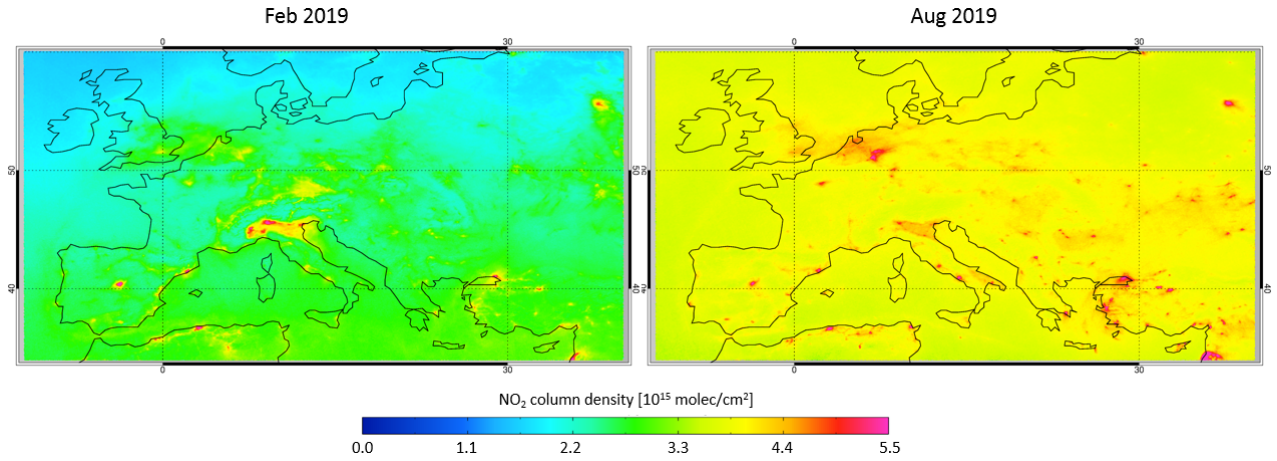
Figure 1. TROPOMI NO$_2$ slant columns (scaled by geometric AMFs) over Europe in February and August 2019.

The spectral effect from the absorption of a species g is determined by the fitted slant column density S_g and associated absorption cross-section $\sigma_g(\lambda)$:

- NO$_2$ absorption at 220K from Vandaele et al. (2002);

- ozone (O$_3$) absorption at 228K from Brion et al. (1998);

- water vapor (H$_2$O$_{vap}$) absorption at 293K from Rothman et al. (2010), rescaled as in Lampel et al. (2015);

- oxygen dimer (O$_4$) absorption at 293K from Thalman and Volkamer (2013);

- liquid water (H$_2$O$_{liq}$) absorption at 297K from Pope and Fry (1997), smoothed as in Peters et al. (2014).

The contribution of the rotational Raman scattering to the measured spectrum, namely the Ring effect (Grainger and Ring, 1962; Solomon et al., 1987), is treated as a pseudo absorber, by means of an additive Ring reference spectrum $R(\lambda)$ and a scaling coefficient α_R as fitting parameter. A linear intensity offset correction $offset(\lambda)$ is fitted as an additional effective cross-section to correct for the stray light in the spectrometer, the inelastic scattering in the ocean, and remaining calibration issues in the level 1 data (Liu et al., 2019b). See additional discussions regarding intensity offset in van Geffen et al. (2020a). The TROPOMI level 1b version 1 spectra are analysed using the QDOAS software developed at BIRA-IASB (Fayt et al., 2011; Danckaert et al., 2017). Figure 1 shows examples of the TROPOMI NO$_2$ slant columns over Europe in February and August 2019, where large NO$_2$ hotspots can be identified. Note that the slant columns are scaled by geometric AMFs to correct for the angular dependencies of TROPOMI measurements.

The NO$_2$ slant columns from single orbits show an across-track striping pattern, a well-known feature of observations of push-broom spectrometers such as OMI (Boersma et al., 2011) and TROPOMI (van Geffen et al., 2020a), which is likely caused by the viewing zenith angle (VZA) dependency of the spectral calibration and detector sensitivity (Boersma et al., 2018). To

reduce the systematic stripes, a de-striping correction is applied to the TROPOMI NO$_2$ slant columns, which ~~amplitude~~ is calculated empirically (Boersma et al., 2011) based on the daily averaged across-track variability of NO$_2$ slant columns over clean regions between 20°S and 20°N. The magnitude of the NO$_2$ de-striping correction is up to 1×10^{14} molec/cm^2 and is stable over time (not shown), in agreement with the operational TROPOMI de-striping that relies on the chemistry transport model data (van Geffen et al., 2020a).

2.2 Stratosphere-troposphere separation

The stratospheric NO$_2$ component is estimated using the STREAM method (Beirle et al., 2016). Belonging to the modified reference sector methods, STREAM uses total NO$_2$ column measurements over clean and remote regions as well as over clouded scenes with negligible tropospheric columns. STREAM calculates weighting factors for each satellite pixel to define the contribution of total columns to the stratospheric estimation: potentially polluted pixels are weighted low, cloudy observations with medium cloud heights are weighted high, and the weights are further adjusted in case of large biases in the tropospheric residues. Depending on these weighting factors, stratospheric NO$_2$ fields are derived by a weighted convolution of the total columns using convolution kernels, which are wider at lower latitudes to account for the low longitudinal variability assumption of stratospheric NO$_2$ and narrower at higher latitudes to reflect the stronger natural variations.

STREAM was developed as a verification algorithm for the TROPOMI instrument, as a complement to the operational stratospheric correction based on data assimilation (van Geffen et al., 2020b). STREAM has been successfully applied to the NO$_2$ measurements from GOME, SCIAMACHY, OMI, and GOME-2 (Beirle et al., 2016; Liu et al., 2019b) with the advantage of requiring no model input. In contrast to previous modified reference sector methods which normally apply a conservative masking approach (flagging pixels as either clean or polluted and skipping the latter for stratospheric estimation) and hardly use information over continents, STREAM introduces an improved treatment of polluted and cloudy pixels by defining weighting factors for each satellite pixel. Due to the use of cloudy pixels, which directly reflect the actual stratospheric column as the tropospheric column is mostly shielded, STREAM reduces the bias caused by the free-tropospheric contamination or tropospheric background in the reference region, in comparison with other modified reference sector methods (Beirle et al., 2016). However, the broad-scale free tropospheric diffuse NO$_2$ might not be fully separated from the stratospheric NO$_2$, which is a general limitation of the modified reference sector methods.

Stratospheric NO$_2$ columns from STREAM differ by up to 3×10^{14} molec/cm^2 as compared to results from data assimilation and other modified reference sector methods, within the general uncertainties of stratosphere-troposphere separation (Beirle et al., 2016; Boersma et al., 2018). The STREAM stratospheric NO$_2$ columns show an average bias of $1 \pm 8 \times 10^{13}$ molec/cm^2 with respect to the ground-based zenith-scattered light differential optical absorption spectroscopy (ZSL-DOAS) measurements (Compernolle et al., 2020).
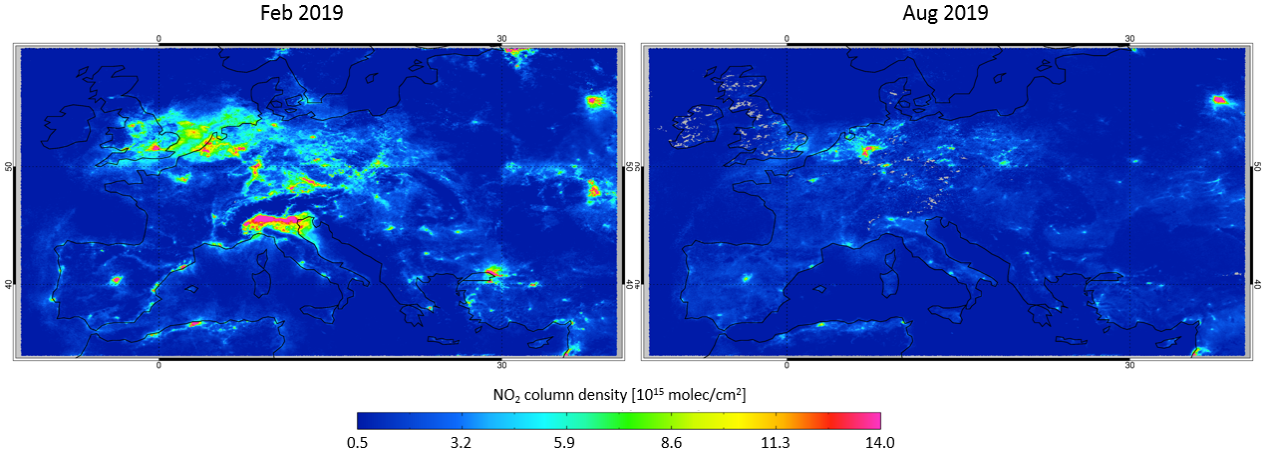
Figure 2. Tropospheric NO$_2$ columns from the reference algorithm over Europe in February and August 2019. Only measurements with cloud radiance fraction less than 0.5 are included.

2.3 AMF calculation

The conversion between the slant column S and the vertical column V is implemented by division with an AMF M:

$$V = \frac{S}{M}. \tag{2}$$

Given the small optical depth of NO$_2$, M can be derived as:

$$M = \frac{\sum_l m_l(\boldsymbol{b}) x_l c_l}{\sum_l x_l}, \tag{3}$$

where m_l is the box-AMFs in layer l, x_l is the partial column from the a priori NO$_2$ profile, and c_l is a correction coefficient to correct for the temperature dependency of the NO$_2$ cross section (Boersma et al., 2004; Nüß et al., 2006; Bucsela et al., 2013). m_l is a function of model inputs $\boldsymbol{b}$, which include TROPOMI measurement geometries, surface albedo, and surface pressure. The box-AMFs m_l values are calculated at 437.5 nm (near the mid-point wavelength of fitting window 405-465 nm), as recommended by Boersma et al. (2018), using the linearised vector code VLIDORT version 2.7 (Spurr, 2006). The light path in the troposphere is affected by scattering on air molecules as well as cloud and aerosol particles, and therefore the tropospheric AMF calculation depends on surface albedo, a priori NO$_2$ profiles, and cloud properties. Table 1 summarises the parameters used in the AMF calculation in several research products and the operational product. Figure 2 shows the tropospheric NO$_2$ columns retrieved from the reference algorithm over Europe in February and August 2019. A large amount of NO$_2$ is located in the troposphere for industrialised and urbanised areas (see Fig. 1).

In the reference algorithm, the surface albedo is described by a monthly climatology based on four years (2004-2007) of OMI LER measurements at 440 nm (Kleipool et al., 2008) with a similar overpass time and viewing conditions as TROPOMI. The surface albedo for each TROPOMI pixel is calculated by an area-weighted tessellation of the OMI monthly averaged surface albedo maps (0.5°×0.5°) and a linear interpolation in time to the measurement day.

Table 1. ~~Parameters used to calculate tropospheric AMFs.~~Overview of tropospheric NO$_2$ column retrievals. See Table 2 for details of the chemistry transport models used to obtain the a priori NO$_2$ profiles for the DLR improved retrieval in this work.

	DLR reference retrieval	DLR improved algorithm	KNMI operational product	POMINO-TROPOMI product	ECCC product
reference	This work	This work	(van Geffen et al., 2020a, b)	(Lin et al., 2014; Liu et al., 2019a)	(Griffin et al., 2019)
Region	Global	Europe	Global	China	Canada
Stratospheric correction	STREAM	DSTREAM	Data assimilation	Same as KNMI	Same as KNMI
Surface albedo	OMI LER climatology	TROPOMI GE_LER data	OMI LER climatology	MODIS BRDF	MODIS albedo climatology
A priori NO$_2$ profile	TM5-MP	POLYPHEMUS/DLR	TM5-MP	GEOS-Chem	GEM-MACH
Cloud parameter	OCRA/ROCINN_CRB version 1.x	OCRA/ROCINN_CAL version 2.1	FESCO-S	Recalculated cloud fraction with aerosol correction	Same as KNMI
Aerosol treatment	Implicit correction	Implicit correction	Implicit correction	Explicit correction	Explicit correction

215   Daily TM5-MP vertical NO$_2$ profiles (Williams et al., 2017) simulated at a global 1°×1° resolution are used as a priori NO$_2$ vertical profiles due to the operational advantage, as summarized in Table 2. The a priori profiles are determined for the satellite overpass time and interpolated to the center of the TROPOMI pixel based on four nearest neighbour TM5-MP cell centers.

In the presence of clouds, the AMF calculation adopts the independent pixel approximation (Cahalan et al., 1994):

$$M = \omega M^{cl} + (1 - \omega)M^{cr}, \tag{4}$$

220   where M^{cl} represents the AMF for completely cloudy sky and M^{cr} for completely clear sky. M^{cl} and M^{cr} are derived with Eq. (3) with M^{cl} mainly relying on the cloud pressure (height) and the cloud albedo (optical depth). The cloud radiance fraction ω is derived from the TROPOMI cloud fraction c_f:

$$\omega = \frac{c_f I^{cl}}{(1 - c_f)I^{cr} + c_f I^{cl}} \tag{5}$$

with I^{cl} and I^{cr} representing the radiances for cloudy and clear scenes, respectively. I^{cl} and I^{cr} are calculated using the
225   LIDORT version 3.6 model (Spurr et al., 2001), depending mostly on TROPOMI viewing geometries, surface albedo, and cloud albedo.

The operational TROPOMI cloud parameters from the OCRA/ROCINN algorithms (Lutz et al., 2016; Loyola et al., 2018) with clouds treated as opaque Lambertian surfaces (CRB model) are applied for the cloud correction. OCRA derives the cloud fraction by separating a spectral scene into cloudy contribution and cloud-free background. With the OCRA cloud fraction and

Table 2. Summary of the chemistry transport model specifications.

	TM5-MP (Huijnen et al., 2010; Williams et al., 2017)	POLYPHEMUS/DLR (Mallet et al., 2007; Bergemann et al., 2012; Khorsandi et al., 2018)
Spatial resolution	$1°×1°$ (latitude, longitude $0.2°×0.3°$ (latitude, longitude)	
Vertical resolution (>150 hPa)	~18 layers	20 layers
Meteorological fields	ECMWF 3 h	WRF 1 h
Tropospheric chemistry	Modified CB05 (Williams et al., 2013)	RACM for trace gases (Stockwell et al., 1997) SORGAM-SIREAM for aerosols (Debry et al., 2007; Schell et al., 2001)
Anthropogenic emission	MACCity (Granier et al., 2011)	TNO-MACC (Denier van der Gon et al., 2010; Kuenen et al., 2014)
Advection	Slopes scheme (Russell and Lerner, 1981)	third-order direct space-time scheme with a Koren-Sweby flux limiter
Convection	ECMWF	WRF (Skamarock et al., 2008)
Diffusion	Holtslag and Boville (1993)	second-order Rosenbrock method (Verwer et al., 2002)

230   the surface albedo from the MERIS black-sky climatology (Popp et al., 2011) as inputs, ROCINN calculates the cloud pressure and cloud albedo by comparing the measured and simulated sun-normalised radiances in and around the O_2 A-band in the NIR.

The original OCRA takes the spectral information from the UV-VIS-NIR part (320 – 800 nm) and transforms the radiances of three predefined spectral ranges to three-color reflectances (RGB: red, green, and blue region of the spectrum). The cloud-free background maps are calculated for each of these three colors. For the TROPOMI application, the OCRA color space

235   approach is applied with two colors (GB) using the UV-VIS (350 – 495 nm) spectra to avoid the spatial misalignment between the UV-VIS and NIR footprints.

Based on the Lambertian cloud assumption, OCRA/ROCINN_CRB tends to retrieve a cloud height (at the optical centroid of the cloud rather than the cloud top) close to the surface altitude for low cloud fraction (Compernolle et al., 2021). The Lambertian cloud assumption is also applied in the Fast Retrieval Scheme for Clouds from the O_2 A-band (FRESCO) algorithm

240   (Koelemeijer et al., 2001; Wang et al., 2008). FRESCO for Sentinel (FRESCO-S) (Wang and Sneep, 2019) is implemented as a support product for the TROPOMI operational NO_2 processing (van Geffen et al., 2020b). FRESCO-S retrieves the cloud fraction and cloud pressure from the reflectance in and around the O_2 A-band. The cloud albedo is assumed to be 0.8, as opposed to OCRA/ROCINN, where cloud albedo is retrieved.
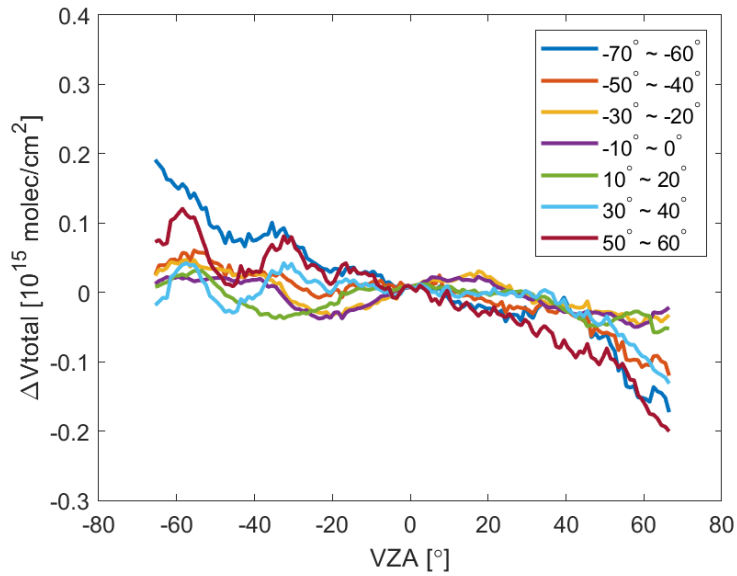
Figure 3. VZA dependency of TROPOMI total NO$_2$ columns (compared to nadir) at different latitudes in January 2019. The VZA is defined negative for observations on the west side of the orbit swath. The de-striping is ~~not~~ implemented here.

3 New Stratosphere-troposphere separation

245 STREAM was originally designed for TROPOMI and optimized for OMI within TROPOMI verification activities (Beirle et al., 2016). STREAM consists basically of two steps: the definition of weighting factors for each satellite pixel and the application of weighted convolution. To identify potentially polluted areas, a climatology of tropospheric NO$_2$ columns is derived in this study using TROPOMI NO$_2$ measurements from 2018-2019, instead of using SCIAMACHY NO$_2$ measurements from 2003-2011 as in the original STREAM. Based on the pollution weight, as well as the cloud weight and tropospheric residue weight,

250 STREAM estimates stratospheric fields for individual orbits using a weighted convolution on $0.5° \times 0.5°$ grid pixels.

As a result of wide swath ($\sim$2600 km), local time differences across a TROPOMI swath are considerable at high latitudes, and the NO$_2$ measurements show dependency on VZA (directly related to local time) due to the diurnal variation of stratospheric NO$_2$ (Dirksen et al., 2011; Belmonte Rivas et al., 2014). Figure 3 shows the total NO$_2$ columns measured by TROPOMI in January 2019 for different latitudes as a function of VZA. The impact of local time changes across the orbit is up to 2×10^{14}

255 molec/cm^2 at the swath edge for latitudes higher than $50°$, in agreement with estimations for OMI measurements (Beirle et al., 2016).

In the following, the concept of a directionally dependent STREAM (DSTREAM) is introduced to estimate the stratospheric NO$_2$ column (Sect. 3.1). The performance of STREAM and DSTREAM is analyzed using synthetic TROPOMI NO$_2$ data (Sect. 3.2), and both algorithms are applied to TROPOMI measurements (Sect. 3.3).

3.1 DSTREAM

To correct for the VZA dependency of stratospheric NO_2, the DSTREAM is developed, which divides the orbit swath into western (VZA from $\sim$-66° to $\sim$-30°), central (VZA from $\sim$-30° to $\sim$30°), and eastern (VZA from $\sim$30° to $\sim$66°) segments. Note that the VZA is defined negative for observations on the west side of the orbit swath throughout the study. For each of the orbit swath containers, the original STREAM is applied based on data from the respective orbit swath segment.

For each individual satellite pixel with a VZA, a directionally dependent stratospheric NO_2 column V_s^{dir} is parameterized using a linear interpolation on the DSTREAM grid results estimated using the eastern, central, and western segments of the orbit swath. As the VZA dependency is negligible for low latitudes (from Fig. 3), and the interpolation error may increase for V_s^{dir} due to less orbital overlap, the final stratospheric NO_2 column V_s is calculated as the weighted mean in dependence on latitude θ:

$$V_s = cos^2(\theta)V_s^{ori} + sin^2(\theta)V_s^{dir}. \tag{6}$$

By this method, the stratospheric NO_2 from the original STREAM V_s^{ori} is applied for equator, and the VZA dependency is captured for polar regions with significant orbital overlap.

3.2 Application to synthetic data

The performance of the original STREAM and the improved DSTREAM for TROPOMI is evaluated with simulated NO_2 fields from the IFS(CB05BASCOE) experiment (Huijnen et al., 2016). Particularly advantageous for stratospheric studies, ~~The IFS(CB05BASCOE) model is particularly advantageous for stratospheric studies due to the extension of~~ the tropospheric chemistry module in the Integrated Forecast System (IFS) is extended with the stratospheric chemistry from the Belgian Assimilation System for Chemical ObsErvations (BASCOE) system. The STREAM and DSTREAM are applied to the synthetic TROPOMI total NO_2 columns, and the estimated stratospheric NO_2 columns are compared with the a priori truth (stratospheric fields from model). See Liu et al. (2019b) for more details on constructing synthetic total and stratospheric NO_2 columns ~~using IFS(CB05BASCOE) data~~.

Figure 4 displays the synthetic total NO_2 columns from IFS(CB05BASCOE), the modelled stratospheric columns, and the estimated stratospheric columns from STREAM and DSTREAM on 1 January and 1 August 2019. The overall latitudinal and seasonal dependencies are reflected in the stratospheric fields from STREAM and DSTREAM. Smaller structures in the synthetic total columns and the modelled stratospheric columns at high latitudes, caused by the diurnal variation of stratospheric NO_2 across the orbital swath, are aliased into the troposphere by STREAM but captured by DSTREAM. The average difference between the estimated and a priori results is 4×10^{14} molec/cm^2 for STREAM and 3.5×10^{14} molec/cm^2 for DSTREAM with improvements mainly for latitudes higher than 50°.

01 Feb 2019　　　　　　　　01 Aug 2019

Vtotal Model

Vstrat Model

Vstrat STREAM

Vstrat DSTREAM

NO$_2$ column density [10^{15} molec/cm^2]
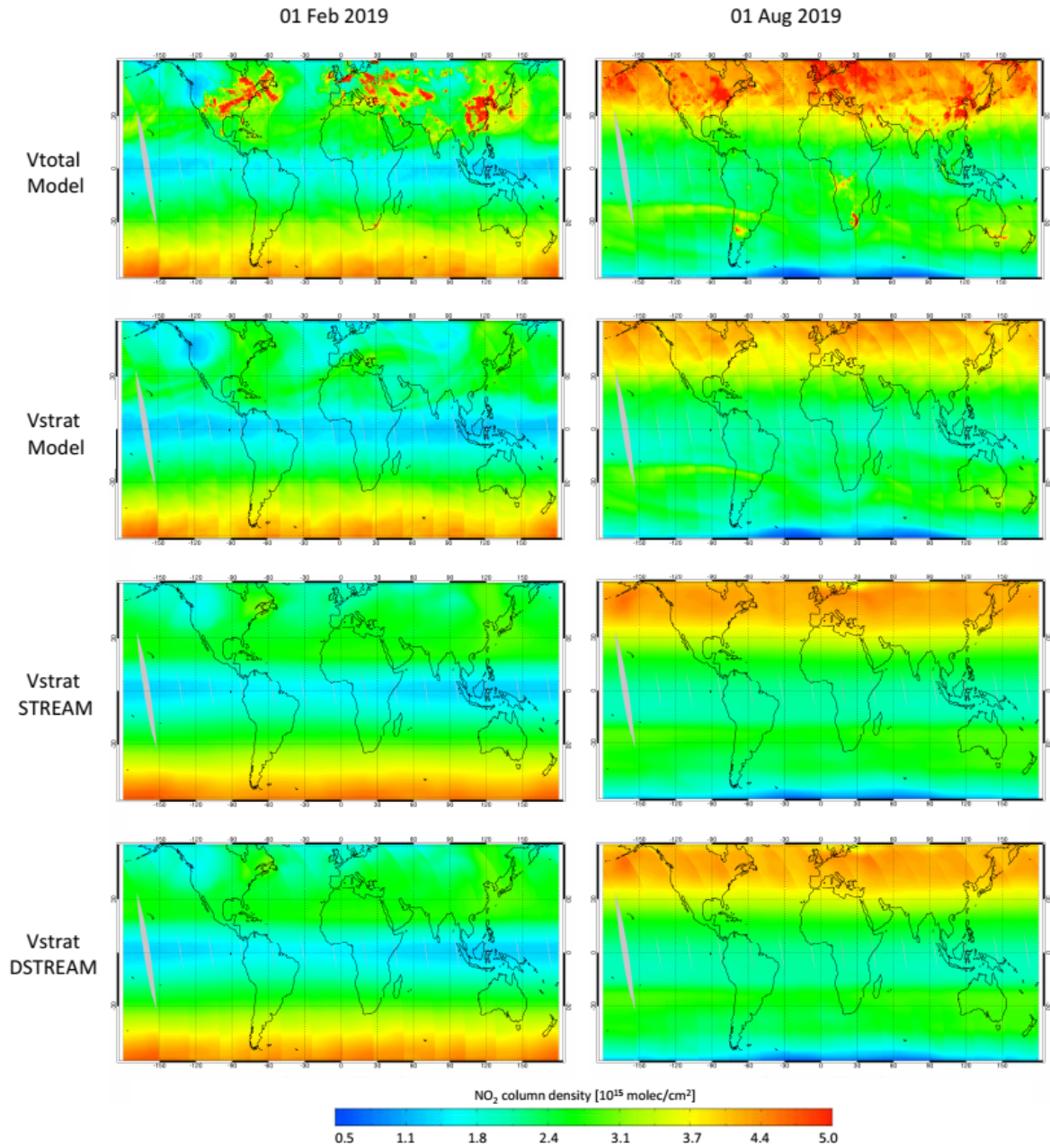
0.5　1.1　1.8　2.4　3.1　3.7　4.4　5.0

Figure 4. Synthetic total NO$_2$ columns, a priori stratospheric NO$_2$ columns from IFS(CB05BASCOE), and estimated stratospheric NO$_2$ columns from STREAM and DSTREAM on 1 February and 1 August 2019.
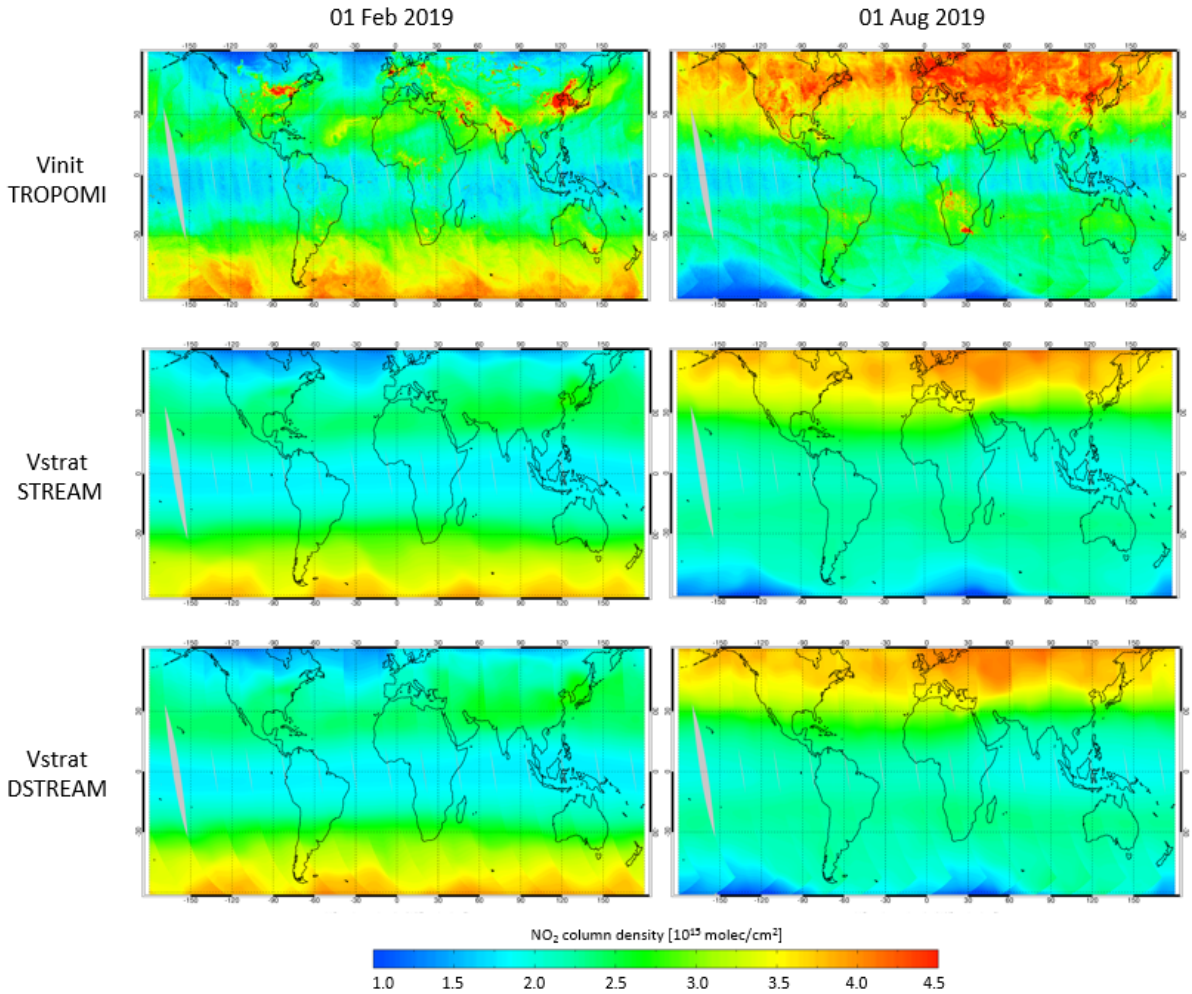
Figure 5. Total NO$_2$ columns and stratospheric NO$_2$ columns estimated using STREAM and DSTREAM, as measured by TROPOMI on 1 February and 1 August 2019.

3.3 Application to TROPOMI measurements

290   Applying STREAM and DSTREAM to TROPOMI data, Fig. 5 shows the total columns from TROPOMI and the estimated stratospheric fields on 1 February and 1 August 2019. For both months, the STREAM and DSTREAM show similar global patterns of stratospheric NO$_2$. The stratospheric and tropospheric contributions over polluted regions are successfully separated due to the use of clean and cloudy measurements at the same latitude where the tropospheric column is shielded. The smooth background at low latitudes is conserved, and the stronger variations of stratospheric NO$_2$ at higher latitudes are captured, e.g.

295   in the polar vortex on 1 February.

14
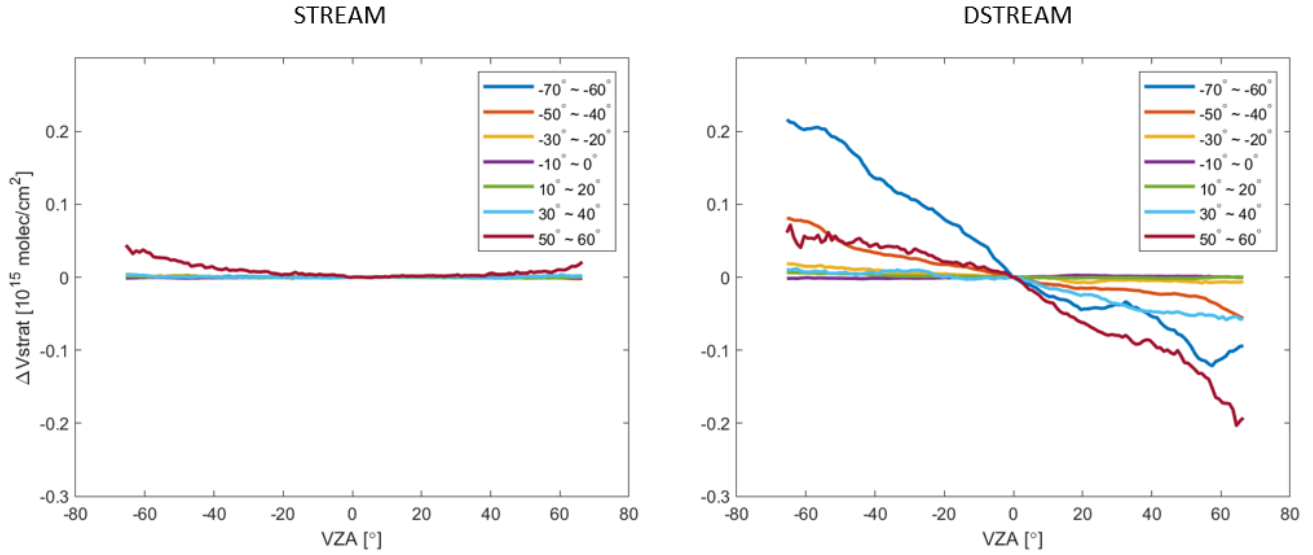
Figure 6. VZA dependency of TROPOMI stratospheric NO₂ columns estimated using STREAM and DSTREAM (compared to nadir) at different latitudes in January 2019. The VZA is defined negative for observations on the west side of the orbit swath.

Figure 6 shows the TROPOMI stratospheric columns estimated using STREAM and DSTREAM for different latitudes as a function of VZA in January 2019. The VZA dependency by up to 2×10^{14} molec/cm² caused by the local time difference in Fig. 3 is captured by DSTREAM, particularly for high latitudes. The overestimation on the west side of swath edge and the underestimation on the east side in the STREAM results are ~~improved~~corrected in DSTREAM.

4   Improved AMF calculation

4.1   Surface albedo

Surface albedo is an important parameter for an accurate retrieval of trace gas columns and cloud properties. The sensitivity of backscattered radiance to the boundary layer NO₂ is strongly related to the surface albedo, especially over polluted areas. In this study, the surface albedo is described using GE_LER retrieved by the FP_ILM algorithm (Loyola et al., 2020b). Unlike conventional approaches (Rodgers, 2000; Doicu et al., 2010), FP_ILM is a machine learning based approach consisting of a training phase wherein an inverse function is derived from synthetic data generated with a radiative transfer model and an operational phase wherein the inverse function is applied to measured spectra. The FP_ILM algorithm has been employed to retrieve ozone profile shapes and sulfur dioxide layer heights from GOME-2 and TROPOMI (Xu et al., 2017; Efremenko et al., 2017; Hedelt et al., 2019).

Combining the DOAS equation Eq. (1) and the conventional forward model, our forward problem can be formulated as an approximation of the DOAS-fitted slant column density (SCD) and the DOAS polynomial (P) using the forward model (F)

with the solar/satellite viewing geometry (Θ), effective ~~surface~~scene pressure (p_e), and surface albedo (A_s):

$$\{SCD, P\} = F(\Theta, p_e, A_s). \tag{7}$$

During the training phase, synthetic TROPOMI spectra in the 405 - 465 nm range are simulated by LIDORT version 3.6 (Spurr et al., 2001) in conjunction with the smart sampling technique (Loyola et al., 2016). The cloud impact is considered in the simulations with the use of the effective ~~surface~~scene pressure p_e, ~~which depends on OCRA cloud fraction, ROCINN_CRB cloud pressure, and surface pressure (Loyola et al., 2020b)~~which is provided in the new version 2.1 processor for OCRA/ROCINN (see Sect. 4.3.1). The aerosol influence is not considered. The DOAS fitting is applied to the simulated spectra using the consistent DOAS settings as introduced in Sect. 2.1. The simulation results from Eq. (7) are grouped as inputs to a multi-layer neural network, and the neural network is trained to learn the inverse function. In the operational phase, GE_LER is generated using the trained neural network and the DOAS results from the measured spectra. An additional polynomial fitting is subsequently included to account for the bidirectional reflectance distribution function (BRDF) effect.

For consistency with the NO$_2$ retrieval, the GE_LER retrieval is performed for every single ground pixel using the same TROPOMI spectrum and DOAS configurations. Global maps are generated from the GE_LER retrievals under clear-sky conditions (OCRA cloud fraction small than 0.05) and updated on a daily basis on a time window between one and four weeks depending on cloudiness. In contrast to the OMI LER climatology, the GE_LER data relies on the measurements from the TROPOMI instrument itself with ~~an improved~~a higher spatial resolution (0.1°×0.1°) and better characterizes the actual surface conditions, particularly for snow/ice scenarios.

Figure 7 compares the climatological OMI LER data and GE_LER data for February and August 2019. ~~The surface LER values from GE_LER are lower than the climatological OMI values by 0.03 on average.~~The mean differences between the surface LER values from GE_LER and OMI climatological values are lower than 0.03. The improved spatial resolution for GE_LER enables a better representation of surface features. Larger differences by more than 0.2 are found in winter over snow/ice regions such as Russia and the Alps, because GE_LER captures the actual snow/ice conditions. The GE_LER values are higher by up to 0.05 over the North Sea, due to the use of only one month of TROPOMI data compared to the multiple years for OMI climatology, which makes GE_LER more likely affected by aerosol contamination or outliers in the input data. In the near future, an improved aerosol screening based on TROPOMI aerosol index data will be implemented in the GE_LER algorithm. An independent Neural Network will be trained and implemented for error estimation.

Figure 8 shows the monthly average differences in the tropospheric NO$_2$ columns retrieved using the climatological OMI LER and the TROPOMI GE_LER in February and August 2019. An effect is noticed mainly in winter under polluted conditions. Consistent with the LER changes in Fig. 7, the general reduced surface LER from GE_LER results in a decrease in the tropospheric AMF and thus an increase in the calculated tropospheric NO$_2$ column by up to 3×10^{15} molec/cm^2. A reduction by up to 1×10^{15} molec/cm^2 is found for snow/ice coverages and aerosol scenes.
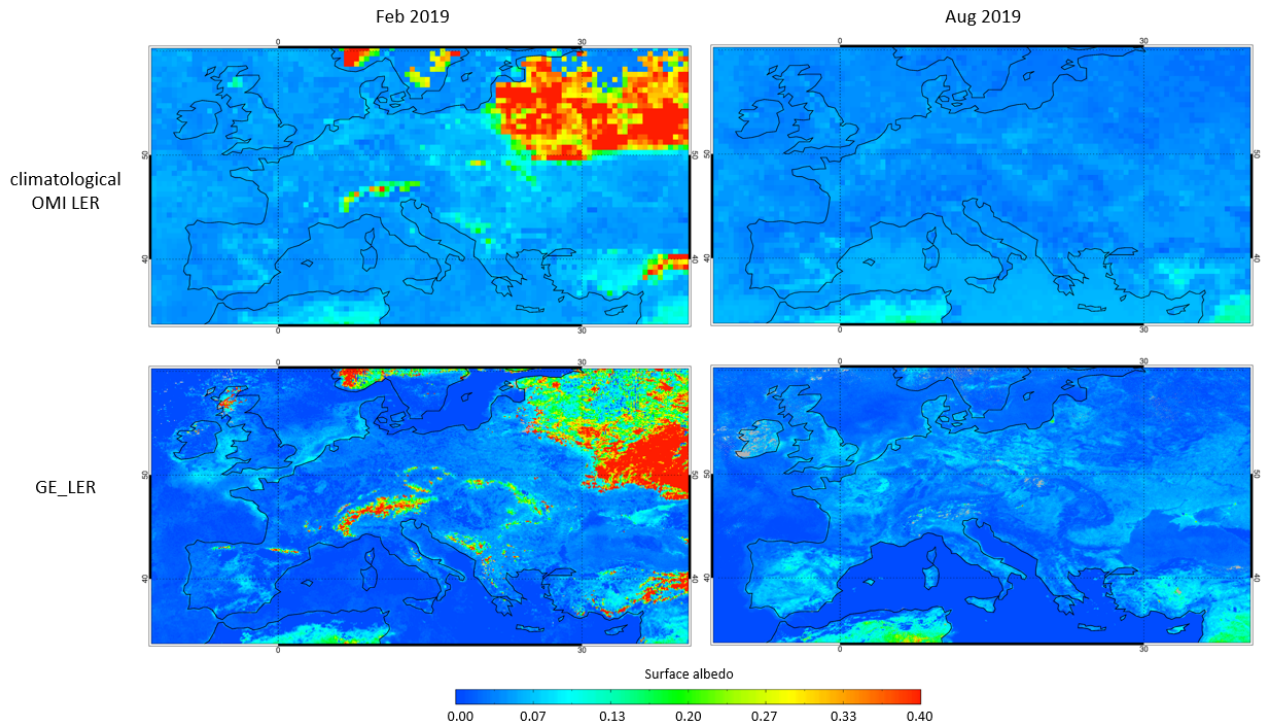
Figure 7. OMI surface LER climatology at 440 nm (Kleipool et al., 2008) and GE_LER retrieved from TROPOMI data in the NO_2 retrieval window (405 - 465 nm) over Europe in February and August 2019.
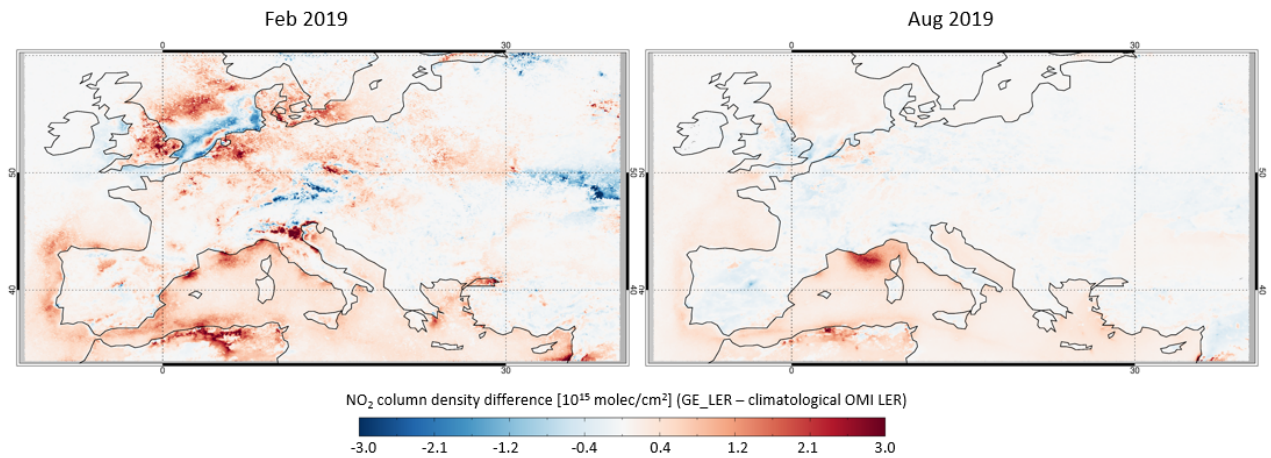

Figure 8. Differences in the tropospheric NO_2 columns retrieved using the climatological OMI LER and GE_LER over Europe in February and August 2019. Only measurements with cloud radiance fraction less than 0.5 are included.

4.2 A priori NO$_2$ profiles

To account for the varying sensitivity of the satellite to NO$_2$ at different altitudes, the POLYPHEMUS/DLR simulations (Mallet et al., 2007) with a spatial resolution of $0.2° \times 0.3°$ (latitude, longitude) and a temporal resolution of 1 h are applied for Europe (34.0°N-60.4°N,12.0°W-40.2°E) in this study. Compared to the reference algorithm using TM5-MP a priori NO$_2$ profiles, it can be expected that the improved resolution of POLYPHEMUS/DLR is better able to capture accurately the local NO$_2$ distribution, particularly for regions with large heterogeneity and variability.

As summarized in Table 2, the meteorological parameters are provided by Weather Research and Forecasting (WRF) Version 3.5 daily forecasts with a 30 km$\times$30 km spatial resolution, initialized by daily Global Forecast System (GSF) global forecast from National Oceanic and Atmospheric Administration (NOAA). The original POLYPHEMUS model is an assembly of several Eulerian and Gaussian models for handling passive tracers, photochemistry, and aerosol dynamics (Mallet et al., 2007) and is developed based on the chemistry transport model Polair3D (Boutahar et al., 2004). In this study, the Regional Atmospheric Chemistry Modeling (RACM) chemical mechanism (Stockwell et al., 1997) is applied along with the Size-REsolved Aerosol Model (SIREAM) and Secondary ORGanic Aerosol Model (SORGAM) size-resolved aerosol model (Debry et al., 2007; Schell et al., 2001). The anthropogenic emissions are extracted from the European TNO-MACC (from 2011 with base year 2005) emission inventory (Denier van der Gon et al., 2010; Kuenen et al., 2014). With a spatial resolution of 7 km$\times$7 km, TNO-MACC defines 10 source categories including road transport and shipping and uses source sector-specific data in a harmonized way. Biogenic emissions from soils are computed as proposed in Simpson et al. (1999). Lightning emissions are not considered.

Figure 9 shows the TM5-MP and POLYPHEMUS/DLR a priori NO$_2$ profiles over Munich in Germany (48.15°N, 11.57°E) on 5 February 2019, with the calculated clear-sky tropospheric AMFs also reported. POLYPHEMUS/DLR shows a higher surface layer NO$_2$ concentration and yields a tropospheric AMF that is reduced by 0.36 (36.7%). Figure 9 additionally shows the low-tropospheric NO$_2$ profile derived from the ground-based MAX-DOAS data (Chan et al., 2020) and the tropospheric AMF calculated using the MAX-DOAS NO$_2$ profile as a priori information (assuming a constant profile shape for the high troposphere). With a typical horizontal sensitivity of a few kilometers, the MAX-DOAS profile shows large amounts of NO$_2$ in the lower troposphere (Irie et al., 2011; Wagner et al., 2011). ~~The profile shape from POLYPHEMUS/DLR agree better with the MAX-DOAS measurements than TM5-MP, with the tropospheric AMF bias improving from 0.32 (48.5%) to -0.04 (-6.0%).~~ In comparison with the tropospheric AMF calculated using the MAX-DOAS NO$_2$ profile, the bias reduces from 0.32 (48.5%) for TM5-MP to -0.04 (-6.0%) for POLYPHEMUS/DLR.

Figure 10 shows the monthly average differences in the tropospheric NO$_2$ columns retrieved using TM5-MP and POLYPHEMUS/DLR a priori NO$_2$ profiles in February and August 2019. POLYPHEMUS/DLR uses the TNO-MACC emission database, which generally shows higher total NO$_2$ emissions at much higher spatial resolution in comparison with the global MACCity inventory. Further tests to investigate the sensitivity of model NO$_2$ profiles have concluded that the horizontal resolution and the representation of the tropospheric boundary layer have the largest influence (not shown). The generally steeper profile shape from POLYPHEMUS/DLR (see Fig. 9) increases the retrieved tropospheric NO$_2$ columns by more than 2×10^{15} molec/cm^2
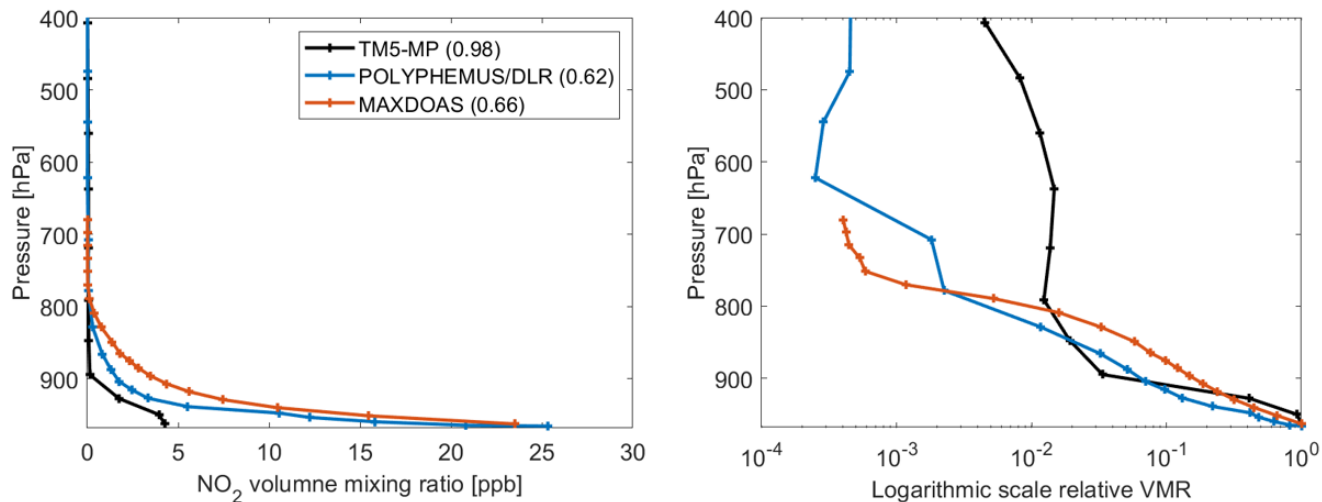
Figure 9. A priori NO$_2$ profiles from the chemistry transport models TM5-MP and POLYPHEMUS/DLR and the low-tropospheric NO$_2$ profile derived from the ground-based MAX-DOAS measurements over Munich in Germany (48.15°N, 11.57°E) on 5 February 2019. The calculated clear-sky tropospheric AMF is given in the bracket next to each label in the legend. Normalized profiles (to the lowest values) are also shown on a logarithm scale.
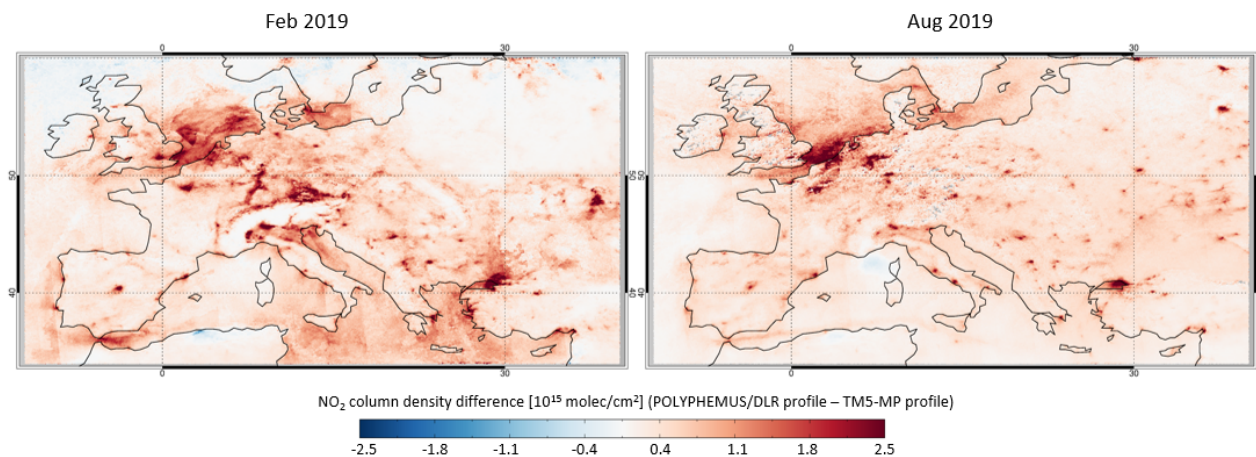

Figure 10. Differences in the tropospheric NO$_2$ columns retrieved using the TM5-MP and POLYPHEMUS/DLR a priori NO$_2$ profiles over Europe in February and August 2019. Only measurements with cloud radiance fraction less than 0.5 are included.

for pollution hot spots, e.g. regions with large population or heavy industry in the Benelux, northern Italy, and western Turkey, as well as highways with intense road traffic in northern Spain, southern France, and western Germany.

    Figure 11 compares the tropospheric NO$_2$ columns from TROPOMI measurements and POLYPHEMUS/DLR simulations. 380 The satellite averaging kernel, which describes the vertical sensitivity of measurements of NO$_2$ concentrations, is applied

19
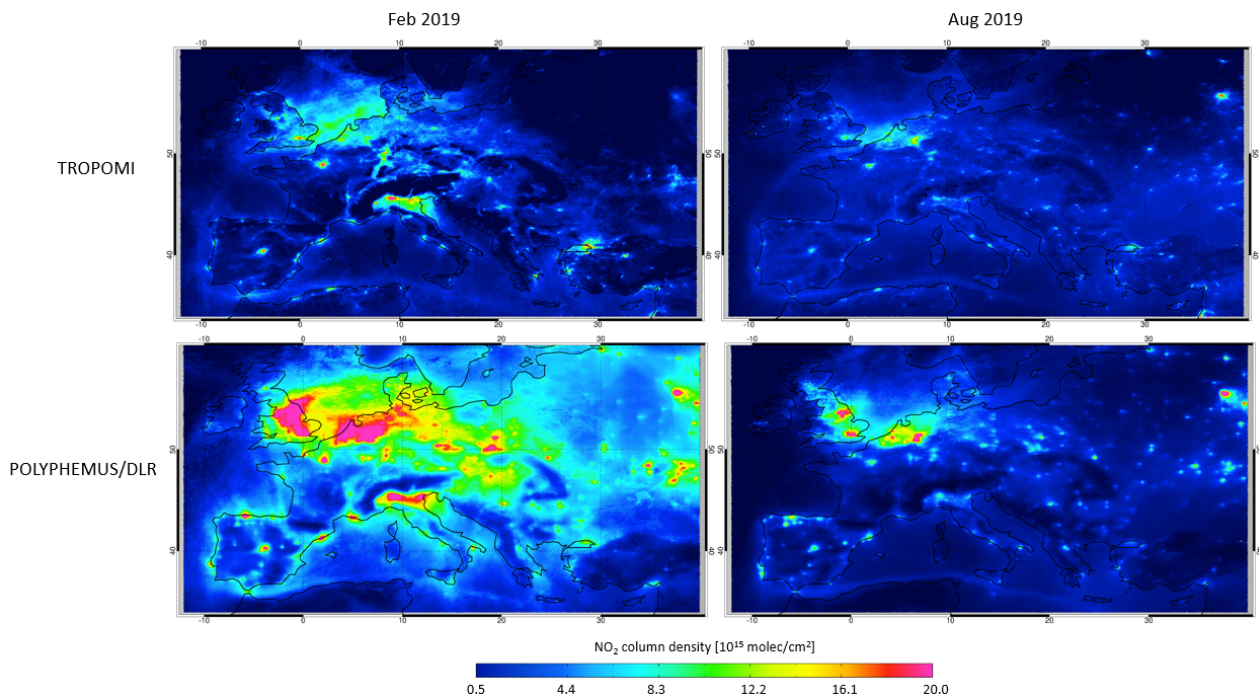
Figure 11. Tropospheric NO$_2$ columns from TROPOMI measurements (retrieved with the POLYPHEMUS/DLR a priori NO$_2$ profiles) and POLYPHEMUS/DLR simulations (using the satellite averaging kernel) over Europe in February and August 2019. Only TROPOMI measurements with cloud radiance fraction less than 0.5 are included.

to reduce the systematic biases caused by unrealistic a priori profile information. From Fig. 11, POLYPHEMUS/DLR NO$_2$ columns are generally higher than satellite measurements, which can be partly related to the use of the TNO-MACC emission dataset (Denier van der Gon et al., 2010). An update of the POLYPHEMUS/DLR model using the more recent TNO-MACC_II emission is planned for the near future. We note here that the profile shape is of far more importance than the column bias for
385   the interpretation of satellite retrievals.

4.3 Cloud correction

4.3.1 New processor for OCRA/ROCINN

With a new version 2.1 ~~OCRA/ROCINN~~ processor in operation since August 2020 (Loyola et al., 2020a), improvements are introduced to the OCRA/ROCINN retrievals. The background maps used in the OCRA cloud fraction determination are calcu-
390   lated based on one year of TROPOMI data (April 2018 - March 2019) instead of the previously used OMI measurements, and the spatial resolution improves from $0.2° \times 0.4°$ to $0.1° \times 0.1°$. In the pre-processing step, a TROPOMI-based VZA dependency correction is applied instead of using the OMI measurements.
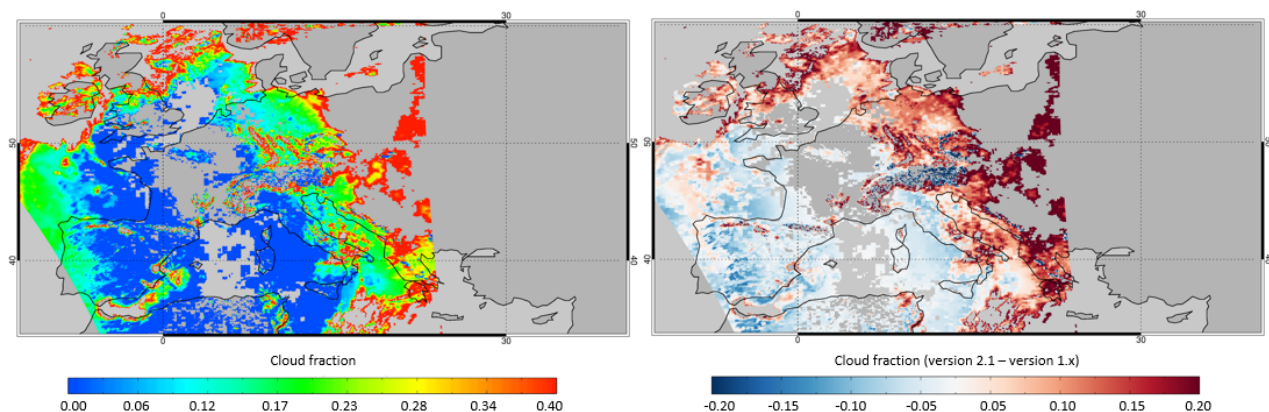
Figure 12. OCRA cloud fractions from the version 2.1 processor (left) and comparisons with version 1.x (right) over Europe for orbit 6939 on 14 February 2019. Only measurements with $0 <$ cloud fraction $<= 0.4$ are included.

For ROCINN, the static MERIS surface albedo climatology (Popp et al., 2011) is replaced with the dynamic on-line GE_LER retrieval in the ROCINN fitting window, which derives the surface properties directly from TROPOMI itself on a daily basis
395 (see Sect. 4.1). The co-registration between UV-VIS band (used by OCRA) and NIR band (used by ROCINN) is optimized with a look-up table containing the fraction of overlapping area between the target and source pixels, and the cloud properties are provided in both spectral bands. Over snow/ice surfaces indicated by the European Centre for Medium Range Weather Forecast (ECMWF) dataset, ~~ROCINN retrieves effective cloud pressure and cloud albedo values assuming a cloud fraction of 0. These values~~ the effective scene pressure and scene albedo values, which are added in the version 2.1 processor, are applied
400 in the NO_2 AMF calculation when the difference between the scene pressure and the surface pressure is less than 2% and the observation is considered to be nearly cloud-free (van der A et al., 2020).

Figure 12 compares the OCRA cloud fractions from the version 1.x (1.0 and 1.1) and 2.1 processors for orbit 6939 on 14 February 2019. The update of cloud-free background maps increases the cloud fractions by more than 0.1 for large cloud fraction values and reduces the values by more than 0.1 for snow/ice covers, e.g. over the Alps and the Ore Mountains.
405 Figure 13 shows the OCRA cloud fractions as a function of VZA. Mainly due to the ~~improved~~updated VZA correction, the overestimation of cloud fractions, particularly at the east side of the orbit swath, are corrected by more than 0.03 for the new version 2.1 processor.

Figure 14 compares the ROCINN_CRB cloud pressures from the version 1.x and 2.1 processors for orbit 6939 on 14 February 2019. The cloud pressure differences are generally small for optically thin clouds with small cloud fractions. Due to
410 the enlarged OCRA cloud fractions for relatively thick clouds in Fig. 12, the new ROCINN shows increased cloud pressures for large cloud fractions. The decreased cloud pressures e.g. over the Adriatic Sea is related to the reduction of surface albedo. Similar variations are observed for ROCINN_CAL cloud top and base pressures.

Figure 15 shows the tropospheric NO_2 columns for orbit 6939 on 14 February 2019 and the effect of upgrading the processor for OCRA/ROCINN ~~processor~~ from version 1.x to version 2.1. The tropospheric NO_2 columns reduce by more than 5×10^{14}
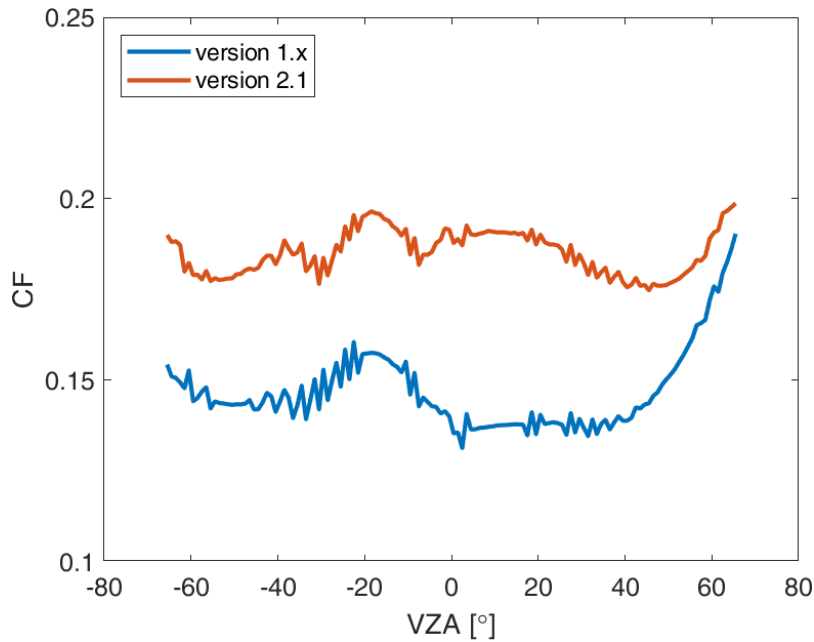
Figure 13. ~~VZA dependency of~~ OCRA cloud fractions from the version 1.x and 2.1 processors ~~(normalized to nadir)~~ in February 2019. Only measurements with $0 <$ cloud fraction $<= 0.4$ are included. The VZA is defined negative for observations on the west side of the orbit swath.
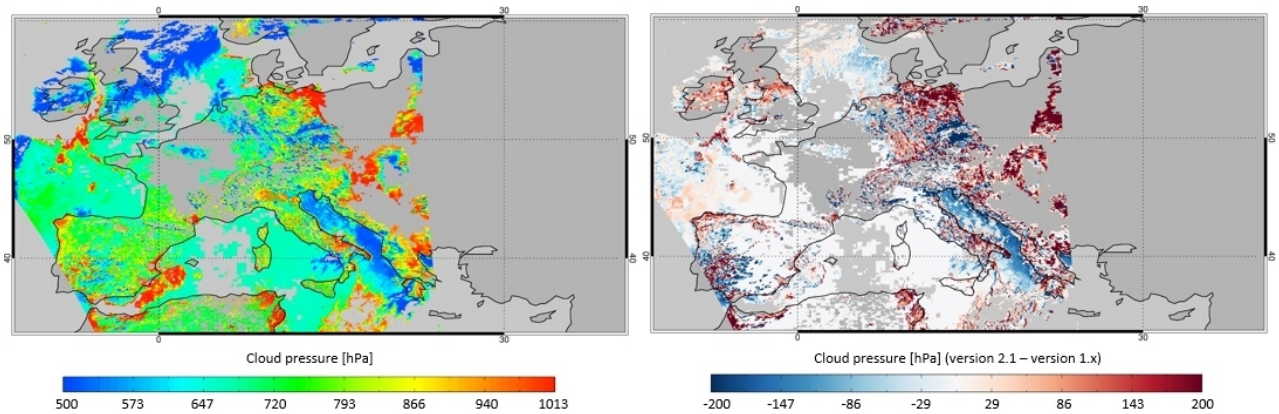

Figure 14. ROCINN_CRB cloud pressures from the version 2.1 processor (left) and comparisons with version 1.x (right) over Europe for orbit 6939 on 14 February 2019. Only measurements with $0 <$ cloud fraction $<= 0.4$ are included.

415 molec/cm^2 for the edge of the swath, such as ~~the Po Valley,~~ Rome and Naples in Italy, and reduce by up to 3.5×10^{14} molec/cm^2 for snow/ice scenarios, for instance the Ore Mountains. For polluted areas with optically thicker clouds (cloud fraction larger than 0.15 and cloud pressure larger than 700 hPa), e.g. northern Germany and the Benelux, the tropospheric NO$_2$ columns

22
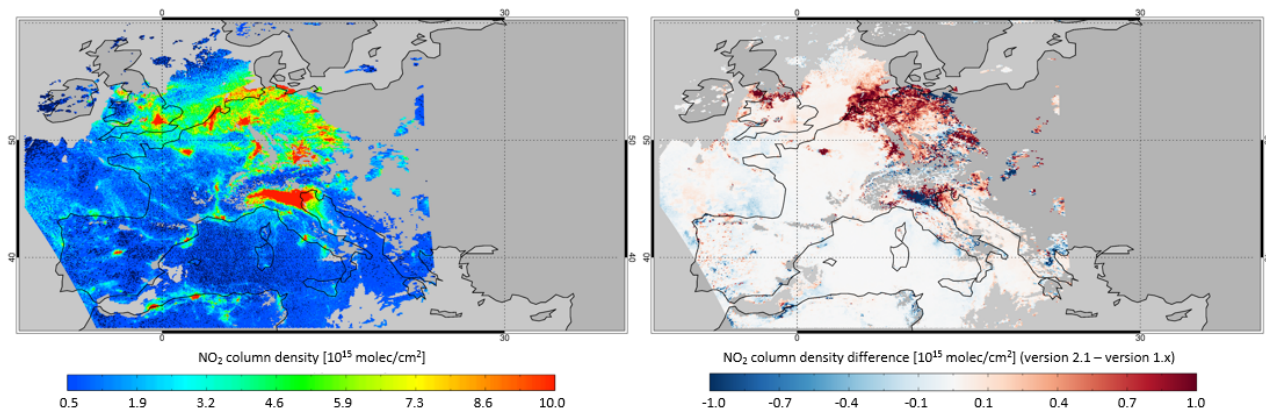
Figure 15. Tropospheric NO$_2$ columns retrieved using the OCRA/ROCINN cloud parameters from the version 2.1 processor (left) and differences with version 1.x (right) over Europe for orbit 6939 on 14 February 2019. Only measurements with a cloud radiance fraction less than 0.5 are included.

increase by more than 1×10^{15} molec/cm^2, because the increase in cloud fraction (and thus cloud radiance fraction) makes the retrieval less sensitive to the NO$_2$ below the cloud. The NO$_2$ reductions over the Po Valley are related to an additional

420   check implemented in the version 2.1 processor: the pixel is assumed to be cloud-free for the almost clear-sky condition (cloud fraction < 0.1) with the retrieved cloud height very close to the surface height (difference < 100 m). This correction improves the data yield of the TROPOMI cloud products compared with other satellite cloud products; the performance of this correction under different surface conditions (dark, bright, snow, ice) or under presence of different types of low-level aerosols (fog, smoke, dust, ash) is under investigation.

425   4.3.2   CAL cloud model

The cloud correction in our TROPOMI NO$_2$ retrieval is improved using the CAL model from the ROCINN cloud algorithm (Loyola et al., 2018). The CAL model, which regards the clouds as optically uniform layers of light-scattering water droplets, is more representative of the real situation than the CRB model, which treats the clouds as idealized Lambertian reflectors with zero transmittance. ~~The CAL model considers the multiple scattering of light inside the cloud and the contribution of the~~

430   ~~atmospheric layer between the cloud bottom and the ground.~~

Figure 16 presents the box-AMFs for clear and cloudy sky calculated using the CRB and CAL cloud models over Munich in Germany (48.15°N, 11.57°E) on 5 February 2019. The cloud pressures and the calculated tropospheric AMFs are also reported. Compared to the clear-sky box-AMFs, the cloudy-sky values increase above the cloud layer (albedo effect) and decrease below the cloud layer (shielding effect). The CRB-based cloud retrieval generally shows a cloud height (pressure) close to the altitude

435   of the middle (Ferlay et al., 2010; Richter et al., 2015), because CRB neglects the oxygen absorption within a cloud layer (Vasilkov et al., 2008) and misinterprets the smaller top-of-atmosphere reflectance as a lower cloud layer (Saiedy et al., 1967).
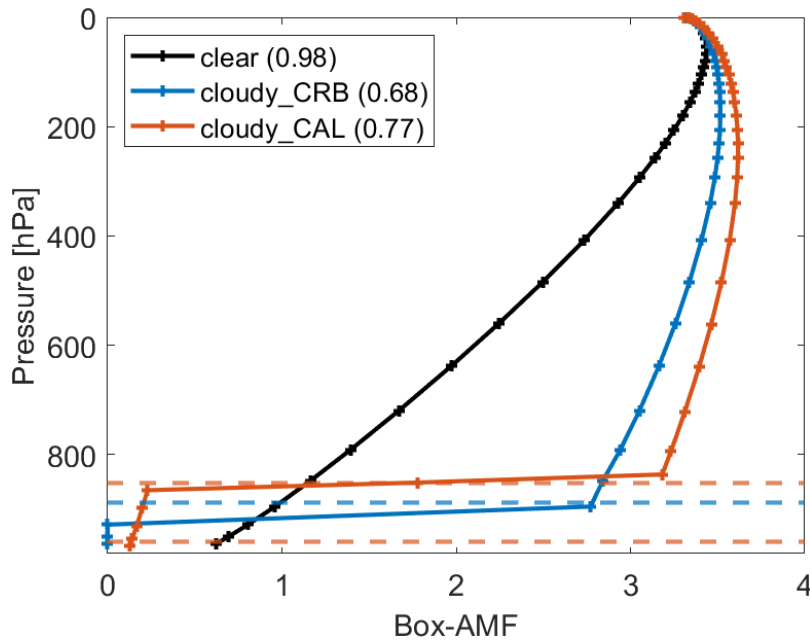
Figure 16. Box-AMFs for clear and cloudy sky using the ROCINN_CRB and ROCINN_CAL cloud models over Munich in Germany (48.15°N, 11.57°E) on 5 February 2019. The calculated tropospheric AMF is given in the bracket next to each label in the legend. The ROCINN_CRB cloud top pressure is shown as a blue horizontal dotted line, and the ROCINN_CAL cloud top and base pressures are shown as brown horizontal dotted lines.

Compared to the CRB-based cloud correction, the use of CAL model considers the sensitivities inside and below the cloud layers and increases the tropospheric AMFs by 0.09 (13.2%) for Munich.

Figure 17 presents the monthly average differences in the tropospheric NO_2 columns retrieved using the ROCINN_CRB and ROCINN_CAL cloud models in February and August 2019. The use of CAL cloud correction decreases the tropospheric NO_2 columns by more than 1×10^{15} molec/cm^2 (18%) for polluted regions in winter, when most of the NO_2 concentrations are located at the surface (as shown in Fig. 9) and the cloud fractions are generally larger due to the seasonal variation of clouds. The effect is less than 5×10^{14} molec/cm^2 (10%) for summer.

5 TROPOMI tropospheric NO$_2$ measurements

5.1 Examples of TROPOMI tropospheric NO$_2$ measurements

Table 3 summarises the tropospheric NO_2 retrieval results for the step-by-step updates listed above. Figure 18 shows the tropospheric NO_2 columns over Europe retrieved using the improved algorithm in February and August 2019. The tropospheric NO_2 columns are higher than 5×10^{15} molec/cm^2 over urban and industrial areas in winter, such as the Po Valley, Germany's Ruhr region, the Benelux, South-East England, and Turkey's Marmara region. City-size polluted regions, e.g. around Paris,
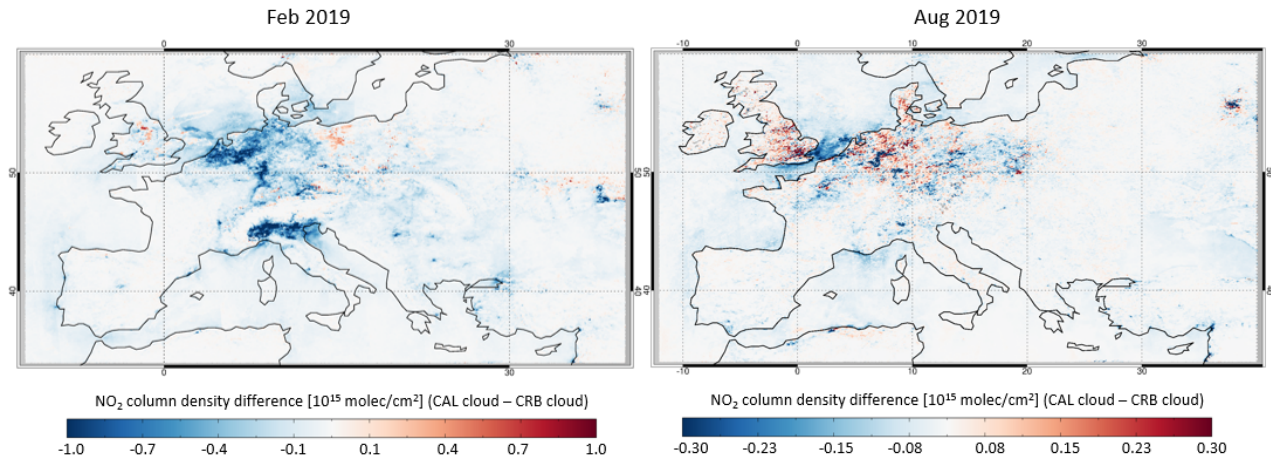
Figure 17. Differences in the tropospheric NO$_2$ columns retrieved using the ROCINN_CRB and ROCINN_CAL cloud models over Europe in February and August 2019. Only measurements with cloud radiance fraction less than 0.5 are included.

Table 3. Main settings for the step-by-step improvements and results of the tropospheric NO$_2$ retrievals for the different steps of the updates for Munich (48.15°N, 11.57°E). The tropospheric NO$_2$ columns (VCDtrop) are given in absolute values (molec/cm^2), and the percentage numbers in the brackets are changes relative to the reference case. The uncertainties in the tropospheric NO$_2$ columns (VCDtropErr) are given in relative numbers.

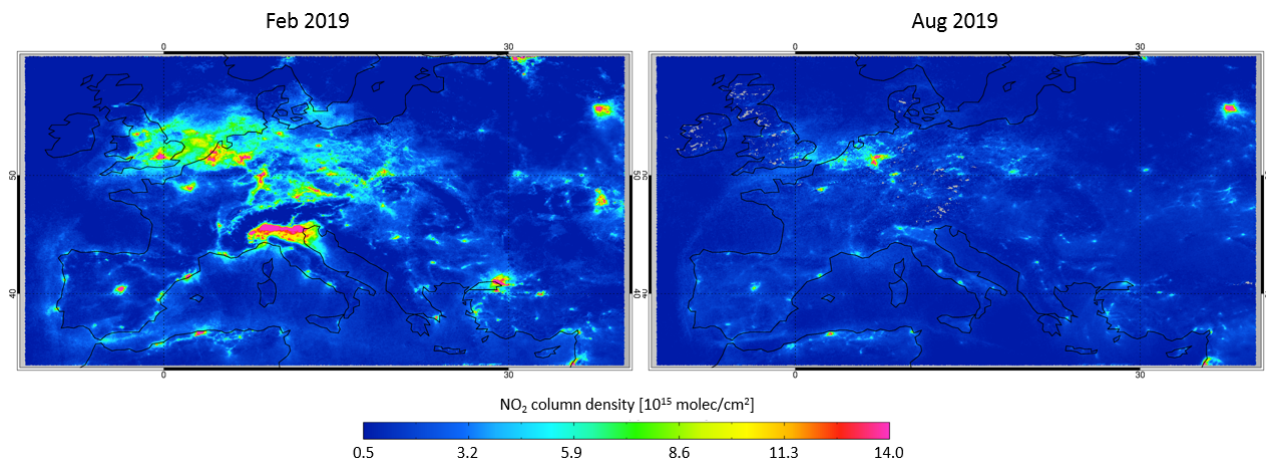|	Sect. 2.3 (Reference)	Sect. 4.1	Sect. 4.2	Sect. 4.3.1	Sect. 4.3.2 (Improved)
Surface albedo	OMI LER climatology	TROPOMI GE_LER data	TROPOMI GE_LER data	TROPOMI GE_LER data	TROPOMI GE_LER data
A priori NO$_2$ profile	TM5-MP	TM5-MP	POLYPHEMUS/DLR	POLYPHEMUS/DLR	POLYPHEMUS/DLR
Cloud parameter	OCRA/ROCINN_CRB version 1.x	OCRA/ROCINN_CRB version 1.x	OCRA/ROCINN_CRB version 1.x	OCRA/ROCINN_CRB version 2.1	OCRA/ROCINN_CAL version 2.1
VCDtrop (Feb. 2019)	1.02×10^{16}	1.07×10^{16} (+4.9%)	1.51×10^{16} (+48.0%)	1.57×10^{16} (+53.9%)	1.43×10^{16} (+40.2%)
VCDtropErr (Feb. 2019)	65%	62%	57%	56%	53%
VCDtrop (Aug. 2019)	3.86×10^{15}	4.03×10^{15} (+4.4%)	5.02×10^{16} (+30.1%)	5.13×10^{16} (+32.9%)	4.59×10^{16} (+18.9%)
VCDtropErr (Aug. 2019)	41%	41%	37%	36%	35%

Figure 18. Tropospheric NO$_2$ columns from the improved algorithm over Europe in February and August 2019. Only measurements with cloud radiance fraction less than 0.5 are included.
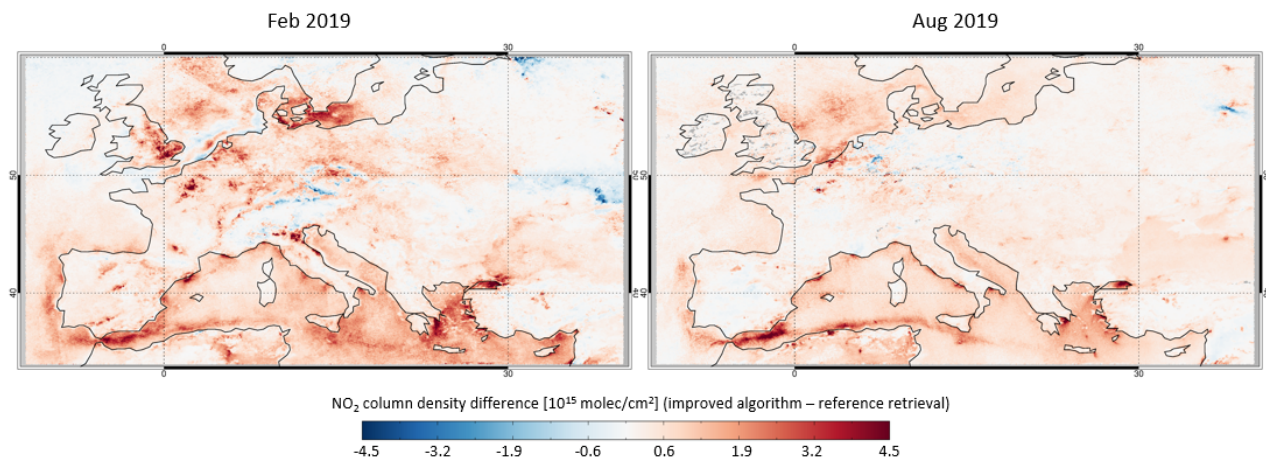

Figure 19. Differences in the tropospheric NO$_2$ columns retrieved using the reference algorithm and improved algorithm over Europe in February and August 2019. Only measurements with cloud radiance fraction less than 0.5 are included.

450 Madrid, Rome, Athens, and Moscow, are captured by the TROPOMI NO$_2$ measurements. NO$_2$ emissions over the shipping routes, e.g. the maritime connection between the Iberian Peninsula and North Africa, as well as emissions over the highways, e.g. the main East-West thoroughfare in Austria, are also detected.

Figure 19 compares the tropospheric NO$_2$ columns retrieved using the reference algorithm and the improved algorithm over Europe in February and August 2019. The tropospheric NO$_2$ columns are on average enhanced by 2×10^{15} molec/cm^2 (37%) 455 in winter and 8×10^{14} molec/cm^2 (15%) in summer mainly due to the combined effect of the improvements in the AMF

calculation. Larger differences by more than 3×10^{15} molec/cm^2 are noticed in polluted regions, such as London, Paris, and the Po Valley, as well as shipping lanes, e.g. in the Mediterranean Sea.

5.2 Uncertainty estimates

Derived by uncertainty propagation (Boersma et al., 2004), the overall uncertainty on the tropospheric NO$_2$ column is directly
460   related to the main retrieval steps, which are performed independently and assumed to be uncorrelated. The slant column uncertainty, estimated following a statistical method (Boersma et al., 2007) based on the spatial variability in the slant columns over the Pacific Ocean (20°S-20°N, 160°E-180°E), is on average 4.5×10^{14} molec/cm^2, in agreement with van Geffen et al. (2020a). The uncertainty in the stratospheric columns is 3.5×10^{14} molec/cm^2 for polluted conditions based on the daily synthetic data (see Sect. 3.2) and 1×10^{14} molec/cm^2 for monthly averages.

465   The tropospheric AMF calculation, which is the largest source of NO$_2$ uncertainty for polluted scenarios (Lorente et al., 2017), is mainly dependent on surface albedo, a priori NO$_2$ profile, cloud fraction, and cloud pressure, as introduced in Sect. 2.3 and 4. The tropospheric AMF uncertainties are calculated based on uncertainty propagation (Boersma et al., 2004) and typical uncertainties of each parameter (De Smedt et al., 2018, Table 8 therein). The uncertainty contribution from the a priori NO$_2$ profile is practically described by a parameter referred to as profile height, defined as the altitude (pressure) below which
470   resides 75% of the integrated NO$_2$ profile (De Smedt et al., 2018). The estimated parameter uncertainties considered in the AMF uncertainty budget include 0.0016 for GE_LER albedo (Loyola et al., 2020b), 75 hPa for POLYPHEMUS/DLR profile (estimated from the profile height standard deviation), 0.05 for the OCRA cloud fraction, and 50 hPa ROCINN cloud pressure (Loyola et al., 2020a).

Figure 20 shows the estimated tropospheric AMF uncertainties due to the errors in the surface albedo, cloud pressure, and
475   a priori NO$_2$ profile. The uncertainty contribution from the a prior NO$_2$ profile is practically described by a parameter referred to as profile height, defined as the altitude (pressure) below which resides 75% of the integrated NO$_2$ profile (De Smedt et al., 2018). As the satellite measurements are normally filtered for cloud radiance fraction smaller than 0.5 or cloud fraction smaller than ∼0.2, the uncertainties related to the cloud fraction are generally smaller than 15% (not shown). From Fig. 20, larger uncertainties are found for small albedo values and for scenarios with large albedo biases such as new snow/ice coverage. The
480   uncertainties due to the cloud pressure and a priori NO$_2$ profile can be up to 70% when the cloud is located below or within the NO$_2$ layer, particularly for thick clouds at low altitudes and for polluted situations (large profile heights).

The presence of aerosols can affect the sensitivity to tropospheric NO$_2$, depending on the particle properties and the NO$_2$ and aerosol vertical distribution (Martin et al., 2003; Leitão et al., 2010). The aerosol effect is not explicitly corrected in this study assuming that the effective cloud parameters from OCRA/ROCINN have partly accounted for the effect of aerosols on the light
485   paths (Boersma et al., 2004, 2011). In comparison to the simple CRB-based cloud correction, which can not fully describe the effects inherent to aerosol particles (Chimot et al., 2019), the use of CAL cloud correction considers the sensitivities inside and below the cloud/aerosol layers and reduces the AMF errors by more than 10% (Liu et al., 2020c).

Note that the use of averaging kernel, which describes the vertical sensitivity of measurements of NO$_2$ concentrations, can remove the uncertainty contributed by the a priori NO$_2$ profile for applications such as data assimilation and validation study
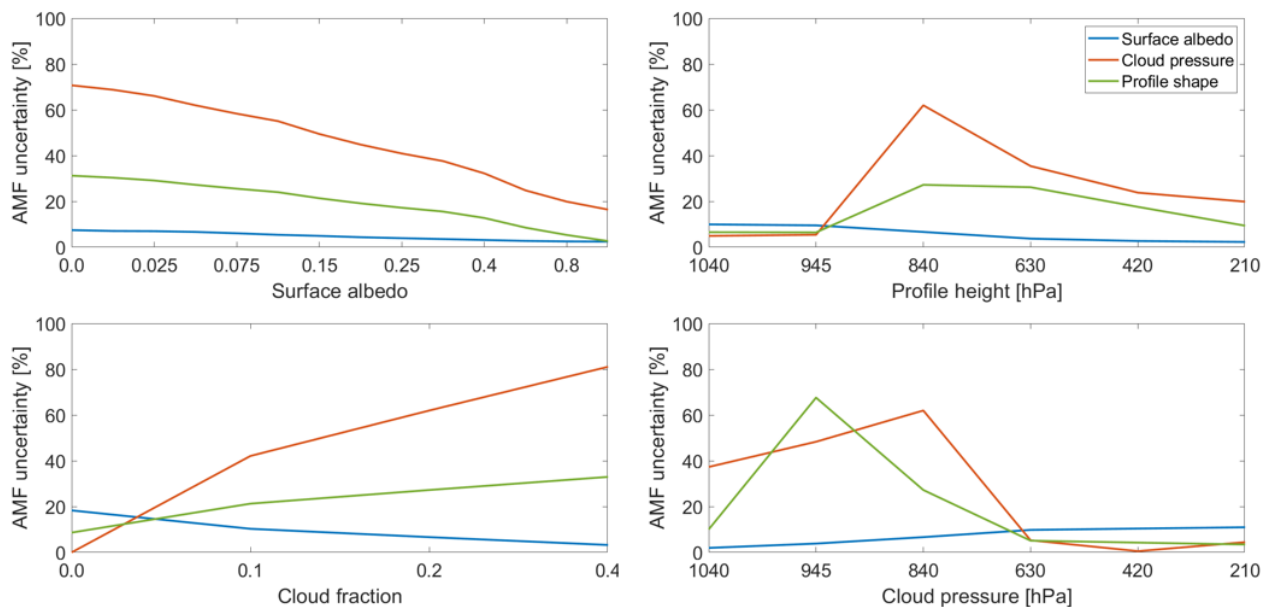
Figure 20. Tropospheric AMF uncertainties related to the surface albedo, cloud pressure, and a priori NO_2 profile errors. By default, the surface pressure is 1050 hPa, the surface albedo is 0.05, the profile height is 840 hPa, the cloud pressure is 840 hPa, the cloud fraction is 0.2. The definition of profile height is given in the text.

490   (Eskes and Boersma, 2003). Therefore, for a typical polluted scene, the tropospheric AMF uncertainty is estimated to be 20% for mostly clear sky and 50% in the presence of clouds, leading to a total uncertainty in the tropospheric NO_2 columns in the 30-60% range.

6   TROPOMI tropospheric NO_2 validation

The validation of the improved TROPOMI tropospheric NO_2 columns is based on ground-based MAX-DOAS measurements
495   from nine stations in Europe. Table 4 provides the information about the stations, most of which are characterised by urban or suburban polluted conditions with heavy traffic and industrial emissions. For the validation of TROPOMI measurements, the satellite data from January 2018 - June 2020 are filtered for clouds (cloud radiance fraction less than 0.5), and the closest valid pixel within 20 km of the stations is compared to the ground-based MAX-DOAS data, which are linearly interpolated to the TROPOMI overpass time if original data exist within 1 h.
500   Figure 21 shows the time series and scatter plot of the comparison of the daily and monthly means between the ~~improved~~new TROPOMI tropospheric NO_2 columns and the ground-based MAX-DOAS measurements in Uccle. The monthly mean values from the TROPOMI and MAX-DOAS measurements show similar seasonal variations in the tropospheric NO_2 column. Figure 21 includes the statistical information on the Pearson correlation coefficient as well as the slope and intercept obtained with

Table 4. An overview of MAX-DOAS stations contributing to the TROPOMI tropospheric NO$_2$ validation in this study. More details on the QA4ECV datasets can be found at http://www.qa4ecv.eu/ecvs.

Station	Location	Institute	Description
Athen	38.05°N, 23.86°E	IUPB	QA4ECV dataset
Bremen	53.10°N, 8.85°E	IUPB	QA4ECV dataset
Cabauw	51.97°N, 4.93°E	KNMI	Vlemmix et al. (2010)
De Bilt	52.10°N, 5.18°E	KNMI	Vlemmix et al. (2010)
Mainz	49.99°N, 8.23°E	MPIC	QA4ECV dataset
Munich	48.15°N, 11.57°E	LMU	Chan et al. (2020)
Thessaloniki_ciri	40.56°N, 22.99°E	AUTH	Drosoglou et al. (2017), QA4ECV dataset
Thessaloniki_lap	40.63°N, 22.96°E	AUTH	Drosoglou et al. (2017), QA4ECV dataset
Uccle	50.80°N, 4.36°E	BIRA-IASB	Gielen et al. (2014), Hendrick et al. (2014), Dimitropoulou et al. (2020)
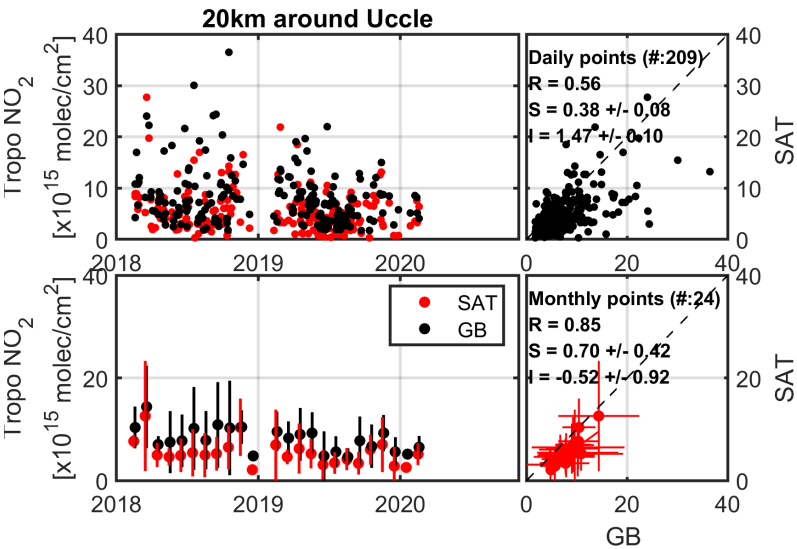
Figure 21. Daily and monthly mean time series and scatter plot of TROPOMI (SAT) and MAX-DOAS (GB) tropospheric NO$_2$ columns (closest valid pixel within 20 km of Uccle). Results are shown for the improved satellite retrieval algorithm.

the robust Theil–Sen estimator (Sen, 1968; Vigouroux et al., 2020). A correlation coefficient of 0.85, a slope of 0.70, and an
505   intercept of -0.52×10^{15} molec/cm^2 are derived when comparing the monthly mean values.

Figure 22 presents the daily and monthly mean absolute and relative differences of TROPOMI and MAX-DOAS measurements in Uccle. The differences are generally within 1×10^{16} molec/cm^2 with a mean difference of -2.6×10^{15} molec/cm^2.
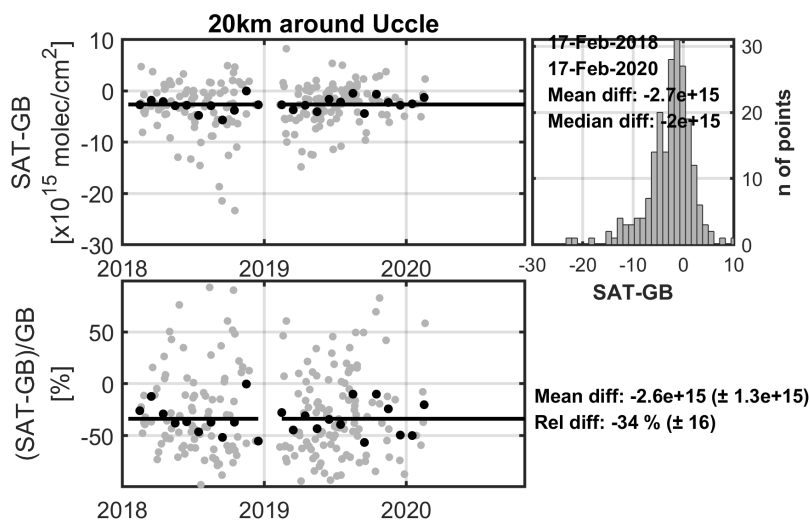
Figure 22. Daily (grey dots) and monthly mean (black dots) absolute and relative TROPOMI (SAT) and MAX-DOAS (GB) time series differences for the Uccle station. Results are shown for the improved satellite retrieval algorithm. The histogram of the daily differences is also given, showing the mean and median difference. The total mean values of absolute and relative monthly differences are given in the bottom-right panel.

The NO_2 levels are underestimated by 34% by TROPOMI with a standard deviation of 16%, which is ~~mostly explained by the relatively low sensitivity of spaceborne measurements near the surface, the aerosol shielding effect, and the gradient smoothing~~

510 ~~effect. These effects are often inherent to the remaining impact of~~ likely explained by comparison errors (such as the gradient smoothing effect, the comparison choices, and the inherent difference in sensitivity), partly by the remaining impact of structural uncertainties (Boersma et al. (2016), such as the impact of the choice of the a priori NO_2 profiles and/or the albedo database assumed for the satellite AMF calculations), and by the different measurement types or the specific conditions of the validation sites.

515   To analyse the gradient smoothing effect for Uccle, TROPOMI measurements for 2018-2020 are aggregated based on an area-weighted tessellation to a resolution of $0.01° \times 0.01°$, and the systematic variation in tropospheric NO_2 columns between the satellite pixel location and the ground-based station position is shown in Fig. 23, following the method from Chen et al. (2009); Ma et al. (2013); Pinardi et al. (2020). From Fig. 23, the smoothing effect is largest for summer (up to 19%), as the NO_2 gradients are large due to the shorter lifetime, in agreement with Ma et al. (2013). For the Uccle site, which is located

520 south of Brussels at a distance of ∼6 km from the city center, the tropospheric NO_2 columns increase by up to 4% outwards until 6 km due to the influence of the surrounding emission sources during summer and autumn. This effect is additionally influenced by the seasonal wind pattern, particularly for winter, when the wind is blowing in the direction of the site from north (Dimitropoulou et al., 2020).
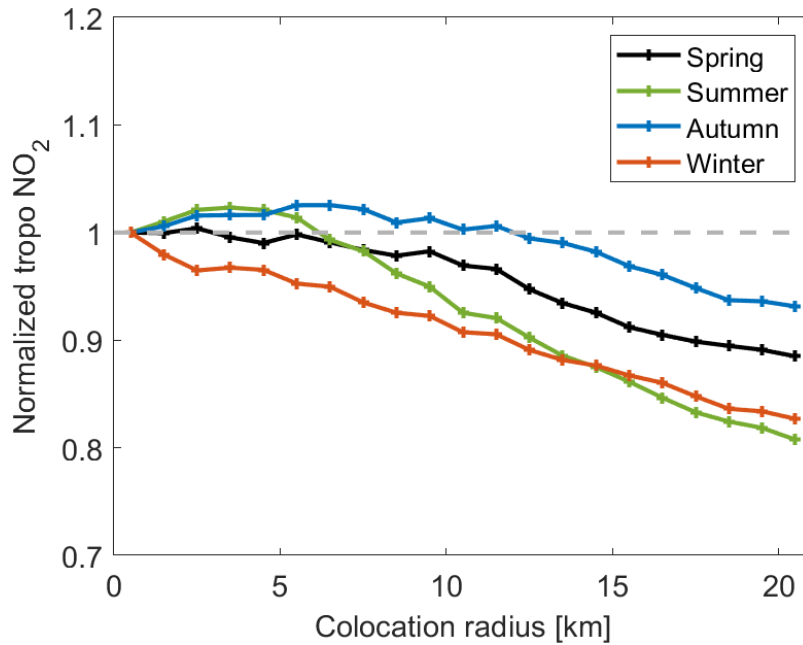
Figure 23. Normalized tropospheric NO₂ columns at increasing colocation radii for the Uccle station, estimated using seasonal mean TROPOMI data in 2018-2020.

Table 5. The Pearson correlation coefficient R, as well as the slope S and intercept I (in 1×10^{15} molec/cm²) obtained with the robust Theil–Sen estimator for the monthly TROPOMI tropospheric NO₂ product compared to MAX-DOAS data. Stations are ordered by increasing mean difference. Values for the DLR improved algorithm (DLRimp) are given, and the values for the DLR reference algorithm (DLRref) and the KNMI operational product (KNMIop) are reported for comparison.

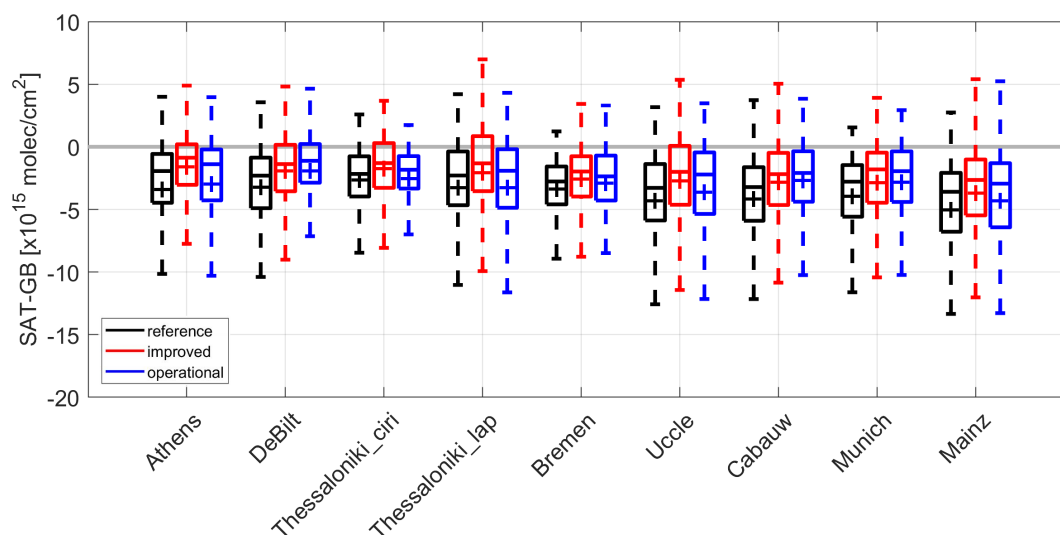| Station	R			S			I		
	DLRimp	DLRref	KNMIop	DLRimp	DLRref	KNMIop	DLRimp	DLRref	KNMIop
Athens	0.85	0.87	0.81	0.65	0.42	0.45	0.33	0.25	0.33
De Bilt	0.63	0.72	0.80	0.42	0.25	0.77	1.69	1.31	-0.57
Thessaloniki_ciri	0.91	0.95	0.91	0.51	0.45	0.26	-0.80	0.14	1.23
Thessaloniki_lap	0.79	0.86	0.90	0.35	0.30	0.37	1.97	1.09	0.93
Bremen	0.85	0.71	0.70	0.58	0.44	0.40	-0.24	-0.20	0.79
Uccle	0.85	0.81	0.44	0.70	0.42	0.27	-0.52	-0.24	2.26
Cabauw	0.75	0.67	0.43	0.41	0.21	0.33	1.08	1.24	1.98
Munich	0.57	0.72	0.63	0.35	0.39	0.42	1.44	0.29	1.35
Mainz	0.85	0.87	0.81	0.39	0.28	0.50	1.65	0.82	0.02

Figure 24. Box and whisker plot of the daily biases and spread of the differences between the TROPOMI (SAT) and MAX-DOAS (GB) data. Results for the reference algorithm, the improved algorithm, and the operational product are compared. Stations are ordered by increasing mean difference. The mean differences are represented by crosses. The median differences are represented by vertical solid lines inside the boxes, which mark the 25 and 75% quantiles. The whiskers cover the 9-91% range of the differences.

Table 6. Similar as Table 5 but for the mean difference (MD, SAT-GB in 1×10^{15} molec/cm^2), standard deviation (STD, in 1×10^{15} molec/cm^2), and relative difference (RD, in %) for the monthly TROPOMI tropospheric NO$_2$ product compared to MAX-DAAS data.

Station	MD			STD			RD		
	DLRimp	DLRref	KNMIop	DLRimp	DLRref	KNMIop	DLRimp	DLRref	KNMIop
Athens	-1.6	-3.5	-3.1	1.2	1.4	1.3	-26	-53	-48
De Bilt	-2.0	-3.5	-2.1	1.8	1.6	1.3	-27	-51	-30
Thessaloniki_ciri	-2.2	-3.4	-3.8	1.5	2.0	4.0	-34	-54	-51
Thessaloniki_lap	-2.4	-3.7	-3.5	2.6	2.6	2.3	-27	-49	-46
Bremen	-2.6	-3.7	-3.1	1.0	1.2	1.4	-45	-61	-46
Uccle	-2.6	-4.5	-4.3	1.3	1.5	2.9	-34	-55	-45
Cabauw	-3.2	-4.7	-2.9	1.8	2.0	2.1	-40	-59	-36
Munich	-3.4	-4.6	-3.3	2.5	2.3	2.8	-39	-56	-38
Mainz	-4.4	-5.6	-5.1	3.0	2.8	2.5	-40	-60	-49

Similar figures as Fig. 21 and 22 for the improved and reference algorithms are gathered in Fig. S1 - S4 in the Supplement for all the stations. Figure 24 shows an overview of the daily differences between satellite and ground-based data for the improved

and reference algorithms. Tables 5 and 6 summarize the monthly comparisons of TROPOMI and MAX-DOAS measurements. High correlations are observed for the improved algorithm for all the stations with an average correlation coefficient of 0.78. The impact of the algorithm improvements leads to a decrease of the mean absolute difference in urban/suburban conditions from -4.13×10^{15} molec/cm^2 to -2.71×10^{15} molec/cm^2 and relative difference from -55.3% to -34.7%. The largest absolute bias (-5.6×10^{15} molec/cm^2 in Mainz) is reduced to -4.4×10^{15} molec/cm^2 (relative bias from -60% to -40%), while the smaller absolute bias (-3.4×10^{15} molec/cm^2 in Thessaloniki_ciri) is reduced to -2.2×10^{15} molec/cm^2 (relative bias from -54% to -34%). The largest reduction is found for Athens (-27% reduction from the reference to improved algorithm).

Smaller biases are found for the improved algorithm, not only in comparison with the reference algorithm but also compared to the operational product in Fig. 24 and Table 6, particularly for Athens, Thessaloniki_ciri, Thessaloniki_lap, Uccle, and Mainz. The relative biases ranging from -26 to -45% in Table 6 are lower than those reported by validation exercises for the operational TROPOMI product, where the NO$_2$ levels are normally found to be underestimated by the TROPOMI instrument by 30% to 50% for polluted conditions (Dimitropoulou et al., 2020; Verhoelst et al., 2020; Wang et al., 2020). These results are not directly comparable to results e.g. obtained by Dimitropoulou et al. (2020), as they use a more elaborated ground-based dataset with several pointing directions and specific area-weighted pixel selections in the MAX-DOAS line-of-sight. Note that the operational tropospheric NO$_2$ columns have been increased with an upgrade of the NO$_2$ processor (version 01.04.00) since 29 November 2020 due to the improved handling of cloud pressures (Eskes et al., 2020).

To investigate the impact of satellite a priori NO$_2$ profiles on the comparison, the satellite averaging kernel ~~(see Sect. Sect. 5.2)~~ is used to relate the MAX-DOAS retrieved NO$_2$ profiles to satellite column measurements by calculating the smoothed MAX-DOAS columns as:

$$V_{GB,smoothed} = \sum_l AK_{SAT,l} \times x_{GB,l}. \tag{8}$$

The smoothed MAX-DOAS NO$_2$ columns $V_{GB,smoothed}$ are derived by convolving the layer (l)-dependent daily profile $x_{GB,l}$ (expressed in partial columns and interpolated to the satellite overpass time) with the satellite averaging kernel $AK_{SAT,l}$.

Figure 25 shows the original and smoothed comparisons of satellite and MAX-DOAS data for the Munich station. The use of the averaging kernel smoothing reduces the MAX-DOAS columns and thus improves the agreement between the satellite and MAX-DOAS columns. When the satellite averaging kernels are used to remove the contribution of the a priori NO$_2$ profile shape, the mean absolute difference reduces from -3.4×10^{15} molec/cm^2 to -1.9×10^{15} molec/cm^2, and the relative difference reduces from -39% to -23%.

7   Conclusions

The DLR retrieval algorithm developed for TROPOMI NO$_2$ measurements follows a three-step scheme. To calculate the NO$_2$ slant columns, a 405-465 nm fitting window is applied in the DOAS fit for consistency with other NO$_2$ retrievals from OMI and TROPOMI. Absorption cross-sections of interfering species and a linear intensity offset correction are applied. The striping
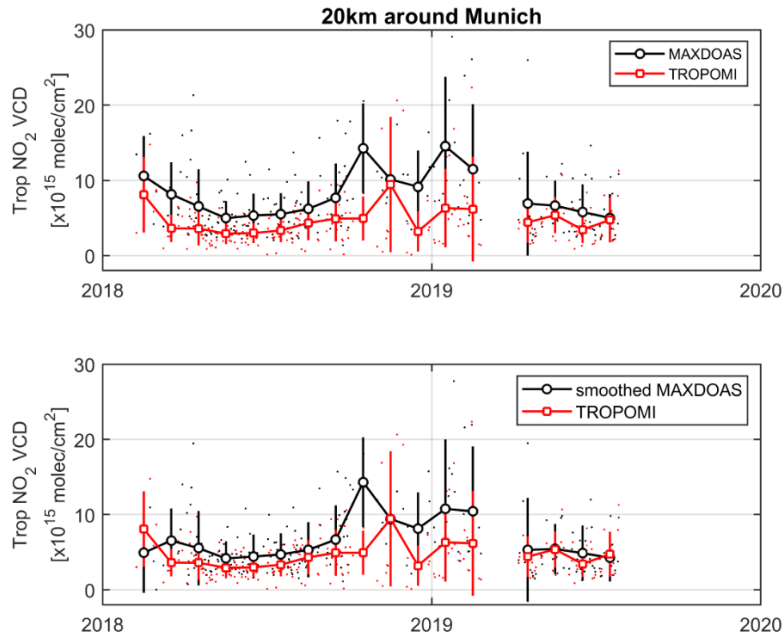
Figure 25. Daily (dots) and monthly mean (circles) time series of TROPOMI and MAX-DOAS tropospheric NO$_2$ columns for the Munich station. Results for the original comparisons and the smoothed comparisons are reported.

pattern of slant columns is corrected using an empirical method based on the daily averaged across-track variability of NO$_2$ slant columns over clean regions.

560   The stratospheric NO$_2$ component is estimated using the STREAM method, which requires no chemistry transport model data as used in data assimilation and provides an improved treatment of polluted and cloudy pixels comparing to other modified reference sector methods. An improved DSTREAM method is used to correct for the VZA dependency of stratospheric NO$_2$ for high latitudes, which is related to the local time changes across the orbit. DSTREAM divides the orbit swath into three segments, applies the original STREAM to data from each of the segments, and calculates the stratospheric NO$_2$ column based on VZA and latitude from the satellite measurement. Applied to synthetic TROPOMI data, constructed using

565   the IFS(CB05BASCOE) model fields, the estimated stratospheric NO$_2$ columns from the original STREAM and the improved DSTREAM show good consistency with the a priori truth. Applied to actual TROPOMI measurements, STREAM and DSTREAM successfully separate the stratospheric and tropospheric fields for polluted regions. The VZA dependency of stratospheric NO$_2$ which amounts up to 2×10^{14} molec/cm^2 at high latitudes is captured by DSTREAM.

     In the tropospheric AMF calculation, the surface albedo from the monthly OMI LER climatology is replaced by the

570   TROPOMI GE_LER data, which is consistently applied in both NO$_2$ and cloud retrievals. GE_LER in the NO$_2$ fitting window is retrieved using the machine learning based approach FP_ILM with inputs from the DOAS fitting. In comparison with the climatological LER values from previous satellite missions, the GE_LER data relies on the real-time measurements from

the TROPOMI instrument itself with an improved spatial resolution of $0.1° \times 0.1°$. Therefore, GE_LER better characterizes the actual surface conditions with an impact on the tropospheric NO_2 columns by up to 3×10^{15} molec/cm^2 under polluted conditions.

Mesoscale-resolution a priori profiles ($0.2° \times 0.3°$), obtained from the regional POLYPHEMUS/DLR chemistry transport model based on the European TNO-MACC emission inventory, provide a better description of the spatial variability in the NO_2 fields for Europe. Compared to the currently used TM5-MP profiles, the POLYPHEMUS/DLR profiles generally show higher surface NO_2 concentrations, which reduce the tropospheric AMFs and thus enhance the tropospheric NO_2 columns by more than 2×10^{15} molec/cm^2 for polluted regions.

The presence of clouds is considered using the TROPOMI operational cloud retrieval algorithms OCRA/ROCINN. In a new version 2.1 processor, OCRA separates a spectral scene (in the UV-VIS wavelength range) into cloudy contribution and cloud-free background using TROPOMI-based background maps ($0.1° \times 0.1°$) instead of OMI-based ones, and ROCINN applies the surface albedo from the GE_LER data in the TROPOMI NIR instead of a static climatology. The overestimation of cloud fractions at the swath edge is corrected. Larger differences in cloud fractions and cloud pressures are found for relatively thick clouds, which affect the tropospheric NO_2 columns by more than 1×10^{15} molec/cm^2. In the tropospheric AMF calculation, the CRB model from ROCINN, in which clouds are idealized Lambertian reflectors, is replaced with the CAL model, in which clouds are represented by uniform layers of water droplets. CAL is more representative of the real situation and preferred for small TROPOMI ground pixels and for low clouds. The application of CAL cloud parameters considers the sensitivities inside and below the cloud layers and reduces the tropospheric NO_2 columns by more than 1×10^{15} molec/cm^2 for polluted regions.

The uncertainty in the NO_2 slant columns is 4.5×10^{14} molec/cm^2, derived from the spatial variability over the Paficic Ocean. The uncertainty in the stratospheric columns is 3.5×10^{14} molec/cm^2 for polluted regions based on daily synthetic TROPOMI data. The tropospheric AMF uncertainty is estimated to be 20% for mostly clear sky and 50% in the presence of clouds, leading to a total uncertainty in the tropospheric NO_2 column in the 30-60% range.

Validation of the improved TROPOMI tropospheric NO_2 columns is performed by comparisons with ground-based MAX-DOAS measurements. The validation is illustrated for nine European stations with urban/suburban conditions. The improved data shows a similar seasonal variation in the tropospheric NO_2 columns as the MAX-DOAS measurements with an average correlation coefficient of 0.78. Compared to the reference data, the improved algorithm shows a significant improvement with absolute differences decreasing from -4.13×10^{15} molec/cm^2 to -2.71×10^{15} molec/cm^2 on average and relative differences from -55.3% to -34.7%. When the satellite averaging kernels are used to remove the contribution of a priori NO_2 profile shape, the absolute difference at the Munich station reduces from -3.4×10^{15} molec/cm^2 to -1.9×10^{15} molec/cm^2, and the relative difference reduces from -39% to -23%.

The TROPOMI NO_2 research product from DLR is a complement to the operational product due to the use of independent approaches for stratosphere-troposphere separation and AMF calculation. Comparing to the other regional TROPOMI NO_2 product listed in Table 1, the DLR European retrieval reduces the potential biases introduced by using inputs from different instruments or climatologies and confirms the importance of applying more realistic input parameters with better resolution for AMF calculation.

In the future, the spectral effect of extending the fitting window to 490 nm will be analysed, when the pixel blooming is better treated in a future update of the TROPOMI level 0-1b processor. An update of the POLYPHEMUS/DLR model using more recent TNO-MACC emission is planned. The operational OCRA/ROCINN cloud parameters will be compared with other cloud products such as FRESCO-S and MICRU. The interpretation of the cloud product for aerosol-dominated scenes and the impact on the NO_2 retrieval algorithm will be further investigated. Aerosol contamination will be removed in the GE_LER retrieval using TROPOMI aerosol index data. An independent Neural Network will be trained and implemented for error estimation.

The NO_2 data quality will be further analysed using data from additional ground-stations covering different pollution conditions and data from validation campaigns with independent instruments. Further improvements in the ground-based validation include using the full MAX-DOAS line-of-sight sensitivity and the intersect with the TROPOMI pixel(s) or having more ground-based instruments located within a TROPOMI pixel. More frequent ground-based measurements and measurements in more than one direction might better sample the temporal and spatial variability around the measurement sites (Richter and Lange, 2021; Dimitropoulou et al., 2020).

The NO_2 retrieval algorithm can be adapted for new instruments and missions, such as the polar-orbiting Sentinel-5 and geostationary Sentinel-4 missions, which offer new perspectives for monitoring NO_2 with a fast revisiting time and a high spatial resolution and provide information on atmospheric variables in support of European policies.

References

Bauwens, M., Compernolle, S., Stavrakou, T., Müller, J.-F., van Gent, J., Eskes, H., Levelt, P. F., van der A, R., Veefkind, J. P., Vlietinck, J., Yu, H., and Zehner, C.: Impact of coronavirus outbreak on NO_2 pollution assessed using TROPOMI and OMI observations, Geophys. Res. Lett., 47, e2020GL087 978, 2020.

650   Beirle, S., Hörmann, C., Jöckel, P., Liu, S., Penning de Vries, M., Pozzer, A., Sihler, H., Valks, P., and Wagner, T.: The STRatospheric Estimation Algorithm from Mainz (STREAM): estimating stratospheric NO_2 from nadir-viewing satellites by weighted convolution, Atmos. Meas. Tech., 9, 2753–2779, 2016.

Beirle, S., Borger, C., Dörner, S., Li, A., Hu, Z., Liu, F., Wang, Y., and Wagner, T.: Pinpointing nitrogen oxide emissions from space, Sci. Adv., 5, eaax9800, 2019.

655   Belmonte Rivas, M., Veefkind, P., Boersma, F., Levelt, P., Eskes, H., and Gille, J.: Intercomparison of daytime stratospheric NO_2 satellite retrievals and model simulations, Atmos. Meas. Tech., 7, 2203–2225, 2014.

Bergemann, C., Meyer-Arnek, J., and Baier, F.: Estimation and causes of uncertainty of air quality forecasts for the Blackforest region, in: Wiss. Mitteil. Inst. f. Meteorol. Univ. Leipzig Band 49(2012), Tagungsband der METTOOLS VIII, Leipzig, Germany, 2012.

Biswal, A., Singh, V., Singh, S., Kesarkar, A. P., Ravindra, K., Sokhi, R. S., Chipperfield, M. P., Dhomse, S. S., Pope, R. J., Singh, T., and
660   Mor, S.: COVID-19 lockdown induced changes in NO_2 levels across India observed by multi-satellite and surface observations, Atmos. Chem. Phys. Discuss., 2020, 1–28, 2020.

Boersma, K. F., Eskes, H. J., and Brinksma, E. J.: Error analysis for tropospheric NO_2 retrieval from space, J. Geophys. Res. Atmos., 109, D04 311, 2004.

Boersma, K. F., Eskes, H. J., Veefkind, J. P., Brinksma, E. J., van der A, R. J., Sneep, M., van den Oord, G. H. J., Levelt, P. F., Stammes, P.,
665   Gleason, J. F., and Bucsela, E. J.: Near-real time retrieval of tropospheric NO_2 from OMI, Atmos. Chem. Phys., 7, 2103–2118, 2007.

Boersma, K. F., Eskes, H. J., Dirksen, R. J., van der A, R. J., Veefkind, J. P., Stammes, P., Huijnen, V., Kleipool, Q. L., Sneep, M., Claas, J., Leitão, J., Richter, A., Zhou, Y., and Brunner, D.: An improved tropospheric NO_2 column retrieval algorithm for the Ozone Monitoring Instrument, Atmos. Meas. Tech., 4, 1905–1928, 2011.

Boersma, K. F., Vinken, G. C. M., and Eskes, H. J.: Representativeness errors in comparing chemistry transport and chemistry climate models
670   with satellite UV–Vis tropospheric column retrievals, Geosci. Model Dev., 9, 875, 2016.

Boersma, K. F., Eskes, H. J., Richter, A., De Smedt, I., Lorente, A., Beirle, S., van Geffen, J. H. G. M., Zara, M., Peters, E., Van Roozendael, M., Wagner, T., Maasakkers, J. D., van der A, R. J., Nightingale, J., De Rudder, A., Irie, H., Pinardi, G., Lambert, J.-C., and Compernolle, S. C.: Improving algorithms and uncertainty estimates for satellite NO_2 retrievals: results from the quality assurance for the essential climate variables (QA4ECV) project, Atmos. Meas. Tech., 11, 6651–6678, 2018.

675   Boutahar, J., Lacour, S., Mallet, V., Quélo, D., Roustan, Y., and Sportisse, B.: Development and validation of a fully modular platform for numerical modelling of air pollution: POLAIR, Int. J. Environ. Pollut., 22, 17–28, 2004.

Bovensmann, H., Burrows, J. P., Buchwitz, M., Frerick, J., Rozanov, V. V., Chance, K. V., and Goede, A. P. H.: SCIAMACHY: Mission objectives and measurement modes, J. Atmos. Sci., 56, 127–150, 1999.

Brion, J., Chakir, A., Charbonnier, J., Daumont, D., Parisse, C., and Malicet, J.: Absorption spectra measurements for the ozone molecule in
680   the 350–830 nm region, J. Atmos. Chem., 30, 291–299, 1998.

Bucsela, E. J., Celarier, E. A., Wenig, M. O., Gleason, J. F., Veefkind, J. P., Boersma, K. F., and Brinksma, E. J.: Algorithm for NO_2 vertical column retrieval from the ozone monitoring instrument, IEEE Trans. Geosci. Remote Sens., 44, 1245–1258, 2006.

Bucsela, E. J., Krotkov, N. A., Celarier, E. A., Lamsal, L. N., Swartz, W. H., Bhartia, P. K., Boersma, K. F., Veefkind, J. P., Gleason, J. F., and Pickering, K. E.: A new stratospheric and tropospheric NO_2 retrieval algorithm for nadir-viewing satellite instruments: applications to OMI, Atmos. Meas. Tech., 6, 2607–2626, 2013.

Burrows, J. P., Weber, M., Buchwitz, M., Rozanov, V., Ladstätter-Weißenmayer, A., Richter, A., DeBeek, R., Hoogen, R., Bramstedt, K., Eichmann, K.-U., Eisinger, M., and Perner, D.: The global ozone monitoring experiment (GOME): Mission concept and first scientific results, J. Atmos. Sci., 56, 151–175, 1999.

Cahalan, R. F., Ridgway, W., Wiscombe, W. J., Bell, T. L., and Snider, J. B.: The albedo of fractal stratocumulus clouds, J. Atmos. Sci., 51, 2434–2455, 1994.

Callies, J., Corpaccioli, E., Eisinger, M., Hahne, A., and Lefebvre, A.: GOME-2-Metop's second-generation sensor for operational ozone monitoring, ESA bulletin, 102, 28–36, 2000.

Celarier, E. A., Brinksma, E. J., Gleason, J. F., Veefkind, J. P., Cede, A., Herman, J. R., Ionov, D., Goutail, F., Pommereau, J.-P., Lambert, J.-C., van Roozendael, M., Pinardi, G., Wittrock, F., Schönhardt, A., Richter, A., Ibrahim, O. W., Wagner, T., Bojkov, B., Mount, G., Spinei, E., Chen, C. M., Pongetti, T. J., Sander, S. P., Bucsela, E. J., Wenig, M. O., Swart, D. P. J., Volten, H., Kroon, M., and Levelt, P. F.: Validation of Ozone Monitoring Instrument nitrogen dioxide columns, J. Geophys. Res. Atmos., 113, D15S15, 2008.

Chan, K. L., Wiegner, M., van Geffen, J., De Smedt, I., Alberti, C., Cheng, Z., Ye, S., and Wenig, M.: MAX-DOAS measurements of tropospheric NO_2 and HCHO in Munich and the comparison to OMI and TROPOMI satellite observations, Atmos. Meas. Tech., 13, 4499–4520, 2020.

Charlson, R. J. and Ahlquist, N. C.: Brown haze: NO_2 or aerosol?, Atmos. Environ., 3, 653–656, 1969.

Chen, D., Zhou, B., Beirle, S., Chen, L., and Wagner, T.: Tropospheric NO_2 column densities deduced from zenith-sky DOAS measurements in Shanghai, China, and their application to satellite validation, Atmos. Chem. Phys., 9, 3641–3662, 2009.

Chimot, J., Veefkind, J. P., Haan, J. F. d., Stammes, P., and Levelt, P. F.: Minimizing aerosol effects on the OMI tropospheric NO_2 retrieval– An improved use of the 477 nm O_2-O_2 band and an estimation of the aerosol correction uncertainty, Atmos. Meas. Tech., 12, 491–516, 2019.

Compernolle, S., Verhoelst, T., Pinardi, G., Granville, J., Hubert, D., Keppens, A., Niemeijer, S., Rino, B., Bais, A., Beirle, S., Boersma, F., Burrows, J. P., De Smedt, I., Eskes, H., Goutail, F., Hendrick, F., Lorente, A., Pazmino, A., Piters, A., Peters, E., Pommereau, J.-P., Remmers, J., Richter, A., van Geffen, J., Van Roozendael, M., Wagner, T., and Lambert, J.-C.: Validation of Aura-OMI QA4ECV NO_2 climate data records with ground-based DOAS networks: the role of measurement and comparison uncertainties, Atmos. Chem. Phys., 20, 8017–8045, 2020.

Compernolle, S., Argyrouli, A., Lutz, R., Sneep, M., Lambert, J.-C., Fjæraa, A. M., Hubert, D., Keppens, A., Loyola, D., O'Connor, E., Romahn, F., Stammes, P., Verhoelst, T., and Wang, P.: Validation of the Sentinel-5 Precursor TROPOMI cloud data with Cloudnet, Aura OMI O_2-O_2, MODIS and Suomi-NPP VIIRS, Atmos. Meas. Tech., 14, 2451–2476, 2021.

Cooper, M. J., Martin, R. V., McLinden, C. A., and Brook, J. R.: Inferring ground-level nitrogen dioxide concentrations at fine spatial resolution applied to the TROPOMI satellite instrument, Environ. Res. Lett., 15, 104 013, 2020.

Crippa, M., Guizzardi, D., Muntean, M., Schaaf, E., Dentener, F., van Aardenne, J. A., Monni, S., Doering, U., Olivier, J. G. J., Pagliari, V., and Janssens-Maenhout, G.: Gridded emissions of air pollutants for the period 1970-2012 within EDGAR v4. 3.2, Earth Syst. Sci. Data, 10, 1987–2013, 2018.

Crutzen, P. J.: The influence of nitrogen oxides on the atmospheric ozone content, Q. J. R. Meteorol. Soc., 96, 320–325, 1970.

Danckaert, T., Fayt, C., Van Roozendael, M., De Smedt, I., Letocart, V., Merlaud, A., and Pinardi, G.: QDOAS software user manual, 2017.

De Smedt, I., Theys, N., Yu, H., Danckaert, T., Lerot, C., Compernolle, S., Van Roozendael, M., Richter, A., Hilboll, A., Peters, E., Pedergnana, M., Loyola, D., Beirle, S., Wagner, T., Eskes, H., van Geffen, J., Boersma, K. F., and Veefkind, P.: Algorithm theoretical baseline for formaldehyde retrievals from S5P TROPOMI and from the QA4ECV project., Atmos. Meas. Tech., 11, 2395–2426, 2018.

Debry, E., Fahey, K., Sartelet, K., Sportisse, B., and Tombette, M.: Technical Note: A new SIze REsolved Aerosol Model (SIREAM), Atmos. Chem. Phys., 7, 1537–1547, 2007.

Denier van der Gon, H. A. C., Visschedijk, A., Van der Brugh, H., and Dröge, R.: A high resolution European emission data base for the year 2005, a contribution to UBA-Projekt PAREST: Particle Reduction Strategies, TNO-report TNO-034-UT-2010-01895 RPTML, Utrecht, 2010.

Dimitropoulou, E., Hendrick, F., Pinardi, G., Friedrich, M. M., Merlaud, A., Tack, F., De Longueville, H., Fayt, C., Hermans, C., Laffineur, Q., Fierens, F., and Van Roozendael, M.: Validation of TROPOMI tropospheric NO_2 columns using dual-scan multi-axis differential optical absorption spectroscopy (MAX-DOAS) measurements in Uccle, Brussels, Atmos. Meas. Tech., 13, 5165–5191, 2020.

Ding, J., van der A, R. J., Eskes, H., Mijling, B., Stavrakou, T., Van Geffen, J., and Veefkind, J. P.: NO_x emissions reduction and rebound in China due to the COVID-19 crisis, Geophys. Res. Lett., 47, e2020GL089 912, 2020.

Dirksen, R. J., Boersma, K. F., Eskes, H. J., Ionov, D. V., Bucsela, E. J., Levelt, P. F., and Kelder, H. M.: Evaluation of stratospheric NO_2 retrieved from the Ozone Monitoring Instrument: Intercomparison, diurnal cycle, and trending, J. Geophys. Res. Atmos., 116, D8, 2011.

Doicu, A., Trautmann, T., and Schreier, F.: Numerical regularization for atmospheric inverse problems, Springer Science & Business Media, 2010.

Drosoglou, T., Bais, A. F., Zyrichidou, I., Kouremeti, N., Poupkou, A., Liora, N., Giannaros, C., Koukouli, M. E., Balis, D., and Melas, D.: Comparisons of ground-based tropospheric NO_2 MAX-DOAS measurements to satellite observations with the aid of an air quality model over the Thessaloniki area, Greece, Atmos. Chem. Phys., 17, 5829–5849, 2017.

Drosoglou, T., Koukouli, M. E., Kouremeti, N., Bais, A. F., Zyrichidou, I., Balis, D., van der A, R. J., Xu, J., and Li, A.: MAX-DOAS NO_2 observations over Guangzhou, China; ground-based and satellite comparisons, Atmos. Meas. Tech., 11, 2239–2255, 2018.

Efremenko, D. S., Loyola, D. G., Hedelt, P., and Spurr, R. J. D.: Volcanic SO_2 plume height retrieval from UV sensors using a full-physics inverse learning machine algorithm, Int. J. Remote Sensing, 38, 1–27, 2017.

Eskes, H. J. and Boersma, K. F.: Averaging kernels for DOAS total-column satellite retrievals, Atmos. Chem. Phys., 3, 1285–1291, 2003.

Eskes, H. J., Velthoven, P. F. J. V., Valks, P. J. M., and Kelder, H. M.: Assimilation of GOME total-ozone satellite observations in a three-dimensional tracer-transport model, Quart. J. R. Met. Soc., 129, 1663–1681, 2003.

Eskes, H. J., Eichmann, K.-U., Lambert, J. C., Loyola, D., Veefkind, J. P., Dehn, A., and Zehner, C.: S5P Mission Performance Centre Nitrogen Dioxide, Tech. rep., S5P-MPC-KNMI-PRF-NO2 issue 1.6, 2020.

European Commission: The EU Environmental Implementation Review: Common challenges and how to combine efforts to deliver better results, Tech. rep., Ref.: SWD(2017)33-60 fina, 2017.

Fayt, C., De Smedt, I., Letocart, V., Merlaud, A., Pinardi, G., and Van Roozendael, M.: QDOAS Software user manual, Tech. rep., IASB/BIRA, Uccle, Belgium, http://uv-vis.aeronomie.be/software/QDOAS, 2011.

Ferlay, N., Thieuleux, F., Cornet, C., Davis, A. B., Dubuisson, P., Ducos, F., Parol, F., Riédi, J., and Vanbauce, C.: Toward new inferences about cloud structures from multidirectional measurements in the oxygen A band: Middle-of-cloud pressure and cloud geometrical thickness from POLDER-3/PARASOL, J. Appl. Meteorol. Climatol., 49, 2492–2507, 2010.

Georgoulias, A. K., Boersma, K. F., van Vliet, J., Zhang, X., van der A, R. J., Zanis, P., and de Laat, J.: Detection of NO_2 pollution plumes from individual ships with the TROPOMI/S5P satellite sensor, Environ. Res. Lett., 15, 124 037, 2020.

Gielen, C., Van Roozendael, M., Hendrick, F., Pinardi, G., Vlemmix, T., De Bock, V., De Backer, H., Fayt, C., Hermans, C., Gillotay, D., and Wang, P.: A simple and versatile cloud-screening method for MAX-DOAS retrievals, Atmos. Meas. Tech., 7, 3509–3527, 2014.

Goldberg, D. L., Anenberg, S. C., Griffin, D., McLinden, C. A., Lu, Z., and Streets, D. G.: Disentangling the impact of the COVID-19 lockdowns on urban NO_2 from natural variability, Geophys. Res. Lett., 47, e2020GL089 269, 2020.

Goldberg, D. L., Anenberg, S., Mohegh, A., Lu, Z., and Streets, D. G.: TROPOMI NO_2 in the United States: A detailed look at the annual averages, weekly cycles, effects of temperature, and correlation with surface NO_2 concentrations, Earth's Future, 9, e2020EF001 665, 2021.

Grainger, J. F. and Ring, J.: Anomalous Fraunhofer line profiles, Nature, 193, 762, 1962.

Granier, C., Bessagnet, B., Bond, T., D'Angiola, A., van Der Gon, H. D., Frost, G. J., Heil, A., Kaiser, J. W., Kinne, S., Klimont, Z., Kloster, S., Lamarque, J.-F., Liousse, C., Masui, T., Meleux, F., Mieville, A., Ohara, T., Raut, J.-C., Riahi, K., Schultz, M. G., Smith, S. J., Thompson, A., van Aardenne, J., van der Werf, G. R., and van Vuuren, D. P.: Evolution of anthropogenic and biomass burning emissions of air pollutants at global and regional scales during the 1980–2010 period, Clim. Change, 109, 163, 2011.

Griffin, D., Zhao, X., McLinden, C. A., Boersma, F., Bourassa, A., Dammers, E., Degenstein, D., Eskes, H. J., Fehr, L., Fioletov, V., Hayden, K., Kharol, S. K., Li, S.-M., Makar, P., Martin, R. V., Mihele, C., Mittermeier, R. L., Krotkov, N., Sneep, M., Lamsal, L. N., Linden, M. t., Geffen, J. v., Veefkind, P., and Wolde, M.: High-resolution mapping of nitrogen dioxide with TROPOMI: First results and validation over the Canadian oil sands, Geophys. Res. Lett., 46, 1049–1060, 2019.

Heckel, A., Richter, A., Tarsu, T., Wittrock, F., Hak, C., Pundt, I., Junkermann, W., and Burrows, J. P.: MAX-DOAS measurements of formaldehyde in the Po-Valley, Atmos. Chem. Phys., 5, 909–918, 2005.

Heckel, A., Kim, S.-W., Frost, G. J., Richter, A., Trainer, M., and Burrows, J. P.: Influence of low spatial resolution a priori data on tropospheric NO_2 satellite retrievals, Atmos. Meas. Tech., 4, 1805–1820, 2011.

Hedelt, P., Efremenko, D. S., Loyola, D. G., Spurr, R., and Clarisse, L.: Sulfur dioxide layer height retrieval from Sentinel-5 Precursor/TROPOMI using FP_ILM., Atmos. Meas. Tech., 12, 5503–5517, 2019.

Hendrick, F., Müller, J.-F., Clémer, K., Wang, P., De Mazière, M., Fayt, C., Gielen, C., Hermans, C., Ma, J. Z., Pinardi, G., Stavrakou, T., Vlemmix, T., and Van Roozendael, M.: Four years of ground-based MAX-DOAS observations of HONO and NO_2 in the Beijing area, Atmos. Chem. Phys., 14, 765–781, 2014.

Holtslag, A. A. M. and Boville, B. A.: Local versus nonlocal boundary-layer diffusion in a global climate model, J. Clim., 6, 1825–1842, 1993.

Hönninger, G., Friedeburg, C. v., and Platt, U.: Multi axis differential optical absorption spectroscopy (MAX-DOAS), Atmos. Chem. Phys., 4, 231–254, 2004.

Huang, G. and Sun, K.: Non-negligible impacts of clean air regulations on the reduction of tropospheric NO_2 over East China during the COVID-19 pandemic observed by OMI and TROPOMI, Sci. Total Environ., 745, 141 023, 2020.

Huber, D. E., Steiner, A. L., and Kort, E. A.: Daily Cropland Soil NO_x Emissions Identified by TROPOMI and SMAP, Geophys. Res. Lett., 47, e2020GL089 949, 2020.

Huijnen, V., Williams, J., van Weele, M., van Noije, T., Krol, M., Dentener, F., Segers, A., Houweling, S., Peters, W., de Laat, J., Boersma, F., Bergamaschi, P., van Velthoven, P., Le Sager, P., Eskes, H. J., Alkemade, F., Scheele, R., Nédélec, P., and Pätz, H.-W.: The global chemistry transport model TM5: description and evaluation of the tropospheric chemistry version 3.0, Geosci. Model Dev., 3, 445–473, 2010.

Huijnen, V., Flemming, J., Chabrillat, S., Errera, Q., Christophe, Y., Blechschmidt, A.-M., Richter, A., and Eskes, H. J.: C-IFS-CB05-BASCOE: stratospheric chemistry in the Integrated Forecasting System of ECMWF, Geosci. Model Dev., 9, 3071–3091, 2016.

Ialongo, I., Virta, H., Eskes, H. J., Hovila, J., and Douros, J.: Comparison of TROPOMI/Sentinel-5 Precursor NO_2 observations with ground-based measurements in Helsinki., Atmos. Meas. Tech., 13, 205–218, 2020.

800 Irie, H., Kanaya, Y., Akimoto, H., Tanimoto, H., Wang, Z., Gleason, J., and Bucsela, E. J.: Validation of OMI tropospheric NO_2 column data using MAX-DOAS measurements deep inside the North China Plain in June 2006: Mount Tai Experiment 2006, Atmos. Chem. Phys., 8, 6577–6586, 2008.

Irie, H., Takashima, H., Kanaya, Y., Boersma, K. F., Gast, L., Wittrock, F., Brunner, D., Zhou, Y., and Roozendael, M. V.: Eight-component retrievals from ground-based MAX-DOAS observations, Atmos. Meas. Tech., 4, 1027–1044, 2011.

805 Khorsandi, E., Baier, F., Erbertseder, T., and Bittner, M.: Air quality monitoring and simulation on urban scale over Munich, in: Remote Sensing Technologies and Applications in Urban Environments III, vol. 10793, p. 1079303, International Society for Optics and Photonics, 2018.

Kleipool, Q. L., Dobber, M. R., de Haan, J. F., and Levelt, P. F.: Earth surface reflectance climatology from 3 years of OMI data, J. Geophys. Res. Atmos., 113, D18 308, 2008.

810 Koelemeijer, R. B. A., Stammes, P., Hovenier, J. W., and De Haan, J. F.: A fast method for retrieval of cloud parameters using oxygen A band measurements from the Global Ozone Monitoring Experiment, J. Geophys. Res. Atmos., 106, 3475–3490, 2001.

Kokhanovsky, A. A. and Rozanov, V. V.: The uncertainties of satellite DOAS total ozone retrieval for a cloudy sky, Atmos. Environ., 87, 27–36, 2008.

Koukouli, M.-E., Skoulidou, I., Karavias, A., Parcharidis, I., Balis, D., Manders, A., Segers, A., Eskes, H., and van Geffen, J.: Sudden changes
815 in nitrogen dioxide emissions over Greece due to lockdown after the outbreak of COVID-19, Atmos. Chem. Phys., 21, 1759–1774, 2021.

Kuenen, J. J. P., Visschedijk, A. J. H., Jozwicka, M., and Denier Van Der Gon, H. A. C.: TNO-MACC_II emission inventory; a multi-year (2003–2009) consistent high-resolution European emission inventory for air quality modelling, Atmos. Chem. Phys., 14, 10 963–10 976, 2014.

Kuhlmann, G., Lam, Y. F., Cheung, H. M., Hartl, A., Fung, J. C. H., Chan, P. W., and Wenig, M.: Development of a custom OMI NO_2 data
820 product for evaluating biases in a regional chemistry transport model, Atmos. Chem. Phys., 15, 5627–5644, 2015.

Lampel, J., Pöhler, D., Tschritter, J., Frieß, U., and Platt, U.: On the relative absorption strengths of water vapour in the blue wavelength range, Atmos. Meas. Tech., 8, 4329–4346, 2015.

Laughner, J. L., Zare, A., and Cohen, R. C.: Effects of daily meteorology on the interpretation of space-based remote sensing of NO_2, Atmos. Chem. Phys., 16, 15 247–15 264, 2016.

825 Laughner, J. L., Zhu, Q., and Cohen, R. C.: The Berkeley High Resolution Tropospheric NO_2 product, Earth Syst. Sci. Data, 10, 2069–2095, 2018.

Leitão, J., Richter, A., Vrekoussis, M., Kokhanovsky, A., Zhang, Q., Beekmann, M., and Burrows, J. P.: On the improvement of NO_2 satellite retrievals–aerosol impact on the airmass factors, Atmos. Meas. Tech., 3, 475–493, 2010.

Leue, C., Wenig, M., Wagner, T., Klimm, O., Platt, U., and Jähne, B.: Quantitative analysis of NO_x emissions from Global Ozone Monitoring
830 Experiment satellite image sequences, J. Geophys. Res. Atmos., 106, 5493–5505, 2001.

Levelt, P. F., Van den Oord, G. H. J., Dobber, M. R., Malkki, A., Visser, H., de Vries, J., Stammes, P., Lundell, J., and Saari, H.: The Ozone Monitoring Instrument, IEEE T. Geosci. Remote Sens., 44, 1093–1101, 2006.

Levelt, P. F., Joiner, J., Tamminen, J., Veefkind, J. P., Bhartia, P. K., Stein Zweers, D. C., Duncan, B. N., Streets, D. G., Eskes, H., van der
A, R., McLinden, C., Fioletov, V., Carn, S., de Laat, J., DeLand, M., Marchenko, S., McPeters, R., Ziemke, J., Fu, D., Liu, X., Pickering,
835   K., Apituley, A., González Abad, G., Arola, A., Boersma, F., Chan Miller, C., Chance, K., de Graaf, M., Hakkarainen, J., Hassinen, S.,
Ialongo, I., Kleipool, Q., Krotkov, N., Li, C., Lamsal, L., Newman, P., Nowlan, C., Suleiman, R., Tilstra, L. G., Torres, O., Wang, H., and
Wargan, K.: The Ozone Monitoring Instrument: overview of 14 years in space, Atmos. Chem. Phys., 18, 5699–5745, 2018.

Li, T., Wang, Y., and Yuan, Q.: Remote Sensing Estimation of Regional NO_2 via Space-Time Neural Networks, Remote Sens., 12, 2514,
2020.

840   Lin, J. T., Martin, R. V., Boersma, K. F., Sneep, M., Stammes, P., Spurr, R., Wang, P., Van Roozendael, M., Clémer, K., and Irie, H.:
Retrieving tropospheric nitrogen dioxide from the Ozone Monitoring Instrument: effects of aerosols, surface reflectance anisotropy, and
vertical profile of nitrogen dioxide, Atmos. Chem. Phys., 14, 1441–1461, 2014.

Liu, F., Page, A., Strode, S. A., Yoshida, Y., Choi, S., Zheng, B., Lamsal, L. N., Li, C., Krotkov, N. A., Eskes, H., van der A, R. J., Veefkind,
P., Levelt, P. F., Hauser, O. P., and Joiner, J.: Abrupt decline in tropospheric nitrogen dioxide over China after the outbreak of COVID-19,
845   Sci. Adv., 6, eabc2992, 2020a.

Liu, M., Lin, J., Boersma, K. F., Pinardi, G., Wang, Y., Chimot, J., Wagner, T., Xie, P., Eskes, H., Van Roozendael, M., Hendrick, F., Wang,
P., Wang, T., Yan, Y., Chen, L., and Ni, R.: Improved aerosol correction for OMI tropospheric NO_2 retrieval over East Asia: constraint
from CALIOP aerosol vertical profile, Atmos. Meas. Tech., 12, 1–21, 2019a.

Liu, M., Lin, J., Kong, H., Boersma, K. F., Eskes, H. J., Kanaya, Y., He, Q., Tian, X., Qin, K., Xie, P., Spurr, R., Ni, R., Yan, Y., Weng, H.,
850   and Wang, J.: A new TROPOMI product for tropospheric NO_2 columns over East Asia with explicit aerosol corrections, Atmos. Meas.
Tech., 13, 4247–4259, 2020b.

Liu, S., Valks, P., Pinardi, G., De Smedt, I., Yu, H., Beirle, S., and Richter, A.: An Improved Total and Tropospheric NO_2 Column Retrieval
for GOME-2, Atmos. Meas. Tech., 12, 1029–1057, 2019b.

Liu, S., Valks, P., Pinardi, G., Xu, J., Argyrouli, A., Lutz, R., Tilstra, L. G., Huijnen, V., Hendrick, F., and Roozendael, M. V.: An improved air
855   mass factor calculation for nitrogen dioxide measurements from the Global Ozone Monitoring Experiment-2 (GOME-2), Atmos. Meas.
Tech., 13, 755–787, 2020c.

Lorente, A., Folkert Boersma, K., Yu, H., Dörner, S., Hilboll, A., Richter, A., Liu, M., Lamsal, L. N., Barkley, M., De Smedt, I., Van Roozen-
dael, M., Wang, Y., Wagner, T., Beirle, S., Lin, J.-T., Krotkov, N., Stammes, P., Wang, P., Eskes, H. J., and Krol, M.: Structural uncertainty
in air mass factor calculation for NO_2 and HCHO satellite retrievals, Atmos. Meas. Tech., 10, 759–782, 2017.

860   Lorente, A., Boersma, K. F., Stammes, P., Tilstra, L. G., Richter, A., Yu, H., Kharbouche, S., and Muller, J.-P.: The importance of surface
reflectance anisotropy for cloud and NO_2 retrievals from GOME-2 and OMI, Atmos. Meas. Tech., 11, 4509–4529, 2018.

Lorente, A., Boersma, K. F., Eskes, H. J., Veefkind, J. P., Van Geffen, J., de Zeeuw, M. B., van der Gon, H. A. C. D., Beirle, S., and Krol,
M. C.: Quantification of nitrogen oxides emissions from build-up of pollution over Paris with TROPOMI, Sci. Rep., 9, 20 033, 2019.

Loyola, D., Pedergnana, M., and García, S. G.: Smart sampling and incremental function learning for very large high dimensional data,
865   Neural Netw., 78, 75–87, 2016.

Loyola, D., Lutz, R., Argyrouli, A., and Spurr, R.: S5P/TROPOMI ATBD Cloud Products, Tech. rep., S5P-DLR-L2-ATBD-400I issue 2.2,
2020a.

Loyola, D., Xu, J., Heue, K.-P., and Zimmer, W.: Applying FP_ILM to the retrieval of geometry-dependent effective Lambertian equivalent
reflectivity (GE_LER) daily maps from UVN satellite measurements., Atmos. Meas. Tech., 13, 985–999, 2020b.

870   Loyola, D. G., Gimeno García, S., Lutz, R., Argyrouli, A., Romahn, F., Spurr, R. J. D., Pedergnana, M., Doicu, A., Molina García, V., and Schüssler, O.: The operational cloud retrieval algorithms from TROPOMI on board Sentinel-5 Precursor, Atmos. Meas. Tech., 11, 409–427, 2018.

Lutz, R., Loyola, D., Gimeno García, S., and Romahn, F.: OCRA radiometric cloud fractions for GOME-2 on MetOp-A/B, Atmos. Meas. Tech., 9, 2357–2379, 2016.

875   Ma, J. Z., Beirle, S., Jin, J. L., Shaiganfar, R., Yan, P., and Wagner, T.: Tropospheric NO_2 vertical column densities over Beijing: results of the first three years of ground-based MAX-DOAS measurements (2008–2011) and satellite validation, Atmos. Chem. Phys., 13, 1547–1567, 2013.

Mallet, V., Quélo, D., Sportisse, B., Ahmed de Biasi, M., Debry, E., Korsakissok, I., Wu, L., Roustan, Y., Sartelet, K., Tombette, M., and Foudhil, H.: The air quality modeling system Polyphemus, Atmos. Chem. Phys., 7, 5479–5487, 2007.

880   Martin, R. V., Chance, K., Jacob, D. J., Kurosu, T. P., Spurr, R. J., Bucsela, E., Gleason, J. F., Palmer, P. I., Bey, I., Fiore, A. M., et al.: An improved retrieval of tropospheric nitrogen dioxide from GOME, J. Geophys. Res. Atmos., 107, 4437, 2002.

Martin, R. V., Jacob, D. J., Chance, K., Kurosu, T. P., Palmer, P. I., and Evans, M. J.: Global inventory of nitrogen oxide emissions constrained by space-based observations of NO_2 columns, J. Geophys. Res. Atmos., 108, 4537, 2003.

McCormick, J.: Acid Earth: the global threat of acid pollution, Routledge, 2013.

885   McLinden, C. A., Fioletov, V., Boersma, K. F., Kharol, S. K., Krotkov, N., Lamsal, L., Makar, P. A., Martin, R. V., Veefkind, J. P., and Yang, K.: Improved satellite retrievals of NO_2 and SO_2 over the Canadian oil sands and comparisons with surface measurements, Atmos. Chem. Phys., 14, 3637–3656, 2014.

Munro, R., Eisinger, M., Anderson, C., Callies, J., Corpaccioli, E., Lang, R., Lefebvre, A., Livschitz, Y., and Albinana, A. P.: GOME-2 on MetOp, in: Proc. of The 2006 EUMETSAT Meteorological Satellite Conference, Helsinki, Finland, vol. 1216, p. 48, 2006.

890   Munro, R., Lang, R., Klaes, D., Poli, G., Retscher, C., Lindstrot, R., Huckle, R., Lacan, A., Grzegorski, M., Holdak, A., Kokhanovsky, A., Livschitz, J., and Eisinger, M.: The GOME-2 instrument on the Metop series of satellites: instrument design, calibration, and level 1 data processing – an overview, Atmos. Meas. Tech., 9, 1279–1301, 2016.

Nüß, H., Richter, A., Valks, P., and Burrows, J.: Improvement of the NO_2 total column retrieval for GOME-2, O3M SAF Visiting Scientist Activity, Final Report, IUP University of Bremen, 2006.

895   Peters, E., Wittrock, F., Richter, A., Alvarado, L. M. A., Rozanov, V. V., and Burrows, J. P.: Liquid water absorption and scattering effects in DOAS retrievals over oceans, Atmos. Meas. Tech., 7, 4203–4221, 2014.

Pinardi, G., Van Roozendael, M., Lambert, J.-C., Granville, J., Hendrick, F., Tack, F., Yu, H., Cede, A., Kanaya, Y., Irie, I., Goutail, F., Pommereau, J.-P., Pazmino, A., Wittrock, F., Richter, A., Wagner, T., Gu, M., Remmers, J., Friess, U., Vlemmix, T., Piters, A., Hao, N., Tiefengraber, M., Herman, J., Abuhassan, N., Bais, A., Kouremeti, N., Hovila, J., Holla, R., Chong, J., Postylyakov, O., and Ma, J.:

900   GOME-2 total and tropospheric NO_2 validation based on zenith-sky, direct-sun and multi-axis DOAS network observations, in: Proc. of the 2014 EUMETSAT Meteorological Satellite Conference, Geneva, Swizerland, EUMETSAT, 2014.

Pinardi, G., Lambert, J.-C., Granville, J., Yu, H., De Smedt, I., van Roozendael, M., and Valks, P.: O3M-SAF validation report, Tech. rep., SAF/O3M/IASB/VR/NO2/TN-IASB-GOME2-O3MSAF-NO2-2015, Issue 1/1, 2015.

Pinardi, G., Van Roozendael, M., Hendrick, F., Theys, N., Abuhassan, N., Bais, A., Boersma, F., Cede, A., Chong, J., Donner, S., Drosoglou,

905   T., Dzhola, A., Eskes, H. J., Frieß, U., Granville, J., Herman, J. R., Holla, R., Hovila, J., Irie, H., Kanaya, Y., Karagkiozidis, D., Kouremeti, N., Lambert, J.-C., Ma, J., Peters, E., Piters, A., Postylyakov, O., Richter, A., Remmers, J., Takashima, H., Tiefengraber, M., Valks, P.,

Vlemmix, T., Wagner, T., and Wittrock, F.: Validation of tropospheric NO_2 column measurements of GOME-2A and OMI using MAX-DOAS and direct sun network observations, Atmos. Meas. Tech., 13, 6141–6174, 2020.

Platt, U. and Stutz, J.: Differential Optical Absorption Spectroscopy, Springer, 2008.

910 Pope, R. M. and Fry, E. S.: Absorption spectrum (380–700 nm) of pure water. II. Integrating cavity measurements, Appl. Opt., 36, 8710–8723, 1997.

Popp, C., Wang, P., Brunner, D., Stammes, P., Zhou, Y., and Grzegorski, M.: MERIS albedo climatology for FRESCO+ O_2 A-band cloud retrieval, Atmos. Meas. Tech., 4, 463–483, 2011.

Qin, W., Fasnacht, Z., Haffner, D., Vasilkov, A., Joiner, J., Krotkov, N., Fisher, B., and Spurr, R.: A geometry-dependent surface Lambertian-
915 equivalent reflectivity product for UV–Vis retrievals–Part 1: Evaluation over land surfaces using measurements from OMI at 466 nm, Atmos. Meas. Tech., 12, 3997–4017, 2019.

Richter, A. and Lange, K.: What is the short-term variability of NO_2 in the atmosphere?, in: MAX-DOAS Workshop, Bremen, Germany, 2021.

Richter, A. et al.: S5P/TROPOMI Science Verification Report, Tech. rep., S5P-IUP-L2-ScVR-RP issue 2.1, 2015.

920 Rodgers, C. D.: Inverse methods for atmospheric sounding: theory and practice, vol. 2, World scientific, 2000.

Rothman, L. S., Gordon, I. E., Barber, R. J., Dothe, H., Gamache, R. R., Goldman, A., Perevalov, V. I., Tashkun, S. A., and Tennyson, J.: HITEMP, the high-temperature molecular spectroscopic database, J. Quant. Spectrosc. Radiat. Transf., 111, 2139–2150, 2010.

Russell, A. R., Perring, A. E., Valin, L. C., Bucsela, E., Browne, E. C., Wooldridge, P. J., and Cohen, R. C.: A high spatial resolution retrieval of NO_2 column densities from OMI: method and evaluation, Atmos. Chem. Phys., 11, 8543–8554, 2011.

925 Russell, G. L. and Lerner, J. A.: A new finite-differencing scheme for the tracer transport equation, J. Appl. Meteorol., 20, 1483–1498, 1981.

Saiedy, F., Jacobowitz, H., and Wark, D.: On cloud-top determination from Gemini-5, J. Atmos. Sci., 24, 63–69, 1967.

Schell, B., Ackermann, I. J., Hass, H., Binkowski, F. S., and Ebel, A.: Modeling the formation of secondary organic aerosol within a comprehensive air quality model system, J. Geophys. Res. Atmos., 106, 28 275–28 293, 2001.

Sen, P. K.: Estimates of the regression coefficient based on Kendall's tau, J. Am. Stat. Assoc., 63, 1379–1389, 1968.

930 Simpson, D., Winiwarter, W., Börjesson, G., Cinderby, S., Ferreiro, A., Guenther, A., Hewitt, C. N., Janson, R., Khalil, M. A. K., Owen, S., Pierce, T. E., Puxbaum, H., Shearer, M., Skiba, U., Steinbrecher, R., Tarrasón, L., and Öquist, M. G.: Inventorying emissions from nature in Europe, J. Geophys. Res. Atmos., 104, 8113–8152, 1999.

Skamarock, W. C., Klemp, J. B., Dudhia, J., Gill, D. O., Barker, D. M., Duda, M. G., Huang, X.-Y., Wang, W., , and Powers, J. G.: A Description of the Advanced Research WRF Version 3, Tech. rep., NCAR Tech. Note NCAR/TN-475+STR, 2008.

935 Solomon, S., Schmeltekopf, A. L., and Sanders, R. W.: On the interpretation of zenith sky absorption measurements, J. Geophys. Res. Atmos., 92, 8311–8319, 1987.

Spurr, R. J.: VLIDORT: A linearized pseudo-spherical vector discrete ordinate radiative transfer code for forward model and retrieval studies in multilayer multiple scattering media, J. Quant. Spectrosc. Radiat. Transf., 102, 316–342, 2006.

Spurr, R. J. D., Kurosu, T. P., and Chance, K. V.: A linearized discrete ordinate radiative transfer model for atmospheric remote-sensing
940 retrieval, J. Quant. Spectrosc. Radiat. Transf., 68, 689–735, 2001.

Stavrakou, T., Müller, J.-F., Bauwens, M., Boersma, K. F., and van Geffen, J.: Satellite evidence for changes in the NO_2 weekly cycle over large cities, Sci. Rep., 10, 1–9, 2020.

Stockwell, W. R., Kirchner, F., Kuhn, M., and Seefeld, S.: A new mechanism for regional atmospheric chemistry modeling, J. Geophys. Res. Atmos., 102, 25 847–25 879, 1997.

945 Tack, F., Merlaud, A., Iordache, M.-D., Pinardi, G., Dimitropoulou, E., Eskes, H., Bomans, B., Veefkind, P., and Van Roozendael, M.:
       Assessment of the TROPOMI tropospheric NO_2 product based on airborne APEX observations, Atmos. Meas. Tech., 14, 615–646, 2021.

Thalman, R. and Volkamer, R.: Temperature dependent absorption cross-sections of O_2-O_2 collision pairs between 340 and 630 nm and at
       atmospherically relevant pressure, Phys. Chem. Chem. Phys., 15, 15 371–15 381, 2013.

Tilstra, L. G., Tuinder, O. N. E., Wang, P., and Stammes, P.: Surface reflectivity climatologies from UV to NIR determined from Earth
950   observations by GOME-2 and SCIAMACHY, J. Geophys. Res. Atmos., 122, 4084–4111, 2017.

Tilstra, L. G., Tuinder, O. N. E., and Stammes, P.: GOME-2 surface LER product - Algorithm Theoretical Basis Document, Tech. rep., KNMI
       Report SAF/AC/KNMI/ATBD/003, Issue 3.1, 2019.

Tilstra, L. G., Tuinder, O. N. E., Wang, P., and Stammes, P.: Directionally dependent Lambertian-equivalent reflectivity (DLER) of the Earth's
       surface measured by the GOME-2 satellite instruments, Atmos. Meas. Tech., 14, 4219–4238, 2021.

955 Valks, P., Pinardi, G., Richter, A., Lambert, J.-C., Hao, N., Loyola, D., Van Roozendael, M., and Emmadi, S.: Operational total and tropo-
       spheric NO_2 column retrieval for GOME-2, Atmos. Meas. Tech., 4, 1491–1514, 2011.

van der A, R. J., de Laat, A. T. J., Ding, J., and Eskes, H.: Connecting the dots: NO_x emissions along a West Siberian natural gas pipeline,
       npj Clim. Atmos. Sci., 3, 1–7, 2020.

van Geffen, J., Boersma, K. F., Eskes, H., Sneep, M., Ter Linden, M., Zara, M., and Veefkind, J. P.: S5P TROPOMI NO_2 slant column
960   retrieval: method, stability, uncertainties and comparisons with OMI, Atmos. Meas. Tech., 13, 1315–1335, 2020a.

van Geffen, J. H. G. M., Boersma, K. F., Van Roozendael, M., Hendrick, F., Mahieu, E., De Smedt, I., Sneep, M., and Veefkind, J. P.:
       Improved spectral fitting of nitrogen dioxide from OMI in the 405–465 nm window, Atmos. Meas. Tech., 8, 1685–1699, 2015.

van Geffen, J. H. G. M., Boersma, K. F., Eskes, H., Maasakkers, J. D., and Veefkind, J. P.: TROPOMI ATBD of the total and tropospheric
       NO_2 data products, Tech. rep., S5P-KNMI-L2-0005-RP issue 1.4.0., 2020b.

965 Vandaele, A. C., Hermans, C., Fally, S., Carleer, M., Colin, R., Merienne, M.-F., Jenouvrier, A., and Coquart, B.: High-resolution Fourier
       transform measurement of the NO_2 visible and near-infrared absorption cross sections: Temperature and pressure effects, J. Geophys. Res.
       Atmos., 107, 4348, 2002.

Vasilkov, A., Joiner, J., Spurr, R., Bhartia, P. K., Levelt, P., and Stephens, G.: Evaluation of the OMI cloud pressures derived from rotational
       Raman scattering by comparisons with other satellite data and radiative transfer simulations, J. Geophys. Res. Atmos., 113, D15S19, 2008.

970 Vasilkov, A., Qin, W., Krotkov, N., Lamsal, L., Spurr, R., Haffner, D., Joiner, J., Eun-Su, Y., and Marchenko, S.: Accounting for the effects of
       surface BRDF on satellite cloud and trace-gas retrievals: a new approach based on geometry-dependent Lambertian equivalent reflectivity
       applied to OMI algorithms, Atmos. Meas. Tech., 10, 333–349, 2017.

Veefkind, J., Aben, I., McMullan, K., Förster, H., De Vries, J., Otter, G., Claas, J., Eskes, H., De Haan, J., Kleipool, Q., van Weele, M.,
       Hasekamp, O., Hoogeveen, R., Landgraf, J., Snel, R., Tol, P., Ingmann, P., Voors, R., Kruizinga, B., Vink, R., Visser, H., and Levelt, P.:
975   TROPOMI on the ESA Sentinel-5 Precursor: A GMES mission for global observations of the atmospheric composition for climate, air
       quality and ozone layer applications, Remote Sens. Environ., 120, 70–83, 2012.

Verhoelst, T., Compernolle, S., Pinardi, G., Lambert, J.-C., Eskes, H. J., Eichmann, K.-U., Fjæraa, A. M., Granville, J., Niemeijer, S., Cede,
       A., Tiefengraber, M., Hendrick, F., Pazmiño, A., Bais, A., Bazureau, A., Boersma, K. F., Bognar, K., Dehn, A., Donner, S., Elokhov,
       A., Gebetsberger, M., Goutail, F., Grutter de la Mora, M., Gruzdev, A., Gratsea, M., Hansen, G. H., Irie, H., Jepsen, N., Kanaya, Y.,
980   Karagkiozidis, D., Kivi, R., Kreher, K., Levelt, P. F., Liu, C., Müller, M., Navarro Comas, M., Piters, A. J. M., Pommereau, J.-P., Portafaix,
       T., Prados-Roman, C., Puentedura, O., Querel, R., Remmers, J., Richter, A., Rimmer, J., Rivera Cárdenas, C., Saavedra de Miguel, L.,
       Sinyakov, V. P., Stremme, W., Strong, K., Van Roozendael, M., Veefkind, J. P., Wagner, T., Wittrock, F., Yela González, M., and Zehner,

46

C.: Ground-based validation of the Copernicus Sentinel-5p TROPOMI NO_2 measurements with the NDACC ZSL-DOAS, MAX-DOAS and Pandonia global networks, Atmos. Meas. Tech., 14, 481–510, 2020.

985 Verwer, J. G., Hundsdorfer, W., and Blom, J. G.: Numerical time integration for air pollution problems, Surveys on Math. for Indus., 10, 107–174, 2002.

Vigouroux, C., Langerock, B., Bauer Aquino, C. A., Blumenstock, T., Cheng, Z., De Mazière, M., De Smedt, I., Grutter, M., Hannigan, J. W., Jones, N., et al.: TROPOMI–Sentinel-5 Precursor formaldehyde validation using an extensive network of ground-based Fourier-transform infrared stations, Atmos. Meas. Tech., 13, 3751–3767, 2020.

990 Vlemmix, T., Piters, A. J. M., Stammes, P., Wang, P., and Levelt, P. F.: Retrieval of tropospheric NO_2 using the MAX-DOAS method combined with relative intensity measurements for aerosol correction, Atmos. Meas. Tech., 3, 1287–1305, 2010.

Wagner, T., Dix, B. v., Friedeburg, C. v., Frieß, U., Sanghavi, S., Sinreich, R., and Platt, U.: MAX-DOAS O_4 measurements: A new technique to derive information on atmospheric aerosols—Principles and information content, J. Geophys. Res. Atmos., 109, D22 205, 2004.

Wagner, T., Beirle, S., Brauers, T., Deutschmann, T., Frieß, U., Hak, C., Halla, J. D., Heue, K. P., Junkermann, W., Li, X., Platt, U., and Pundt-
995 Gruber, I.: Inversion of tropospheric profiles of aerosol extinction and HCHO and NO_2 mixing ratios from MAX-DOAS observations in Milano during the summer of 2003 and comparison with independent data sets, Atmos. Meas. Tech., 4, 2685–2715, 2011.

Wang, C., Wang, T., Wang, P., and Rakitin, V.: Comparison and validation of TROPOMI and OMI NO_2 Observations over China, Atmosphere, 11, 636, 2020.

Wang, P. and Sneep, M.: Sentinel-5 L2 Prototype Processor – Algorithm Theoretical Baseline Document for Cloud, Tech. rep., KNMI-ESA-
1000 S5L2PP-ATBD-005 issue 3.1, 2019.

Wang, P., Stammes, P., van der A, R., Pinardi, G., and van Roozendael, M.: FRESCO+: an improved O_2 A-band cloud retrieval algorithm for tropospheric trace gas retrievals, Atmos. Chem. Phys., 8, 6565–6576, 2008.

Williams, J. E., van Velthoven, P. F. J., and Brenninkmeijer, C. A. M.: Quantifying the uncertainty in simulating global tropospheric composition due to the variability in global emission estimates of Biogenic Volatile Organic Compounds, Atmos. Chem. Phys., 13, 2857–2891,
1005 2013.

Williams, J. E., Boersma, K. F., Le Sager, P., and Verstraeten, W. W.: The high-resolution version of TM5-MP for optimized satellite retrievals: description and validation, Geosci. Model Dev., 10, 721–750, 2017.

Wittrock, F., Oetjen, H., Richter, A., Fietkau, S., Medeke, T., Rozanov, A., and Burrows, J. P.: MAX-DOAS measurements of atmospheric trace gases in Ny-Ålesund-Radiative transfer studies and their application, Atmos. Chem. Phys., 4, 955–966, 2004.

1010 World Health Organization: WHO Air quality guidelines for particulate matter, ozone, nitrogen dioxide and sulfur dioxide: global update 2005: summary of risk assessment, Tech. rep., World Health Organization, 2006.

Xu, J., Schüssler, O., Rodriguez, D. G. L., Romahn, F., and Doicu, A.: A novel ozone profile shape retrieval using full-physics inverse learning machine (FP-ILM), IEEE J. Sel. Top. Appl. Earth Observ. Remote Sens., 10, 5442–5457, 2017.

Zara, M., Boersma, K. F., De Smedt, I., Richter, A., Peters, E., van Geffen, J. H. G. M., Beirle, S., Wagner, T., Van Roozendael, M.,
1015 Marchenko, S., Lamsal, L. N., and Eskes, H. J.: Improved slant column density retrieval of nitrogen dioxide and formaldehyde for OMI and GOME-2A from QA4ECV: intercomparison, uncertainty characterisation, and trends, Atmos. Meas. Tech., 11, 4033–4058, 2018.

Zhao, X., Griffin, D., Fioletov, V., McLinden, C., Cede, A., Tiefengraber, M., Müller, M., Bognar, K., Strong, K., Boersma, F., Eskes, H., Davies, J., Ogyu, A., and Lee, S. C.: Assessment of the quality of TROPOMI high-spatial-resolution NO_2 data products in the Greater Toronto Area, Atmos. Meas. Tech., 13, 2131–2159, 2020.